AJUR

American Journal of
Undergraduate Research

Volume 17 | Issue 4 | March 2021

www.ajuronline.org

Print Edition ISSN 1536-4585
Online Edition ISSN 2375-8732

AJUR
American Journal of
Undergraduate Research

Volume 17 | Issue 4 | March 2021 *www.ajuronline.org*

2 **AJUR History and Editorial Board**

3 **Factors Controlling Coral Skeletal U/Ca Ratios with Implications for their Use as a Proxy for Past Ocean Conditions**
Emily Patterson, Spencer Eanes, Penelope Lancrete, Anne Gothman, & Paul Roback

19 **Analyzing Trends in Water Table Elevations at the Marcell Experimental Forest, Minnesota, U.S.A.**
Anna Stockstad, Ella Gray, Stephen Sebestyen, Nina Lany, Randall Kolka, &Marcella Windmuller-Campione

33 **Treatment Outcomes in a Partial Hospital Program for Patients with Social Anxiety Disorder: The Effects of Comorbid Major Depression**
Allison Graham, Douglas R. Terrill, Simone I. Boyd, Isabel Benjamin, Madeline Ward, & Mark Zimmerman

41 **Evaluation of Physical Activity Participation, Self-Efficacy and Outcome Expectancy for Employees Participating in Exercise Is Medicine® On Campus Program**
Maximilian Gastelum-Morales, Lisa J. Leininger, Joanna L. Morrissey, Ryan Luke, & Mark DeBeliso

49 **Axisymmetric Thermal Finite Element Analysis of Effects of Intraocular Projector in the Human Eye**
John A. Stark, Craig D. Foster, & Charles Yu

59 **Prime Factors and Divisibility of Sums of Powers of Fibonacci and Lucas Numbers**
Spirit Karcher & Mariah Michael

71 **A Survey of Inhibitors for the Main Protease of Coronaviruses with the Potential for Development of Broad-Spectrum Therapeutics**
Alyssa Sanders, Samuel Ricci, Sarah Uribe, Bridget Boyle, Brian Nepper, & Nathaniel Nucci

American Journal of Undergraduate Research (AJUR) *is a national, independent, peer-reviewed, open-source, quarterly, multidisciplinary student research journal. Each manuscript of AJUR receives a DOI number. AJUR is archived by the US Library of Congress. AJUR was established in 2002, incorporated as a cheritable not-for-profit organization in 2018. AJUR is indexed internationally by EBSCO and Crossref with ISSNs of 1536-4585 (print) and 2375-8732 (web).*

Factors Controlling Coral Skeletal U/Ca Ratios with Implications for their Use as a Proxy for Past Ocean Conditions

Emily Patterson, Spencer Eanes, Penelope Lancrete, Anne Gothmann[a], & Paul Roback*[b]

[a]*Department of Environmental Studies and Physics, St. Olaf College, Northfield, MN*
[b]*Department of Mathematics, Statistics, and Computer Science, St. Olaf College, Northfield, MN*

https://doi.org/10.33697/ajur.2020.031

Students: patter5@stolaf.edu, eanes1@stolaf.edu, lancre1@stolaf.edu
Mentors: gothma1@stolaf.edu, roback@stolaf.edu*

ABSTRACT
Seawater temperature, salinity and carbonate chemistry have been shown to influence the uranium/calcium (U/Ca) ratios of scleractinian coral skeletons. This apparent sensitivity of U/Ca to multiple environmental parameters calls into question whether there is one environmental variable that most strongly controls coral U/Ca, and whether U/Ca can be straightforwardly applied as a paleoenvironmental proxy due to the tendency of environmental variables to covary in space and time. In this study, uranium concentration data from an existing compilation of tropical scleractinian coral U-series measurements is paired with environmental data from the World Ocean Atlas (WOA) and the Global Ocean Data Analysis Project (GLODAP) to examine the sensitivity of coral skeletal U/Ca to multiple seawater properties including temperature, salinity, pH, and saturation state. First, univariate linear regressions and multiple linear regressions were used to compare relationships between uranium and environmental parameters in the dataset with relationships observed in previous studies. Next, principal component analysis and regularized regression were used to identify the most likely predictors of coral U/Ca in order to create a multiple linear regression model. Results indicate that pH, Ω, alkalinity, and temperature are all significant predictors of uranium concentrations in coral. The magnitude and strength of relationships between U/Ca and environmental variables also differ across different genera. Seawater properties with strong correlations and small ranges make interpretation of these results difficult. However, results of these analyses indicate that U/Ca is dependent on multiple environmental parameters and that previously developed univariate regressions may be insufficient to characterize the full range of variables that influence coral [^{238}U].

KEYWORDS
Coral; Paleoceanography; Proxy Calibration; Uranium; Multiple Linear Regression; Regularized Regression; Environmental Change; Oceanographic Databases

INTRODUCTION

Understanding how and why the environment has changed naturally over Earth's history can provide valuable insight into how Earth's climate system will respond to ongoing anthropogenic perturbations. Instrumental records of oceanic changes do not exist beyond the last ~100 years, however, so to access information about ocean changes further in the past, indirect indicators of environmental change, referred to as 'proxies', are used. Scleractinian corals skeletons are one of the most fruitful proxies for past climate and environmental change because their age can be precisely determined, they tend to record environmental properties of the seawater in which they grow, it is possible to make multiple measurements of environmental properties on the same sample due to their relatively large size, and they can capture sub-annual environmental variability.[1, 2] In recent years, the U/Ca ratio of corals has been explored as a proxy that responds linearly to changes in seawater properties including seawater temperature,[3] salinity,[4] pH,[5] and carbonate ion concentration.[6] The ability of coral U/Ca to capture past seawater salinity, pH, and/or carbonate ion concentration, in particular, would be a valuable addition to the arsenal of coral-based proxies, due to the relative lack of proxies for these important environmental variables. In particular, indicators of pH and carbonate ion concentration could help us better understand the relationship between changes in atmospheric CO_2 and ocean acidification.[7] An understanding of past changes in seawater salinity can provide insight into the relationship between salinity and ocean circulation and also can be used to learn about the relationship between changes in climate and the hydrological cycle.[8]

There is reason to expect U/Ca in corals to be sensitive to seawater pH and/or carbonate ion concentration. Inorganic aragonite precipitation experiments conducted by DeCarlo *et al.* (2015) suggest that U is incorporated into the aragonite mineral in proportion to the ratio of $[U]/[CO_3^{2-}]$ in seawater.[9] These results support the idea that corals, which make aragonite skeletons, may also incorporate uranium in proportion to the concentration of carbonate ion in seawater. A potential problem is the fact

that corals do not appear to precipitate their aragonite skeletons directly from seawater, but rather from a semi-enclosed space referred to as the calcifying fluid.[10–12] Because corals are able to manipulate the chemical composition of this calcifying fluid (through active pumping of protons, for example), the calcifying fluid has a carbonate chemistry that is distinct from external seawater.[13–15] As a result, coral U/Ca could be more dependent on other environmental parameters that have strong effects on the coral skeletal growth process.

There is also evidence that coral U/Ca may be dependent on sea surface salinity. First, Swart and Hubbard (1982) showed that coral U/Ca ratios appear to be dependent mainly on the absolute concentration of U in seawater.[16] As a result, they postulated that U/Ca in coral could record salinity variations as a result of changes in the absolute concentration of U. Results of Shen and Dunbar (1995), showing that U/Ca in tropical coral skeletons decreased during times of greater local rainfall, generally support this idea.[17]

Many published studies have also examined relationships between U/Ca and seawater temperature.[3, 18–23] While it does not appear that U/Ca is sensitive to temperature in inorganic aragonite,[7] U/Ca is correlated with temperature in natural samples over seasonal cycles.[24] As a result, U/Ca may be related to seawater temperature through an effect of temperature on the coral skeletal growth process.

To date, the studies calibrating environmental proxies based on coral skeletal U/Ca ratios come from natural samples collected from a single geographic location,[17, 24] or from laboratory-based culture experiments in which one environmental variable is varied while others are held constant.[5] However, if paleoclimatologists hope to apply proxies over a broad geographic range and far into the past (when seawater boundary conditions may have looked quite different), it is important to quantify whether U/Ca depends on a single, or multiple, environmental parameters. It is also important to quantify how precisely environmental variations could be reconstructed from coral U/Ca.

One common approach in proxy development is the 'space-for-time' approach, which trains proxies based on modern spatial variability in environmental parameters. For example, in the case of ocean sediment cores, measurements of chemical, geological, physical or biological variables are made in the top few centimeters of ocean sediment and are examined for correlations with environmental variables in the water column overlying the sediment core location. Recent studies have combined core-top measurements of Mg/Ca ratios in foraminifera with oceanographic databases to refine the foraminifera-based Mg/Ca paleothermometer.[25, 26] An assumption embedded in the 'space-for-time' calibration strategy is that the relationships between environmental changes and the proxy of interest are common across space and at a single location over hundreds, thousands, or even millions of years.

This study attempts to conduct a calibration of U/Ca's sensitivity to environmental changes using a 'space-for-time' approach whereby modern and Recent (Holocene and younger) tropical coral U data are compared with environmental data from the World Ocean Atlas (WOA) and the Global Ocean Data Analysis Project (GLODAP). A wealth of coral U data exists in the literature due to the fact that tropical corals have been measured by U-series dating as a way to generate sample ages for decades (*e.g.* Robinson *et al.* 2014).[27] In order to obtain U-series ages from coral, the abundance of [^{238}U], which makes up >99% of the U in the coral skeleton, is determined. As a result, U-series measurements made over the past few decades also produce measurements of coral [U]. Recently, Chutcharavan *et al.* (2018) compiled coral U-series measurements from the literature and analyzed the data to determine whether seawater [^{234}U]/[^{238}U] ratios appear to have changed over time.[28] In the present study, the compilation of Chutcharavan *et al.* (2018) is used to investigate whether the [U] of recent corals appears to vary significantly with environmental variables such as temperature, salinity, pH, and/or carbonate ion concentration.

METHODS AND PROCEDURES

Data Compilation

Coral U-series data compiled in Chutcharavan *et al.* (2018) was used to evaluate the relationship between coral skeleton [U] and the environmental properties of seawater in which the corals grew.[28] The main variables of interest alongside the genus, age, calcite abundance (as % calcite), and [^{238}U] of the corals include sea surface temperature (SST), salinity (SSS), pH, total alkalinity, dissolved inorganic carbon, and saturation state with respect to aragonite (Ω). The two most abundant genera from the coral U-series data were included in our analyses. A summary of these variables for these two genera can be found in **Table 1**. Coral [^{238}U] data is converted to coral U/Ca molar ratios using the atomic weight of U and by assuming that Ca concentrations in the tropical coral skeletons are 9.52 mmol Ca/g coral aragonite. Analyses of Ca concentrations in coral skeletons show that [Ca] in tropical coral skeletons varies by ~0.4%.[29, 30] As such, U/Ca variations in coral skeletons are dominated by variability in [^{238}U]. All samples for which [^{238}U] were labeled as "not reported" and/or genus was reported as "nd", "unknown", or "unidentified" were excluded from the analysis.

While the coral samples in Chutcharavan *et al.* (2018) range in age from modern to ~55 kyr, we restrict our investigation to n=737 samples of Holocene age, specifically <10 kyr. These samples indicate stable seawater $[^{234}U]/[^{238}U]$ ratios over the last 10 kyr. Restricting our samples to those of Holocene age and younger ensures that we retain a relatively large number of samples for our analyses. Additionally, the Holocene is a time of relatively stable climate, such that we expect the modern spatial variability in environmental variables covered by our samples from different sites to be much greater than the Holocene environmental changes at any given site. Although recent studies have demonstrated variability in SSTs of up to 1°C during the Holocene at high latitudes, SSTs in the tropics appear to vary by ~0.5°C during this time.[31, 32] Discrepancies in environmental records from the Holocene generated by different proxies also remain, making it difficult to explicitly correct for climatic variability in Holocene-age samples.[32]

Variable	5th Percentile	Median	Mean	95th Percentile
$[^{238}U]$ (ppm)	0.93	1.14	1.20	1.66
Age (ka)	0.01	0.46	2.4	9.00
Calcite Abundance (%)	0.00	0.50	0.44	1.00
Salinity (g/kg)	33.05	35.11	34.72	35.94
Temperature (°C)	24.29	26.65	26.63	29.35
pH (total scale)	8.05	8.11	8.10	8.13
Total Alkalinity (µmol/kg)	2180.89	2264.88	2272.45	2364.90
TCO_2 (µmol/kg)	1870.91	1953.53	1943.54	2001.25
Ω	3.16	3.76	3.69	4.18
$\delta^{234}U$ initial (‰)	141.23	144.83	144.66	148.51

Table 1. Data summary of key coral and environmental variables.[29–32] These values include all non-missing values with age under 10,000 years from the two most abundant genera in the Chutcharavan *et al.* (2018) compilation.

Complementary environmental data from the World Ocean Atlas (WOA) and the Global Ocean Data Analysis Project (GLODAP) was paired with the coral U-series dataset. Both projects have been updated with recent oceanographic data, mapped at 1° by 1° gridded points with latitudes, longitudes, and depths associated with each point. This feature makes the WOA and GLODAP datasets appropriate to compare directly with one another and with our coral dataset. The mean oceanographic temperature and salinity data from the WOA is based on the analysis of historical oceanographic profiles and select surface-only data as described in greater detail in Zweng *et al.* (2018) and Locarnini *et al.* (2018).[33, 36] All other environmental variables were accessed as mapped climatologies from GLODAPv2.[34, 35] Additional detail on the methodologies used to create these mapped climatologies can be found in Lauvset *et al.* (2016).[34]

To pair coral data from a particular geographic location with environmental data, a distance function was created which measures the distance from each coral sample included in Chutcharavan *et al.* (2018) to the grid locations where each of the environmental variables were measured. Since the GLODAP and WOA data are built on a grid and use interpolation from measured data, coral environmental parameters were estimated by taking the weighted average of the three closest values to each fossil coral sample. The function was coded in C++ for efficiency and run in R using the Rcpp library.[37–39] The function measured the distance between any two points on earth, that is the coral and each environmental grid location, measured in latitude and longitude, taking the earth's curvature into account. In the case that latitudes or longitudes were not reported in Chutcharavan *et al.* (2018) or in the original scientific papers cited by Chutcharavan *et al.*, the original scientific papers reporting coral U-series data were searched for coral collection sites, and the longitudes and latitudes corresponding to these sites were identified.

Data Cleaning

The coral samples compiled in Chutcharavan *et al.* (2018) were constrained to those of Holocene age (*i.e.* ~10,000 years of age and younger). At ages beyond about 15,000 years, there are fewer coral samples in the compilation for a given time point such that the data are sparser. After filtering for age, the resulting dataset contains 737 of the original 1860 samples. Filtering the coral samples to those younger than ~10,000 years results in $[^{238}U]$ vs. Age slopes close to zero as seen in **Figure 1** below.

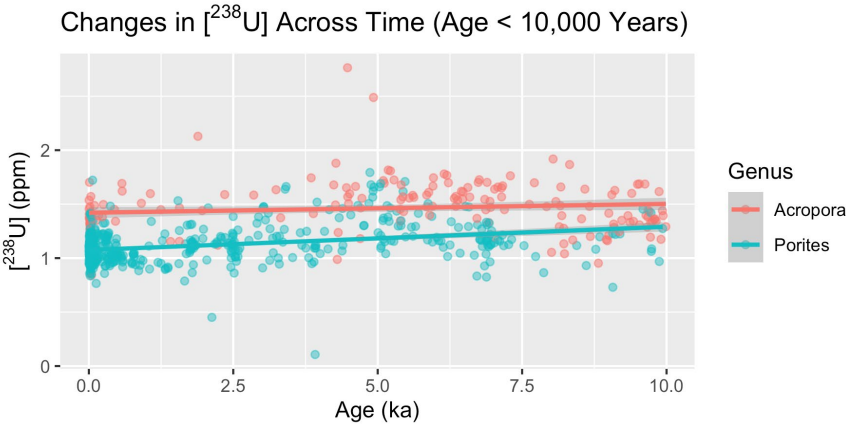

Figure 1. This plot uses coral [^{238}U] data as a function of age for samples of the genera *Acropora* and *Porites* across the entire Chutcharavan *et al.* (2018) dataset, filtered to remove NA's and filtered for samples younger than 10,000 years. Age slopes were close to zero for each genus: *Acropora* (0.008 (+/- 0.004)) and *Porites* (0.022* (+/- 0.003)), and when including both genera (0.03* (+/- 0.003)).
*indicates significance at the .05 level. Results include coefficient estimates followed by standard errors.

Next, the relationship between [^{238}U] and % calcite was explored. The presence of calcite in the coral skeleton can overprint the original geochemical composition of coral skeletons at the time of growth because U incorporation in calcite and coral aragonite differ.[40] Some labs reported % calcite as a range of values, in which case the maximum reported value was used in order to avoid underestimating the % calcite of the sample. The data was assessed on variable and genus levels for differences between corals with different amounts of calcite. Calcite values were divided into three groups: less than or equal to one percent, greater than one percent, and those with no values listed (≤ 1 = 120 samples, > 1 = 37 samples, N/A = 580 samples). The threshold chosen was 1% because this value corresponds to the detection limit of many X-ray diffraction measurements that quantify calcite abundance.[28] The directions of the slopes for the group where calcite > 1% differs from that of the calcite ≤ 1% group for pH and Ω. There were no significant differences in slopes between calcite groups for temperature or salinity (**Figure A1** in Appendix). To optimize U data quality, the 37 samples with values of calcite greater than 1% were removed from the working dataset. We also note that the majority of samples younger than 1 kyr did not record percent calcite.[28] The original studies corresponding to these published samples assess preservation by qualitative measures including scanning electron microscopy, or otherwise note that there are no detectable traces of calcite in the samples.[41, 42] Our univariate regression results for temperature, salinity, and pH all did not change significantly between the case where samples were restricted to only those with calcite values ≤ 1% (*i.e.* samples with calcite values of N/A were removed) and the case where samples with calcite values of N/A were included. As such, the final dataset presented here contains samples with calcite values of ≤ 1% and N/A, in order to obtain a more robust analysis with greater sample sizes.

The next data integrity check was to examine [^{238}U] values at the lab level for outliers. Labs 1, 3, 9, 11 and 16 were investigated as their means fell greater than one standard deviation from the mean of all the samples. A multiple linear regression model was trained on all the other lab data and used to create prediction intervals for the data from those five more extreme labs. Only six out of 104 observations fell outside of a 95% prediction interval across all sites for those five outlying labs, so no lab exclusions were made (**Figure 2**). Additional details can be found in the project GitHub repository, a link to which is provided in the Appendix.

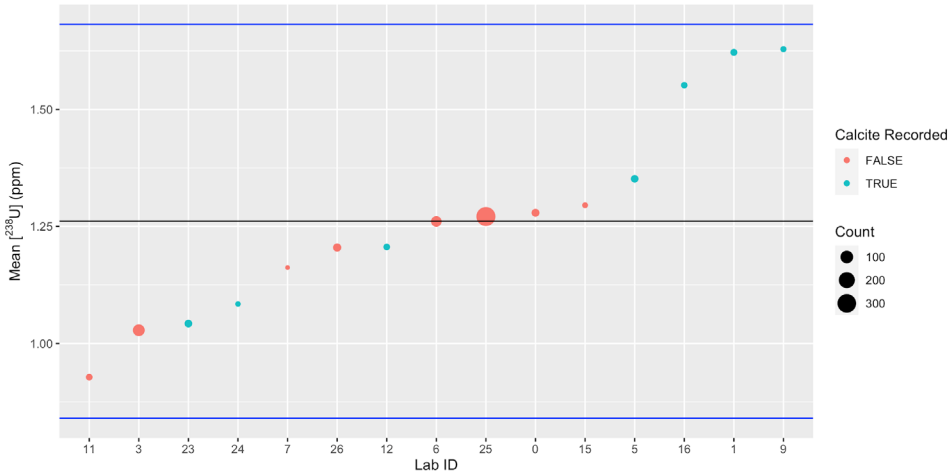

Figure 2. Each lab's mean [^{238}U] was calculated for all samples, and points sized by number of samples. Points are colored by whether or not the lab reported calcite values for their sample. The black horizontal line is the global mean, and the blue lines are +/- two standard errors from the lab aggregated mean.

An additional analysis conducted to validate the data was to check if any sites had unusual or strongly correlated environmental data values. Since environmental data is resolved at the site level, there are 51 unique sites, and thus 51 values for each of the environmental variables (temperature, salinity, pH, Ω, alkalinity, TCO_2). As seen in **Figure 3**, salinity values above and below 34 g/kg seemed to cluster in regard to their pH and temperature values, leading to a further investigation of the sites with low salinity values.

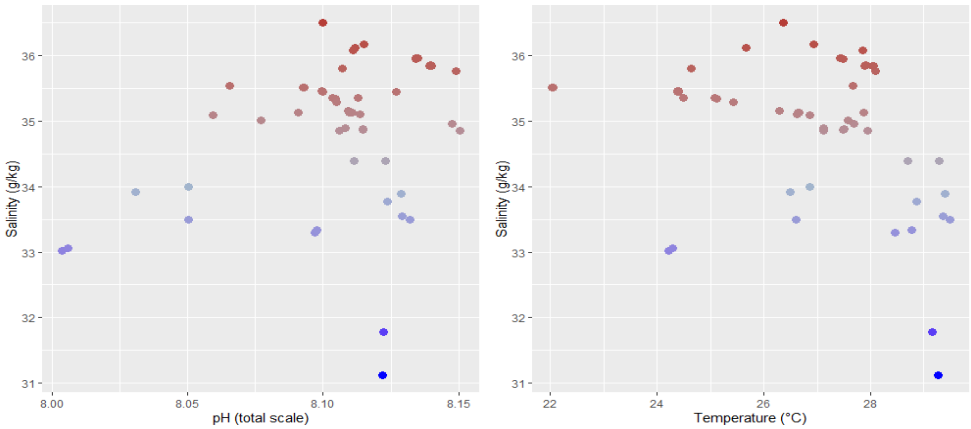

Figure 3. Salinity values associated with each geographic site in our data set, plotted against pH and temperature, colored by salinity.

These points of interest came from a broad region of low mean salinity waters in the Indo-Pacific, and their salinity, temperature, and pH values are reasonable for this geographic location (**Figure 4**).

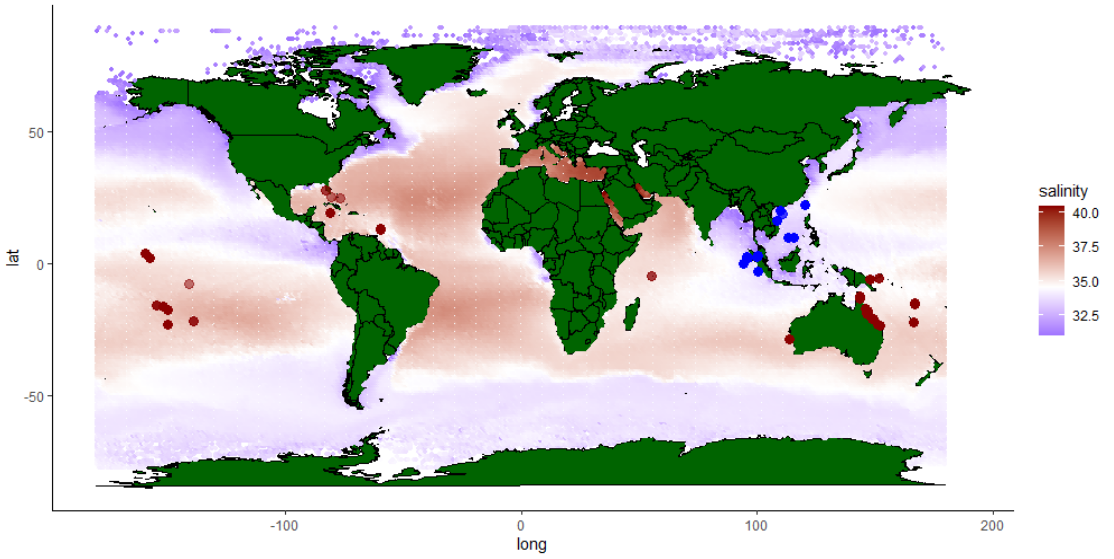

Figure 4. Global map with gridded ocean salinity data colored from blue (low) to red (high).[36]

Variability in relationships between [U] and environmental variables were also examined by genus; only corals with genera that had more than 50 samples were selected. It is notable that 297 samples had no genus listed and were excluded. After selecting the top two genera, filtering for age and calcite abundance, and finding no issues with locations or labs, 700 samples remained out of the original 1860 (**Table 2**). After data cleaning, 51 sites remained out of the original 78. The original data distribution can be found in **Table A1** in Appendix.

Genus	Number of Samples	Percent of Total
Porites	533	76%
Acropora	167	24%
Both Genera	700	100%

Table 2. After filtering for age and calcite and keeping genera with more than 50 samples.

Statistical Methods

Univariate linear regression was used to test if [^{238}U] can be used as a proxy for temperature, salinity, and pH separately, as has been done in previous studies.[3, 6, 18–24, 43, 44] Additionally, multiple linear regression was used in order to account for additional variables which cannot be controlled for in an observational setting. In order to perform multiple linear regression, predictors need to be chosen, a process known as feature selection. Regularized regression (*e.g.* lasso and ridge regression) has been widely used in recent years due to its demonstrated prediction prowess on data with many predictors of unknown relationships. Regularized regression is suited to this task because the underlying relationships are expected to be linear, not categorical or tree-like. The technique of regularized regression solves a linear regression minimization problem for a best fit linear model to data but includes a penalty parameter proportional to a measure of coefficient size. Thus, this technique prefers more parsimonious models with coefficients of smaller magnitude. There are multiple flavors of regularized regression with different methods to measure the magnitude of models' coefficients, the two most common being ridge regression, which uses the sum of the squared coefficients, and lasso regression, which uses the sum of the absolute value of the coefficients. Elastic net is a more general form of regularized regression that uses a linear combination of squared and absolute value coefficients.[45]

To compare the regularized regression methods, two stages of 10-fold cross validation were employed. The first stage is used to reserve some out-of-bag test data in order to compare regularized regression techniques. For each of the folds of the first-stage, 10-fold cross-validation is again performed to select the minimum and one standard error penalty parameter for each of the three techniques: ridge, lasso, and elastic net. Then, minimum and one standard error models for each of the techniques were used to compute a root mean squared error (RMSE) on the initial reserved out-of-bag data from the first stage of cross-validation. RMSE is a technique used to compare model accuracy in regression by taking the mean of the squared differences of actual and predicted values, and then taking the square root of that mean. A lower RMSE indicates a more accurate model. The RMSE is then averaged for the 10 folds of the first stage of cross-validation. The minimum penalty parameter always performed better than the

one standard error penalty parameter across the three models, and the RMSE was within .01% for the minimum penalty parameter across the three methods. Thus, since there was on average essentially no difference in RMSE between the techniques, lasso was chosen for simplicity.

Bootstrapping, the technique of resampling the data with replacement, was employed to ensure stable estimates from variable selection. Due to the randomness of sampling in cross-validation of lasso modeling, bootstrapping the data was necessary to quantify random differences and stabilize the results. The data was bootstrapped 5,000 times, a lasso model was fit to the bootstrap sample, and the selected variables, their coefficients, and the penalty parameter were all recorded.

Best subset selection was implemented for comparison with the bootstrapped lasso approach. This involved fitting every possible combination of linear models with a given set of predictors, of which there are 2^p possible models, where p is the number of predictors in the data. These models can then be compared with a selection of characteristics, such as adjusted R-squared, or information criterion like AIC (Akaike information criterion) and BIC (Bayesian information criterion).[46] Information criterion are frequently used and often preferred when comparing models with different sets of predictors, as they can help account for the differing complexities between models.[47] BIC was selected since it more heavily penalizes additional predictors than AIC, and it was valuable to achieve a parsimonious model to compare against the results of bootstrap lasso.

Finally, principal component analysis (PCA) was performed on the data to help understand the relationships between the predictors. PCA has previously been applied to questions in the broad field of paleoceanography to identify structure in data when multiple variables are involved.[48–50] For example, Lough (2004) used PCA to determine whether scleractinian coral proxy-based sea-surface temperature records captured variability in El-Niño Southern Oscillation.[50] PCA allows the collapse of high dimensional data into a few independent components. Singular value decomposition is applied to the input data and results in a linear transformation of the data such that the first new predictor describes most of the variability in the data, and each subsequent predictor describes less. The original predictors can also be visualized in "PCA-space" to give some understanding of how they relate to one another.

RESULTS

Comparison to Previous Studies

Temperature

Linear regression was used to test if there was a significant association between explanatory variables and [^{238}U], when applying an age restriction of 10,000 years and excluding percent calcite values greater than 1%. The first test was between temperature and [^{238}U] (**Figure A2**). When including both genera of interest (*Porites* and *Acropora*), there was significant evidence of a negative association between temperature and [^{238}U] ($t = -16.66$, p-value < 0.001). When looking at each individual genus, a highly significant negative association between temperature and [^{238}U] was found for both *Porites* ($t = -10.79$, p-value < 0.001) and for *Acropora* ($t = -8.89$, p-value < 0.001). Negative relationships between [^{238}U] and temperature are consistent with results from previous studies on *Porites* coral (**Table 3**, **Figure 5**). Comparisons between the results in this study with and without filtering for age can be found in **Table A2**.

Primary Results			Previous Lab Studies			
Intercept	**Temperature**	**Genus**	**Intercept**	**Temperature**	**Genus**	**Source**
2.295* (+/- 0.108)	-0.044* (+/- 0.004)	*Porites*	1.928	-0.033*	*Porites*	Ourbak *et al.* (2006)
3.600* (+/- 0.239)	-0.083* (+/- 0.009)	*Acropora*	2.232	-0.0456*	*Porites*	Min *et al.* (1995)
3.169* (+/- 0.116)	-0.074* (+/- 0.004)	Both Genera	2.106	-0.0367*	*Porites*	Correge *et al.* (2000)
			1.488	-0.0212*	*Porites*	Armid *et al.* (2011)
			1.957	-0.029*	*Porites*	Wei *et al.* (2000)
			2.057	-0.034*	*Porites*	Felis *et al.* (2009)
			2.26	-0.044*	*Porites*	Fallon *et al.* (1999)
			2.24	-0.046*	*Porites*	Sinclair *et al.* (1998)

Table 3. Primary results, which showed a negative association between temperature and [^{238}U], compared to previous lab studies.
*indicates significance at the .05 level. Primary results include coefficient estimates followed by standard errors.

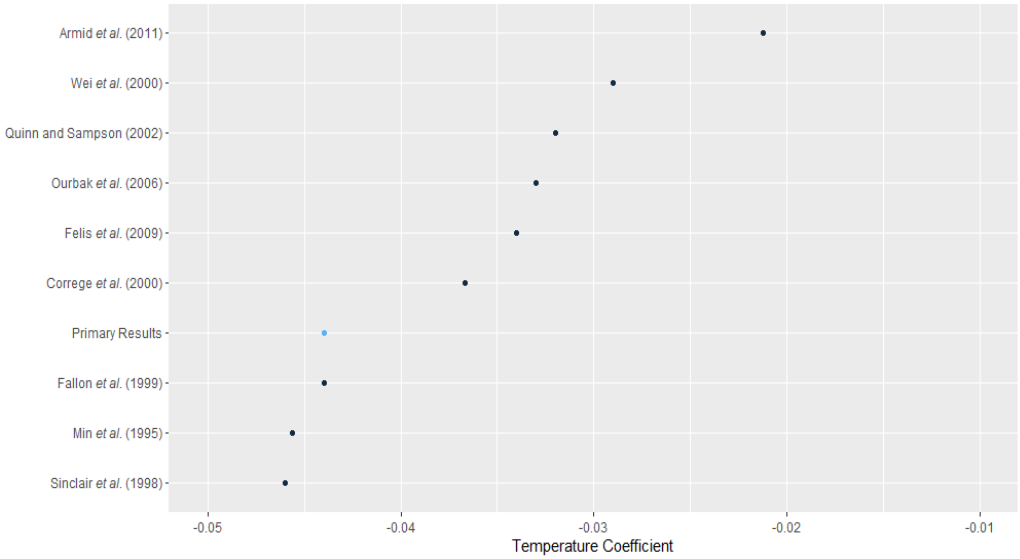

Figure 5. Coefficients from primary result using only *Porites* compared to other reported *Porites* slopes using univariate OLS regression.

Salinity

Salinity was added to the previous set of models to once again examine the relationship between temperature and [^{238}U], this time holding salinity constant. Adjusting for salinity in this set of models gives insight into the true relationship between temperature and [^{238}U] since salinity is more variable in this large-scale observational study than in lab studies. The model with both genera included revealed that a significant negative relationship between temperature and [^{238}U] remained after accounting for salinity ($t = -12.13$, p-value < 0.001). When breaking the analysis down by genus, this negative relationship was still significant for both *Porites* ($t = -7.89$, p-value < 0.001) and for *Acropora* ($t = -8.04$, p-value < 0.001). Compared to Ourbak *et al.* (2006), both the *Porites* model and the larger model including both genera in this study followed a similar pattern, revealing a significant negative relationship between temperature and [^{238}U] after accounting for salinity.

After accounting for temperature, the model with both genera showed a positive effect of salinity on [^{238}U] ($t = 6.58$, p-value < 0.001). However, when breaking the analysis down by genus, this positive effect of salinity after adjusting for temperature was only significant for *Porites* ($t = 4.59$, p-value < 0.001) and not for *Acropora* ($t = 1.10$, p-value $= 0.271$). Salinity results for *Porites* revealed a significant positive relationship between salinity and [^{238}U] after adjusting for temperature, which is directionally consistent with Ourbak *et al.* (2006) (**Table 4**).

Ourbak *et al.* (2006)			
Intercept	**Temperature**	**Salinity**	**Genus**
0.162 (+/- 0.019)	-0.022* (+/- 0.003)	0.162* (+/- 0.019)	*Porites*
Primary Results			
Intercept	**Temperature**	**Salinity**	**Genus**
0.986* (+/- 0.299)	-0.035* (+/- 0.031)	0.031* (+/- 0.007)	*Porites*
1.599 (+/- 1.804)	-0.080* (+/- 0.010)	0.054 (+/- 0.048)	*Acropora*
0.887* (+/- 0.359)	-0.059* (+/- 0.005)	0.054* (+/- 0.008)	Both Genera

Table 4. Primary results for temperature and salinity compared to previous lab studies.
*indicates significance at the 0.05 level. Primary results include coefficient estimates followed by standard errors.

pH

Linear regression was also used to test whether pH was significantly associated with [^{238}U] (**Figure A2**). For the model including both genera, there was evidence that pH was significantly positively associated with [^{238}U] ($t = 3.24$, p-value $= 0.001$). When looking at each individual genus, pH was significantly related to [^{238}U] for both *Porites* ($t = 2.17$, p-value $= 0.031$) and *Acropora* ($t = -5.34$, p-value < 0.001), although this relationship was positive for *Porites* and negative for *Acropora*. The negative relationship

between pH and [^{238}U] in the *Acropora* model was directionally similar to the results of Inoue *et al.* (2011) which also modeled only *Acropora*. However, the magnitude of our primary results was about 28 times larger than was seen in Inoue *et al.* for the intercept, and about 47 times larger for the slope (**Table 5**). After accounting for temperature or temperature and salinity in the *Acropora* models, the intercept was large but insignificant, and the models revealed no significant relationship between [^{238}U] and pH in *Acropora* (**Table 6**).

Inoue *et al.* (2011)		
Intercept	**pH**	**Genus**
2.96	-0.21*	*Acropora*
Primary Results		
Intercept	**pH**	**Genus**
-2.451 (+/- 0.836)	0.441* (+/- 0.199)	*Porites*
82.319* (+/-14.961)	-9.974* (+/- 1.845)	*Acropora*
-6.116* (+/- 2.215)	0.903* (+/- 0.274)	Both Genera

Table 5. Primary results for pH compared to previous lab studies.
*indicates significance at the 0.05 level. Primary results include coefficient estimates followed by standard errors.

pH *Acropora* models			
Intercept	**pH**	**Temperature**	**Salinity**
82.319* (+/-14.961)	-9.974* (+/- 1.845)		
11.854 (+/- 19.386)	-1.932 (+/- 2.423)	-0.091* (+/- 0.014)	
-9.362 (+/- 19.564)	1.399 (+/- 2.486)	-0.086* (+/- 0.015)	0.048 (+/- 0.050)

Table 6. Comparing univariate pH model to multivariate models for *Acropora*.
*indicates significance at 0.05 level. Primary results include coefficient estimates followed by standard errors.

Further Analysis - Variable Selection

In this observational study, [^{238}U] is not adequately explained by one or two variables as described in previous studies. Multiple regression modeling can be utilized in this context as an attempt to replicate how certain conditions can be carefully controlled in lab studies (**Table 7**). Three multiple regression models were built, one for each genus of corals, and one overall (for both genera combined), controlling for all six variables of interest simultaneously. These multiple regression models confirmed some relationships the univariate models in this study have previously shown; for example, pH has a positive relationship with [^{238}U] for both genera, modeled individually and overall, when controlling for temperature, Ω, total alkalinity, salinity and total CO_2. Interestingly, this positive relationship is significant in *Acropora* when controlling for all other parameters, contrary to the negative linear relationship found between pH and [^{238}U] in the univariate regression results (**Tables 6** and **7**). The relationship between temperature and [^{238}U] is negative in both genera modeled individually and overall, after accounting for the other five parameters, which is consistent with our primary results in **Tables 3** and **4**.

	Porites	*Acropora*	Both Genera
Intercept	-43.853* (+/-13.323)	-303.493* (+/-107.097)	-69.259* (+/- 16.004)
pH	5.469* (+/-1.581)	36.652* (+/-12.814)	8.622* (+/- 1.896)
Temperature	-0.044* (+/-0.007)	-0.018 (+/-0.034)	-0.065* (+/- 0.008)
Ω	-0.620* (+/-0.189)	-3.613* (+/-0.839)	-1.098* (+/- 0.222)
Total Alkalinity	0.003* (+/-0.001)	0.002 (+/-0.009)	0.005* (+/- 0.002)
Salinity	-0.030* (+/-0.013)	0.142 (+/-0.080)	-0.014 (+/- 0.015)
TCO_2	-0.001 (+/-0.002)	-0.006 (+/-0.012)	-0.003 (+/- 0.002)

Table 7. Multiple Linear Regression with all variables for the two major genera. Amount of explained variance for the three models: *Porites* adj. $R^2 = 0.317$, *Acropora* adj. $R^2 = 0.389$, Both Genera adj. $R^2 = 0.435$.
*indicates significance at the 0.05 level. Primary results include coefficient estimates followed by standard errors.

While it is beneficial to see which environmental parameters are most significantly related to [^{238}U] when including all variables of interest in multiple linear regression, feature selection can be used to further identify the subset of predictors that are most significantly related to the response, [^{238}U]. First, principal component analysis was performed to identify how predictors are related to one another (**Figure 6**, **Figure A3**). The first PCA component captures 51.7% of the variability in the explanatory variables, and the second captures 38.7% (**Figure A4**). This means that the set of explanatory variables can be projected into two dimensions while capturing 90.4% of the variability in the data. One notable piece of information derived from PCA is variable loading, or how strongly predictors align with one PCA dimension. It is clear that pH is very highly loaded on the second dimension because it points nearly parallel to that axis. Salinity and total alkalinity are highly loaded on dimension one, though to a lesser extent than pH is loaded on dimension two. Finally, temperature and TCO_2 measure a very similar parameter, but are negatively correlated.

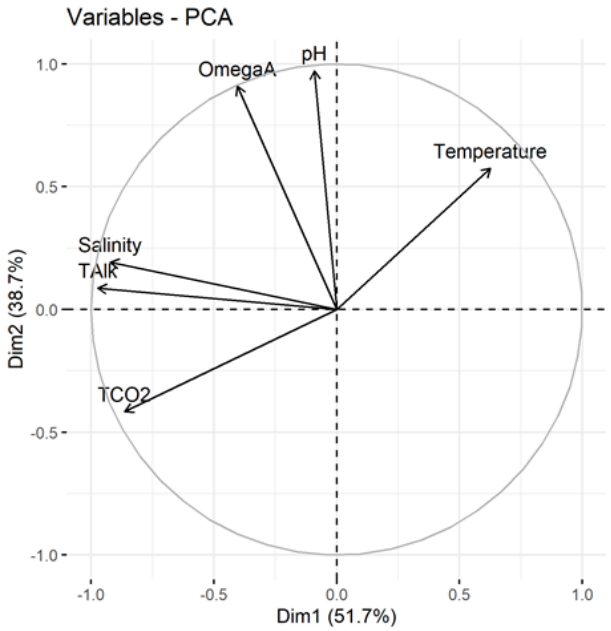

Figure 6. Visualization of predictors projected onto the first two PCA dimensions, which shows how predictors relate to each other in a reduced dimension space.

To perform feature selection, lasso models were fit from many bootstrapped samples of the data to account for instabilities in lasso estimates. The variables of interest in these analyses were temperature, salinity, pH, Ω, total alkalinity, and TCO_2. The data

was bootstrapped, and each bootstrap sample was fit with a lasso model to create a bootstrapped confidence interval for predictor coefficients (**Figure 7**).

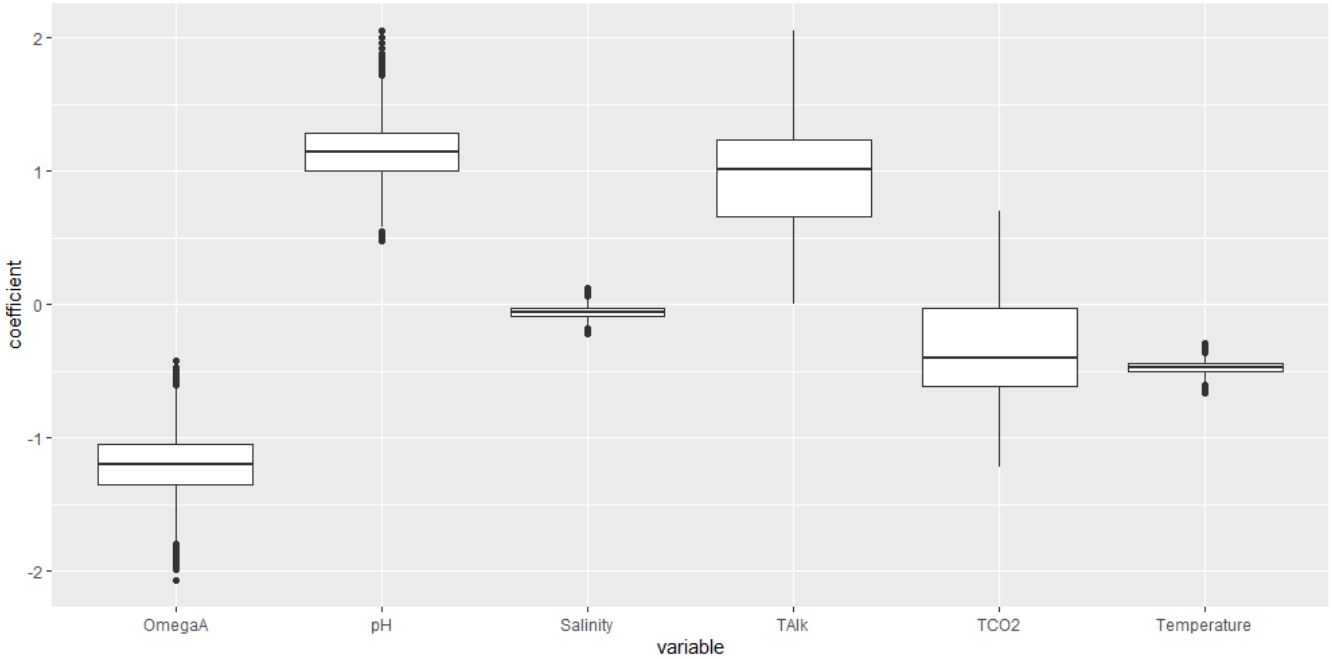

Figure 7. Box plots of slopes of standardized variables resulting from minimum penalty parameter lasso run on 5,000 bootstraps of the data. Lasso sets unimportant variables to zero, thus plots that are centered or overlapping with zero are considered unimportant, while those that do not overlap zero are selected.

It can be seen that when using the minimum error penalty parameter, Ω, pH, temperature, and alkalinity were always non-zero (that is, selected by the model). Best subset selection identified the same subset of predictors when using all possible combinations of predictors and using both AIC or BIC as the criterion. Thus, results indicate that Ω, pH, temperature, and alkalinity all control [^{238}U] to some extent, and a final multiple linear regression model was built using all four as predictors for both genera of interest to quantify these relationships. This final model reveals that [^{238}U] has negative linear relationships with temperature and Ω, and positive linear relationships with pH and alkalinity (**Table 8**). The negative linear relationship between temperature and [^{238}U] is consistent with previous calibrations. While the relationship between pH and [^{238}U] is not consistent with past studies, this is likely due to measuring the effect of pH while controlling Ω, which is very difficult to measure in practice as these variables are closely coupled. These relationships also likely differ by genus.

	Both Genera
Intercept	-84.511* (+/- 12.917)
pH	10.428* (+/- 1.529)
Temperature	-0.062* (+/- 0.008)
Ω	-1.125* (+/- .220)
Total Alkalinity	0.003* (+/- 0.001)

Table 8. Multiple linear regression with variables selected from lasso and best subset selection.
*indicates significance at the 0.05 level. Primary results include coefficient estimates followed by standard errors.

DISCUSSION

This study reveals that using a large observational dataset of coral fossils yields results consistent with several existing, lab-based studies measuring temperature and salinity with smaller sample sizes. Specifically, this study confirms previous lab calibrations that describe the univariate relationship between ocean temperature and [^{238}U] in fossil coral.[3, 4, 18–24] After accounting for salinity, a significant negative relationship remains between temperature and [^{238}U]. Additionally, after adjusting for temperature, a significant positive relationship was found between salinity and [^{238}U]. Both relationships are consistent with the results of Ourbak *et al.* (2006).[4] Interestingly, the relationship between pH and [^{238}U] differed from past lab studies. Specifically, an overall positive relationship between pH and [^{238}U] was found, inconsistent with results from lab studies such as Inoue *et al.* (2011).[5] This discrepancy was found in the model for *Porites* alone and when modeling both genera together, but not in the model of only *Acropora*. However, after adjusting for temperature, there was no statistically significant relationship between pH and [^{238}U] in the *Acropora* model. This may be reconciled in two ways. First, univariate relationships are generally insufficient to describe this observational data. Secondly, existing lab studies[5] did not decouple pH, Ω, and other carbonate system variables, making it difficult to identify which variable might in reality be controlling U/Ca. This analysis reveals a negative relationship between Ω and [^{238}U], generally consistent with Inoue *et al.* (2011).[5] Indeed, previous univariate model results showing pH as a good predictor of [^{238}U] may be related to pH's high loading on PCA dimension 2. The observation that pH corresponds nearly exactly with a PCA dimension shows that it likely captures some information from other parameters that are also highly loaded on PCA dimension 2 like Ω and temperature. Thus, slopes reported for pH from previous experiments may indicate control by either Ω and/or temperature and not by pH itself.

Based on this work, univariate relationships are insufficient to fully describe the complex interactions of corals and seawater conditions. This result suggests that it would likely be challenging to apply a simple proxy for inferring past oceanic conditions as represented by coral [^{238}U], since many parameters control [^{238}U]. However, if there is evidence that other variables remain constant in some regions or time periods, it could be possible to predict other variables from [^{238}U]. Specifically, since the relationship between temperature and [^{238}U] remained even after accounting for salinity, it is possible that [^{238}U] could be used as a proxy for measuring temperature. The relationship between pH and [^{238}U] does not appear as simple.

A major difference with this observational data compilation and lab studies is that lab studies often fix all experimental parameters besides the one or two they are studying. Furthermore, a study to determine which combination of many possible parameters best describe [^{238}U] in corals has not been done. However, the difficulty is that in observational ocean data, and in many lab experiments, environmental parameters may covary. While it would be valuable to further test these results in additional laboratory experiments, this difficulty can be somewhat addressed with careful variable selection by statistically approximating the control of parameters using multiple linear regression, although when two parameters are highly correlated it is difficult to evaluate the effect of changes in one while holding the other constant. When including all parameters of interest in variable selection through bootstrap lasso and best subset selection, pH, Ω, alkalinity, and temperature are all significant predictors of [^{238}U]. Genus also seems to play a key role in these relationships.

The authors acknowledge that the current study still suffers from limitations including the need to filter by genus (rather than by species) to include large enough sample sizes. Hence, there could be species-specific effects that are not captured. Additionally, a stable climate was assumed for the last 10,000 years, but this is an oversimplification. Previous work has highlighted regional changes in climate over this time period that are unaccounted for in this examination, but may be possible to include in future studies once regional Holocene climate changes are better constrained.[31, 32] Furthermore, many of the environmental variables of interest are highly correlated, which can make regression results difficult to interpret. Finally, the range in the environmental variables is relatively small (*e.g.* pH values from 8.00 to 8.15), especially compared to lab calibrations. Though significant conclusions can still be drawn, values over larger data ranges, as can be obtained through further lab experiments, would help to more fully understand the relationships identified in this study.

CONCLUSIONS

In this study, a compilation of U-series measurements in tropical corals from a range of geographic locations was used in combination with environmental variables from two oceanographic databases to quantify relationships between coral [^{238}U] and seawater temperature, salinity, aragonite saturation state, and pH. Univariate linear regressions and multiple linear regressions were used to compare relationships between U and environmental parameters. Though there is some fragility to multiple linear regression models on these data, results of variable selection analyses indicate that U is dependent on multiple environmental parameters and that previously developed univariate regressions may be insufficient to characterize the full range of variables that influence coral [^{238}U]. In addition, relationships between [^{238}U] and environmental variables vary by genus. Laboratory culture experiments, in which larger ranges of environmental variability can be explored, may prove useful in further testing the multivariate relationships found here and for identifying the physical, chemical, and biological mechanisms driving the dependences of coral uranium abundance on environmental change.

ACKNOWLEDGEMENTS

The authors thank Ella Hagopian (Class of 2020), Henry Henson (Class of 2020), Brendan Ireland (Class of 2019), Katie Murney (Class of 2019), and Matthew Richey (Professor of Mathematics, Statistics and Computer Science) from St. Olaf College for their contributions to the initial stages of this research. They also acknowledge the Center for Interdisciplinary Research at St. Olaf College and its Director, Katie Ziegler-Graham, for support.

REFERENCES

1. Druffel, E. (1997) Geochemistry of corals: Proxies of past ocean chemistry, ocean circulation, and climate. *Proc. Natl. Acad. Sci.* 94, 8354–8361. *https://doi.org/10.1073/pnas.94.16.8354*
2. Edwards, R.L., Gallup, C.D., Cheng, H. (2003) Uranium-series Dating of Marine and Lacustrine Carbonates. *Rev.Mineral. Geochem.*52, 363–405. *https://doi.org/10.2113/0520363*
3. Correge, T., Delcroix, T., Recy, J., Beck, W., Cabioch, G., Le Cornec, F. (2000), Evidence for stronger El Nino-Southern Oscillation (ENSO) events in a mid-Holocene massive coral, *Paleoceanography* 15, 465–470. *https://doi.org/10.1029/1999PA000409*
4. Ourbak, T., Correge, T., Malaize, B., Le Cornec, F., Charlier, K., and Peypouquet, J.-P. (2006) A high-resolution investigation of temperature, salinity, and upwelling activity proxies in corals. *Geochem. Geophys. Geosyst.* 7, Q03013. *https://doi.org/10.1029/2005GC001064*
5. Inoue, M., Suwa, R., Suzuki, A., Sakai, K., and Kawahata, H., (2011). Effects of seawater pH on growth and skeletal U/Ca ratios of *Acropora digitifera* coral polyps. *Geophys. Res. Lett.* 38, 12801–12804. *https://doi.org/10.1029/2011GL047786*
6. Anagnostou, E., Sherrell, R. M., Gagnon, A. C., LaVigne, M., Field, M. P., and McDonough, W. F., (2011). Seawater nutrient and carbonate ion concentrations recorded as P/Ca, Ba/Ca, and U/Ca in the deep-sea coral *Desmophyllum dianthus. Geochim.Cosmochim. Acta* 75, 2529–2543. *https://doi.org/10.1016/j.gca.2011.02.019*
7. Rae, J.W.B., Foster, G.L., Schmidt, D.N., Elliot, T. (2011) Boron isotopes and B/Ca in benthic foraminifera: Proxies for the deep ocean carbonate system. *Earth. Planet. Sci. Lett.* 302, 403-413. *https://doi.org/10.1016/j.epsl.2010.12.034*
8. Nyadjro, E. S., & Subrahmanyam, B. (2016). Spatial and temporal variability of central Indian Ocean salinity fronts observed by SMOS. Remote Sensing of Environment, 180, 146–153. *https://doi.org/10.1016/j.rse.2016.02.049*
9. DeCarlo, T.M., Gaetani, G.A., Holcomb, M., Cohen, A.L., (2015). Experimental determination of factors controlling U/Ca of aragonite precipitated from seawater: Implications for interpreting coral skeleton. *Geochimica et Cosmochimica Acta* 162, 151–165. *https://doi.org/10.1016/j.gca.2015.04.016*
10. McConnaughey, T. (1989) ^{13}C and ^{18}O isotopic disequilibrium in biological carbonates: II. *In vitro* simulation of kinetic isotope effects. *Geochim. Cosmochim. Acta* 53, 163–171. *https://doi.org/10.1016/0016-7037(89)90282-2*
11. Adkins J. F., Boyle E. A., Curry W. B. and Lutringer A. (2003) Stable isotopes in deep-sea corals and a new mechanism for "vital effects." *Geochim. Cosmochim. Acta* 67, 1129–1143. *https://doi.org/10.1016/S0016-7037(02)01203-6*
12. Tambutté, E., Tambutté, S., Segonds, N., Zoccola, D., Venn, A., Erez, J. and Allemand, D. (2012) Calcein labelling and electrophysiology: insights on coral tissue permeability and calcification. *Proc. R. Soc. B Biol. Sci.* 279, 19–27. *https://doi.org/10.1098/rspb.2011.0733*
13. Comeau, S., Tambutte, E., Carpenter, R., Edmunds, P., Evensen, N, Allemand, C., Ferrier-Pages, C., Tambutte, S., Venn A. (2017) Coral calcifying fluid pH is modulated by seawater carbonate chemistry not solely seawater pH. *Proc. R. Soc. B Biol. Sci.* 284, 20161669. *https://doi.org/10.1098/rspb.2016.1669*
14. Al-Horani, F.A., Al-Moghrabi, S.M., de Beer, D. (2003) The mechanism of calcification and its relation to photosynthesis and respiration in the scleractinian coral *Galaxea fascicularis. Mar. Biol.* 142, 419-426. *DOI 10.1007/s00227-002-0981-8*
15. Zoccola D., Tambutté E., Kulhanek E., Puverel S., Scimeca J.-C., Allemand D. and Tambutté S. (2004) Molecular cloning and localization of a PMCA P-type calcium ATPase from the coral Stylophora pistillata. *Biochim. Biophys. Acta - Biomembr.* 1663, 117–126. *https://doi.org/10.1016/j.bbamem.2004.02.010*
16. Swart, P. K., and Hubbard, J. A. E. B., (1982). Uranium in Scleractinian Coral Skeletons. *Coral Reefs* 1, 13–19. *https://doi.org/10.1007/BF00286535*
17. Shen, G. T., and Dunbar, R. B., (1995). Environmental controls on uranium in reef corals. *Geochim. Cosmochim. Acta* 59, 2009–2024. *https://doi.org/10.1016/0016-7037(95)00123-9*
18. Quinn, T.M. and Sampson, D.E. (2002) A multiproxy approach to reconstructing sea surface conditions using coral skeleton geochemistry, *Paleoceanogr. Paleoclimatol.* 17. *doi:10.1029/2000PA000528*
19. Armid, A., Asami, R., Fahmiati, T., Sheikh, M.A., Fujimura, H., Higuchi, T., Tair, E., Shinjo, R., Oomori, T. (2011) Seawater temperature proxies based on DSr, DMg, and DU from culture experiments using the branching coral *Porites cylindrica. Geochem. Cosmochim. Acta* 75, 4273–4285. *https://doi.org/10.1016/j.gca.2011.05.010*
20. Wei, G., Sun, M., Li, X., Nie, B. (2000) Mg/Ca, Sr/Ca, and U/Ca ratios of a porites coral from Sanya Bay, Hainan Island, South China Sea and their relationships to sea surface temperature. *Paleogeog., Paleoclim., Paleoecol.* 162, 59–74. *https://doi.org/10.1016/S0031-0182(00)00105-X*

21. Felis, T., Suzuki, A., Kuhnert, H., Dima, M., Lohmann, G., Kawahata, H. (2009) Subtropical coral reveals abrupt early-twentieth-century freshening in the western North Pacific Ocean. *Geology* 37, 527–530. *https://doi.org/10.1130/G25581A.1*

22. Fallon, S.J., McCulloch, M.T., van Woesik, R., Sinclair, D.J. (1999) Corals at their latitudinal limits: laser ablation trace element systematics in *Porites* from Shirigai Bay, Japan. *Earth Planet. Sci. Lett.* 172, 221–238. *https://doi.org/10.1016/S0012-821X(99)00200-9*

23. Sinclair, D.J., Kinsley, L.P.J., McCulloch, M.T. (1998) High resolution analysis of trace elements in corals by laser ablation ICP-MS. *Geochim. Cosmochim. Acta* 62, 1889-1901. *https://doi.org/10.1016/S0016-7037(98)00112-4*

24. Min, G. R., Edwards, R. L., Taylor, F. W., Recy, J., Gallup, C. D., and Beck, J. W., (1995). Annual cycles of U/Ca in coral skeletons and U/Ca thermometry. *Geochim. Cosmochim. Acta* 59, 2025–2042. *https://doi.org/10.1016/0016-7037(95)00124-7*

25. Saenger, C.P., Evans, M.N. (2019) Calibration and Validation of Environmental Controls on Planktic Foraminifera Mg/Ca Using Global Core-Top Data. *Paleoceanogr.Paleoclimatol.* 34, 1249–1270. *https://doi.org/10.1029/2018PA003507*

26. Tierney, J.E., Malevich, S.B., Gray, W., Vetter, L., Thirumalai K. (2019) Bayesian Calibration of the Mg/Ca Paleothermometer in Planktic Foraminifera, *Paleoceanogr. Paleoclimatol.* 34, 2005–2030. *https://doi.org/10.1029/2019PA003744*

27. Robinson, L.F., Adkins, J.F., Frank, N., Gagnon, A.C., Prouty, N.G., Roark, E.B., van de Flierdt, T. (2014) The geochemistry of deep-sea coral skeletons: A review of vital effects and applications for paleoceanography. *Deep Sea Research Part Ii: Topical Studies in Oceanography* 99, 184-198. *https://doi.org/10.1016/j.dsr2.2013.06.005*

28. Chutcharavan, P. M., Dutton, A., Ellwood, M. J., (2018). Seawater $^{234}U/^{238}U$ recorded by modern and fossil corals. *Geochim. Cosmochim. Acta* 224, 1–17. *https://doi.org/10.1016/j.gca.2017.12.017*

29. Sun, Y., Sun M., Lee, T., Nie, B. (2005) Influence of seawater Sr content on coral Sr/Ca and Sr thermometry. *Coral Reefs* 24, 23-29. *doi 10.1007/s00338-004-0467-x*

30. Allison, N., Finch, A.A., Sutton, S.R., Newville, M. (2001) Strontium heterogeneity and speciation in coral aragonite: Implications for the strontium paleothermometer. *Geochim. Cosmochim. Acta* 65, 2669-2676. *https://doi.org/10.1016/S0016-7037(01)00628-7*

31. Marcott, S.A., Shakun, J.D., Clark, P.U., Mix, A.C. (2013) A Reconstruction of Regional and Global Temperature for the Past 11,300 Years. *Science* 339, 1198-1201. *doi: 10.1126/science.1228026*

32. Rodriguez, L. G., Cohen, A. L., Ramirez, W., Oppo, D. W., Pourmand, A., Edwards, R. L., et al. (2019). Mid- Holocene, coral-based sea surface temperatures in the western tropical Atlantic. *Paleoceanogr. Paleoclimatol.*, 34, 1234–1245. *https://doi.org/10.1029/2019PA003571*

33. Locarnini, R. A., A. V. Mishonov, O. K. Baranova, T. P. Boyer, M. M. Zweng, H. E. Garcia, J. R. Reagan, D. Seidov, K. Weathers, C. R. Paver, and I. Smolyar, (2018). *World Ocean Atlas 2018, Volume 1: Temperature.* A. Mishonov Technical Ed.; NOAA Atlas NESDIS 81, 52 pp. *https://archimer.ifremer.fr/doc/00651/76338/*

34. Lauvset, S.K., Key, R.M., Olsen, A., van Heuven, S., Velo, A., Lin, X., Schirnick, C., Kozyr, A., Tanhua, T., Hoppema, M., Jutterstrom, S., Steinfeldt, R., Jeansson, E., Ishii, M., Perez, F.F., Watelet, S. (2016) A new global interior ocean mapped climatology: the 1 x 1 GLODAP version 2, *Earth Syst. Sci. Data* 8, 325–340. *DOI 10.5194/essd-8-325-2016*

35. Olsen, A., Key, R.M., van Heuven, S., Lauvset, S.K., Velo, A., Lin, Z., Schirnick, C., Kozyr, A., Tanhua, T., Hoppema, M., Jutterstrom, S., Steinfeldt, R., Jeansson, E., Ishii, M., Perez, F.F., Suzuki, T. (2016). The Global Ocean Data Analysis Project version 2 (GLODAPv2) - an internally consistent data product for the world ocean *Earth Syst. Sci. Data* 8, 297–323. *https://doi.org/10.5194/essd-8-297-2016*

36. Zweng, M. M., J. R. Reagan, D. Seidov, T. P. Boyer, R. A. Locarnini, H. E. Garcia, A. V. Mishonov, O. K. Baranova, K. Weathers, C. R. Paver, and I. Smolyar, (2018) *World Ocean Atlas 2018, Volume 2: Salinity.* A. Mishonov Technical Ed.; NOAA Atlas NESDIS 82, 50 pp. *https://archimer.ifremer.fr/doc/00651/76339/*

37. Eddelbuettel D, François R (2011). Rcpp: Seamless R and C++ Integration. *J. Stat. Softw*, **40**, 1–18. *doi: 10.18637/jss.v040.i08*.

38. Eddelbuettel D (2013). *Seamless R and C++ Integration with Rcpp*. Springer, New York. doi: 10.1007/978-1-4614-6868-4, ISBN 978-1-4614-6867-7.

39. Eddelbuettel D, Balamuta JJ (2017). "Extending extitR with extitC++: A Brief Introduction to extitRcpp." *PeerJ Preprints*, **5**, e3188v1. ISSN 2167-9843, *doi: 10.7287/peerj.preprints.3188v1, https://doi.org/10.7287/peerj.preprints.3188v1*.

40. Gothmann, A.M., Higgins, J.A., Adkins, J.F., Broecker, W., Farley, K.A., McKeon, R., Stolarski, J., Planavsky, N., Wang, X., Bender, M.L. (2019) A Cenozoic record of seawater uranium in fossil corals. *Geochim. Cosmochim. Acta* 250, 173–190. *https://doi.org/10.1016/j.gca.2019.01.039*

41. Rashid, R., A. Eisenhauer, P. Stocchi, V. Liebetrau, J. Fietzke, A. Ruggeberg, and € W-C. Dullo (2014), Constraining mid to late Holocene relative sea level change in the southern equatorial Pacific Ocean relative to the Society Islands, French Polynesia, Geochem. Geophys. Geosyst., 15, 2601–2615, *doi:10.1002/ 2014GC005272*

42. Cobb, K.M., Charles, C.D., Cheng, H., Kastner, M., Edwards, R.L. (2003) U/Th-dating living and young fossil corals from the central tropical Pacific. *Earth Planet. Sci. Lett.* 210, 91-103. *https://doi.org/10.1016/S0012-821X(03)00138-9*

43. Armid, A., Takaesu, Y., Fahmiati, T., Yoshida, S., Hanashiro, R., Fujimura, H., Higuchi, T., Taira, E., and Oomori, T., (2008). U/Ca as a possible proxy of carbonate system in coral reef *in Proceedings of the 11th International Coral Reef Symposium*, 92–96.

44. Inoue, M., Nakamura, T., Tanaka, Y., Suzuki, A., Yokoyama, Y., Kawahata, H., Sakai, K., Gussone, N. (2018) A simple role of coral-algal symbiosis in coral calcification based on multiple geochemical tracers. *Geochim. Cosmochim. Acta* 235, 76–88. *https://doi.org/10.1016/j.gca.2018.05.016*

45. Zou, H., Hastie, T. (2005) Regularization and variable selection via the elastic net. *J. R. Statist. Soc. B.* 67, 301-320. *https://doi.org/10.1111/j.1467-9868.2005.00503.x*

46. Efron B., Hastie, T. (2016) Statistical Inference: Algorithms, Evidence, and Data Science. 1st ed., 91-104, Cambridge University Press.

47. Hastie, T., Tibshirani, R., Friedman, J. (2008) The Elements of Statistical Learning, 2nd ed., 605-624.

48. Yuan, Z., Liu, D. Masque, P., Zhao, M., Song, X., Keesing, J.K. (2020) Phytoplankton responses to climate-induced warming and interdecadal oscillation in North-Western Australia. *Paleoceanogr. Paleoclimatol.*, 35, e2019PA003712. *https://doi.org/10.1029/2019PA003712*

49. Iwamori, H., K. Yoshida, H. Nakamura, T. Kuwatani, M. Hamada, S. Haraguchi, and K. Ueki (2017), Classification of geochemical data based on multivariate statistical analyses: Complementary roles of cluster, principal component, and independent component analyses, *Geochem. Geophys. Geosyst.,* 18, 994– 1012, *doi:10.1002/2016GC006663*

50. Lough, J.M. (2004) A strategy to improve the contribution of coral data to high-resolution paleoclimatology. *Palaeogeogr. Palaeoclimatol. Palaeoecol.* 204, 115-143, *https://doi.org/10.1016/S0031-0182(03)00727-2*

ABOUT STUDENT AUTHORS

Emily Patterson recently graduated from St. Olaf College in May, 2020, with a B.A. degree in Psychology and a concentration in Statistics and Data Science. She is now working as an Associate Data Scientist at the Allant Group. In the future, she plans to pursue a career in data science with a focus on the fields of healthcare or environmental science.

Spencer Eanes graduated from St. Olaf College in May, 2020, with a B.A. degree in Mathematics and Computer Science, and a concentration in Statistics and Data Science. He is now working as a Software Developer at Epic Systems, where he develops a telemedicine video conferencing solution.

Penelope Lancrete graduated from St. Olaf College in May, 2020, with a B.A. degree in Mathematics and Ancient Studies, and a concentration in Statistics and Data Science. She is now working as a Catastrophe Risk Analyst at TigerRisk Partners.

PRESS SUMMARY

An understanding of past environmental conditions provides context for evaluating modern climate changes, but there is a lack of data for periods before the existence of instrument-based environmental records. To reconstruct conditions hundreds to millions of years into the past, proxies are needed - indirect indicators of past conditions measured from data or samples that are currently accessible. Coral skeletons are one good example of an environmental proxy. They are globally distributed, can be reliably dated, and have potential to record high-resolution climate information through their chemical composition and physical structure.

Recently, the uranium/calcium ratio in fossil coral skeletons has been investigated as a proxy for past ocean pH, temperature, salinity, and carbonate ion concentration. However, existing calibrations are either lab-based or were developed using small numbers (n~15) of natural samples. This study explores whether existing calibrations can describe the relationship between uranium concentrations and seawater environmental conditions, such as seawater pH, temperature, salinity, and carbonate ion concentration for a large observational dataset of 700 fossil coral samples. Results suggest that no single variable most strongly controls U/Ca, but rather that multiple environmental variables are needed to capture it. Specifically, pH, Ω, alkalinity, and temperature are all significant predictors of U/Ca. Genus also plays a key role in these relationships. These results provide further insight into whether the fossil coral uranium proxy can be used to accurately and precisely reconstruct past ocean conditions.

Analyzing Trends in Water Table Elevations at the Marcell Experimental Forest, Minnesota, U.S.A.

Anna Stockstad[*a], *Ella Gray,*[a] *Stephen Sebestyen*[b], *Nina Lany*[c], *Randall Kolka*[b], *& Marcella Windmuller-Campione*[a]

[a]*Department of Forest Resources, University of Minnesota- Twin Cities, St. Paul, Minnesota*
[b]*USDA Forest Service Northern Research Station, Grand Rapids, Minnesota*
[c]*USDA Forest Service Northern Research Station, Durham, New Hampshire*

https://doi.org/10.33697/ajur.2020.032

Student: stock523@umn.edu[*]
Mentor: mwind@umn.edu

ABSTRACT
Water table fluctuations in peatlands are closely coupled with the local climate setting and drive critical ecosystem processes such as nutrient cycling. In Minnesota, USA, peatlands cover ten percent of the surface area, approximately 2.5 million hectares, some of which are actively managed for forest products. To explore the relationship between peatland water tables and precipitation, long-term data (1961 to 2019) were used from the Marcell Experimental Forest in northern Minnesota. Starting in 1961, water table data from seven peatlands, including two types of peatlands (bogs and fens), were measured. We used the Theil-Sen estimator to test for monotonic trends in mean monthly water table elevations for individual peatlands and monthly precipitation. Water levels in bogs were both more variable and had mean water table elevations that were closer to the surface. Individual trends of water table elevations differed among peatlands. Water table elevations increased over time in three of the bogs studied and decreased over time in two of the bogs studied. Trends within fens were notably nonlinear across time. No significant linear trend was found for mean monthly precipitation between 1961 and 2019. These results highlight differences in peatlands types, local physiography, and the importance of understanding how changes in long-term dynamics coupled with changing current conditions will influence the effects of water table fluctuations on ecosystem services. The variability of water table elevations in bogs poses potential difficulties in modeling these ecosystems or creating adaptive management plans.

KEYWORDS
Peatlands; Hydrology; Water tables; Bogs; Fens; Monitoring; Minnesota; Climate Change

INTRODUCTION

Worldwide northern (boreal and subarctic) peatlands have stored carbon (estimated at 500 Pg of carbon) due to slow decomposition rates.[1-3] Theoretically, aboveground ecosystem productivity increases as a function of belowground carbon.[4-6] In peatlands, however, aboveground productivity presents as extremely low growth rates due to infertile conditions, regardless of the surplus of belowground carbon.[4-7] Northern peatland carbon stores were historically considered "stable" or "inactive". In response to a changing climate, however, hydrological and biogeochemical feedbacks have revealed the extreme sensitivity of peatland carbon stocks to fluctuations in decomposition rates.[1, 2]

Water table dynamics in peatlands control biogeochemical cycles in these systems and are closely linked with local and global climate.[1] Understanding the feedback processes between water tables and climate in peatlands is critical in predicting the future dynamics of these ecosystems. Subsequently, the magnitude of ecosystem services provided by peatlands, such as carbon storage and biodiversity, are influenced by these feedback processes.[2] Carbon cycling within peatlands is linked with fluctuations of the water table since decomposition rates are controlled by soil moisture content.[1-3, 8] Slight changes in peatland hydrology can cause significant feedbacks in local carbon dynamics and productivity, and thus have major implications for the global carbon cycle.[8, 9, 10, 11]

Long-term changes in water tables may lead to changes in forest composition, notably shifts in understory species, which has major implications for forest management.[12, 13, 14] Local hydrology strongly influences the composition of plant communities as well as the growth of vegetation. For example, some species, especially the evergreen plants of the heath family Ericaceae, are

adapted to survive in growth-limiting conditions such as acidic and low fertility soils. If these growing conditions were to change, the species composition would likely shift as well.[13] Temperature and hydrology are key drivers of change in forest composition and productivity, as demonstrated by McPartland et al.[14] Decreases in shrub cover were seen in the drought-only experiments (*i.e.* water table drawdown), while drought treatments with warming were correlated with an increase in shrub cover.[12] In contrast, the relationship between water tables and tree species in peatlands, specifically black spruce (*Picea mariana*), is less clear. A study within bogs at the MEF analyzed the long-term correlation (1963 to 2010) of black spruce growth to several climatic factors, and found a weak relationship between annual tree growth and water table elevation.[12] These various growth strategies suggest a possible decoupling of evapotranspiration and water table elevation due to the perched root systems of black spruce located in *Sphagnum* hummocks above high water tables.[12] In addition, rooting depth may increase with declines in water table elevation, which would likely shift vegetation community structure.[15] Thus, multiple feedback responses due to changes in climatic conditions, including changes in water table elevation, may determine the transition of peatland plant communities. These relationships suggest that the long-term management of peatlands, and specifically black spruce, will become increasingly complex under a changing climate. Fluctuations in water tables may cause a cascading effect on forest composition and local hydrology, which may influence forest productivity and health on an ecosystem scale. Therefore, forest managers must consider the several feedbacks between local hydrology, forest composition, and structure in order to adaptively manage these systems.

Differences in peatland hydrology strongly influence feedback responses. Hydrological characteristics, vegetation, and chemistry are used to classify peatland type (*i.e.* bog or fen). Both bogs and fens have organic soils. Bogs are perched above local aquifers and only receive precipitation inputs. Bog soils are acidic and low in plant available nutrients. By contrast, fens intersect local aquifers and receive groundwater inputs in addition to precipitation.[4] Soils and water in fens are less acidic than in bogs (*i.e.* poor fens) and may even be neutral to alkaline (*i.e.* rich fen).[4, 8,] Water tables in bogs are typically more variable than in fens since these systems do not receive water inputs from local aquifers and only receive precipitation inputs.[1, 2, 4, 9] Water table elevation is inversely correlated to decomposition rates. A lowering of the water table will generally result in increased decomposition rates.[9] The concentration of dissolved minerals is also generally higher in fens compared to bogs.[3, 4] Consequently, the dynamics of peatland hydrology and biogeochemical processes are tightly linked and can influence forest composition and subsequently have major implications for forest management.[12, 13, 14]

The timing, intensity, and frequency of precipitation, runoff, and ET influence the hydrology of peatlands, and these processes are not stationary as climate changes. To explore trends, long-term monitoring is required. The Marcell Experimental Forest (MEF), located in northern Minnesota, USA, includes a long-term monitoring station of both bogs and fens. Specifically, peatland water table and meteorological monitoring have been ongoing since 1961.[4] Therefore, the MEF provides records of peatland water table elevations in both bogs and fens which can be utilized to quantify trends and differences in annual and decadal patterns in types of peatlands.

Given the complexity and interacting feedbacks within peatlands systems, long-term data are required to identify trends in hydrological patterns. The Marcell Experimental Forest (MEF) research program, located in northern Minnesota, USA, includes monitoring of peatland water table and meteorological data since 1961.[4] Therefore, these records of peatland water table elevations in both bogs and fens which can be utilized to quantify trends and differences in annual and decadal patterns in types of peatlands. Using MEF data, we evaluated trends in water table elevations in bogs and fens at the MEF, the relationship of those trends to precipitation, and the magnitude of peatland responses to climate. We hypothesized that water tables within bogs would be more variable than that of fens due to the reduced influence of local aquifers in bogs than in fens. Secondly, we hypothesized that precipitation would demonstrate a significant linear trend during the period of record. Our results can aid natural resource managers in the development adaptive management plans that consider the site-specific responses of these stands to climate.

METHODS AND PROCEDURES

Study region

Northern Minnesota, USA, represents the southern edge of the boreal forest.[11] The composition of Minnesota's boreal forests includes a mix of upland conifer species, wet hardwood forests, and conifer peatland forests.[16, 17] Minnesota's conifer peatland forests are dominated by three species, tamarack (*Larix laricina*), black spruce, and northern white cedar (*Thuja occidentalis*), and represent approximately 450,000 hectares, 550,000 hectares, and 245,000 hectares of forest land, respectively. All three species are managed for commercial timber production; black spruce is the second most harvested pulpwood species after aspen (*Populus* spp.), representing millions of dollars in direct and indirect revenue within Minnesota.[18]

Study site[4]

The 1114-hectare MEF is located forty kilometers north of Grand Rapids, Minnesota, USA. Formally established as a long-term monitoring site in 1962 to study peatland ecology and hydrology, the site is funded and operated by the USDA Forest Service.

The MEF contains both fens and bogs, as well as upland terrestrial ecosystems. Both forested and open peatlands exist within the MEF. Vegetation in fens may include tamarack, black spruce, willow (*Salix* spp.), speckled alder (*Alnus incana* ssp. *rugosa*), sedges (*Carex* spp.), and other species. Several species of Ericaceae are found in bogs. Black spruce and eastern tamarack are the major overstory trees in forested bogs.[4] Due to nutrient limitation in bogs, overstory trees have low productivity and slow growth.[11] *Sphagnum* mosses are the predominant understory species within bogs and fens.

Climate at the MEF is defined as sub-humid continental with an average annual temperature of 3C and average annual precipitation of 78.0 cm (± 1 standard deviation of 11.0 cm; 75% of which occurs during snow-free periods). Average January temperature is -1 °C and average July temperature is 19°C.[4] Typical of northern latitudes, large diurnal and seasonal fluctuations in temperature occur.

The MEF is divided into six research watersheds, each having a central peatland and surrounding upland. These six research watersheds have been extensively researched with additional information on each watershed, instrumentation, and research methods summarized by Sebestyen et. al.[4]

We investigated the water table elevations of the S1, S2, S3, S4, S5, and S6 peatlands. We also analyzed a research site (not a watershed) called Bog Lake Peatland. The bogs are located within the S1, S2, S4, S5, and S6 watersheds. The S3 watershed contains a rich fen and Bog Lake Peatland is a poor fen. Soil classification is similar across peatlands at the MEF (**Table 1**). Typic borohemists contain wood fragments, intermediately decomposed (hemic), and are reddish in color.[4] Typic borosaprists are composed of a surface layer of *Sphagnum* moss and ericaceous shrubs, with partially and fully decomposed organic layers below (saprist).[4] Soil water chemistry, specifically pH, differs between the two peatland types, with bogs being more acidic than fens (**Table 1**).

Watershed	Starting date of record (Year-month)	Size (hectares)	Soil series	Description	Soil water pH
S1 bog	1961-01	8.1	Greenwood	Typic Borohemist	3.9 ± 0.2
S2 bog	1961-01	3.2	Loxley	Typic Borosaprist	3.9 ± 0.2
S3 fen	1961-04	18.6	Moose Lake; Lupton	Typic Borosaprist; Typic Borohemist	6.9 ± 0.1
S4 bog	1962-04	8.1	Greenwood	Typic Borohemist	4.1 ± 0.3
S5 bog	1962-03	6.1	Moose Lake; Lupton	Typic Borosaprist; Typic Borohemist	4.1
S6 bog	1965-01	2.0	Seelville peat	Typic Borosaprist	4.9
Bog Lake Peatland (fen)	1990-07	NA	Greenwood	Typic Borohemist	4.1

Table 1. Description of peatland soil classification and chemistry at the Marcell Experimental Forest.[4]

Trees in the S1 bog and S3 fen at the MEF were experimentally harvested several decades ago. Black spruce were strip cut from the S1 bog in 1969, and the remaining strips were then removed in 1974. The S3 fen was clearcut and slash was burned during the winter of 1972 to 1973. The other peatlands have not been experimentally manipulated and are reference sites.

Statistical analysis

Monthly mean water table elevation (mWTE) was calculated by averaging the daily maximum water table elevation dataset for each month during the period of record.[19, 20] To standardize across the different elevations of the peatlands in the landscape, monthly mean water table elevations were mean-centered by subtracting the overall mean water table elevation during the full period of record from mWTE for each peatland. The selected time range for all data was 1961 (oldest available data) to 2019

(most recent available data). The starting date of record differed slightly for individual peatlands based on when observational studies were first established (**Table 1**) Peatland water table elevations at the MEF were monitored using float-driven well levels, with a precision of ±0.3 cm. Additional details on the data collection instrumentation and methods were summarized by Sebestyen et al.[4] Each watershed dataset contained one peatland type.

Long-term trends in water table elevations in individual peatlands were initially visualized in RStudio v. 1.1.463.[21] For each individual peatland, a time series plot of mWTE with regression line, autocorrelation function, decomposition function of the time series, and monthly box plot were created. Coefficients of variation were calculated for each peatland.

Precipitation (1961-2019) was measured in forest clearings at the S2 and S5 watersheds.[19, 20] Precipitation data at the MEF was measured to the closest 0.03 cm. To match the frequency of the water table data, monthly precipitation data was aggregated from daily precipitation values. Trends in monthly precipitation were tested using nonparametric regression with the Theil-Sen estimator in the "openair" package.[22, 23] Total, seasonal, and de-seasoned regressions were calculated for each precipitation record. Seasonal data was divided into spring (March, April, May), summer (June, July, August), autumn (September, October, November), and winter (December, January, February). A statistical test was considered significantly different when a p-value was less than 0.05.

The direction and significance of trends in water table elevation were also analyzed using the Theil-Sen estimator in the "openair" package.[22, 23] Total, seasonal, and de-seasoned regressions were tested for each peatland.[22, 23] Mean-centered water table elevation was used in the regression to standardize across absolute elevations. De-seasoned regressions were conducted as a part of the Theil-Sen function in the "openair" package in order to identify irregular patterns in mean-centered water table elevation. Trends in fens were non-monotonic and thus were excluded from the analysis. A time series plot was used to visualize trends in mWTE in the S3 fen and Bog Lake Peatland. Separate time series plots over the 1990 to 2019 period were used to compare the bogs to the two fens, as limited by the shorter record from the Bog Lake Peatland.

RESULTS

Trends in water table elevation for individual peatlands

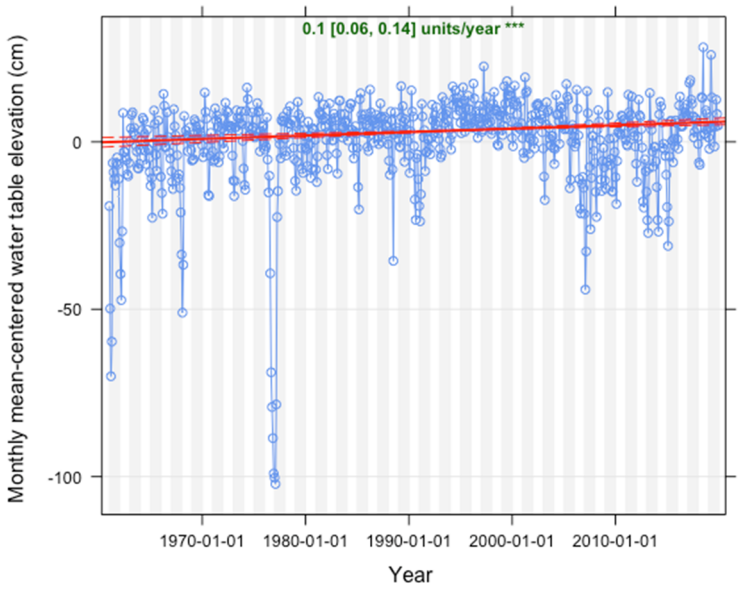

Figure 1a. Changes in monthly mean-centered water table elevation for the S1 bog. The linear trend was statistically significant ($p < 0.001$). The values at the top of the figure denote the slope of the line (cm/year) and the 95% confidence interval (cm).

Figure 1 shows the change in monthly mean-centered water table for each bog through the period of record. Slopes of trend lines (cm/year) and 95% confidence intervals (cm) are included for each bog. Trends in mean-centered WTE and mWTE varied across peatlands (**Figure 1, 2**). Peatlands that are in close spatial proximity on the landscape exhibited different trends in mWTE. Trends within peatland type (bog versus fen) were not consistent. There was a net decrease in mWTE in the Bog Lake Peatland, while the S3 fen had a net increase over the full period of record. It is important to note that the period of study began in 1990 for the Bog Lake Peatland, and in 1961 for the S3 fen (**Table 1**). The trend in the S3 fen, when reevaluated over

the same period from 1990 to 2019 was similar to the trend for Bog Lake Peatland. When viewed over the same time period (**Figure 3**), the bogs demonstrated trends which are visually different from the trends in the fens. For each peatland, the autocorrelation function, decomposition function, and monthly boxplots were used mainly as exploratory analyses of the data, and thus will not be discussed here.

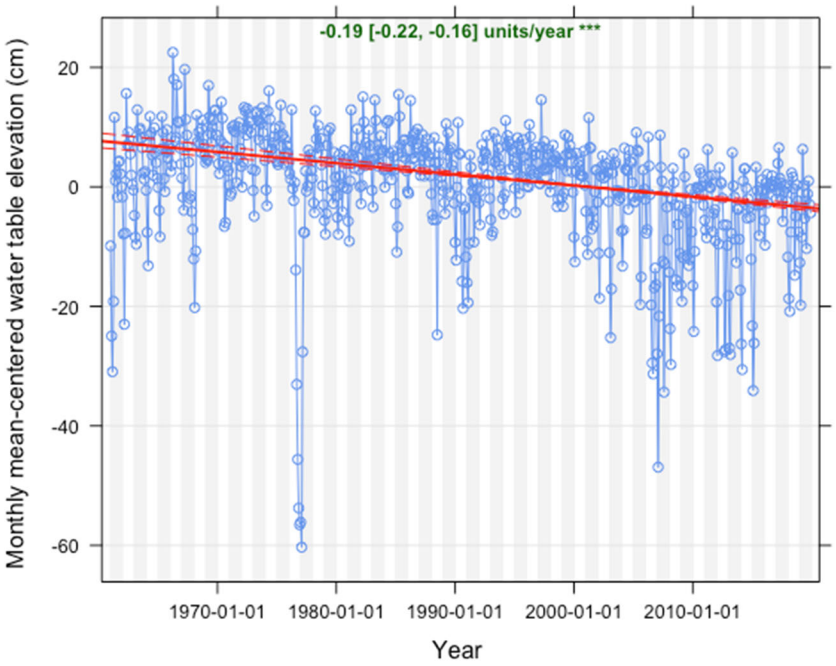

Figure 1b. Changes in monthly mean-centered water table elevation for the S2 bog. The linear trend was statistically significant ($p < 0.001$). The values at the top of the figure denote the slope of the line (cm/year) and the 95% confidence interval (cm).

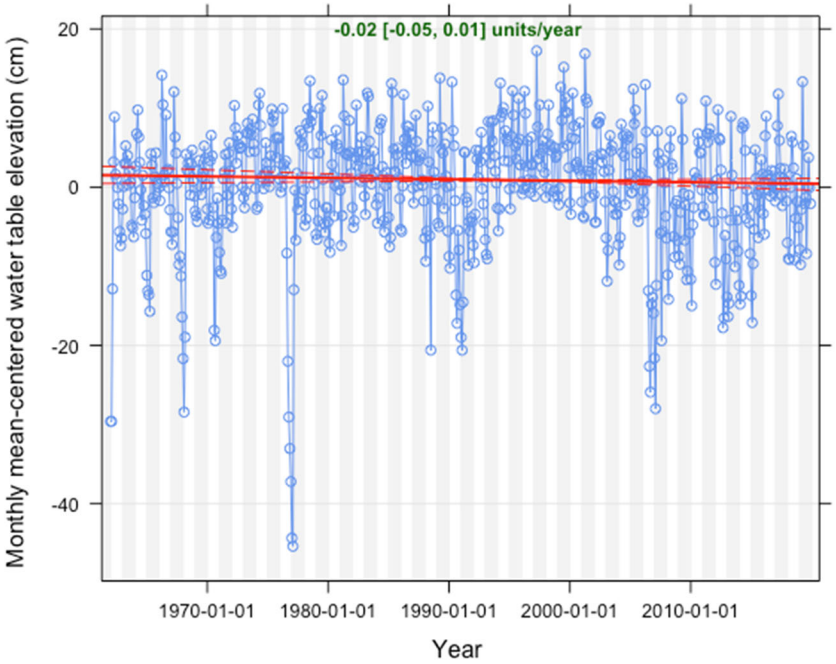

Figure 1c. Changes in monthly mean-centered water table elevation for the S4 bog. The linear trend was not statistically significant ($p > 0.05$). The values at the top of the figure denote the slope of the line (cm/year) and the 95% confidence interval (cm).

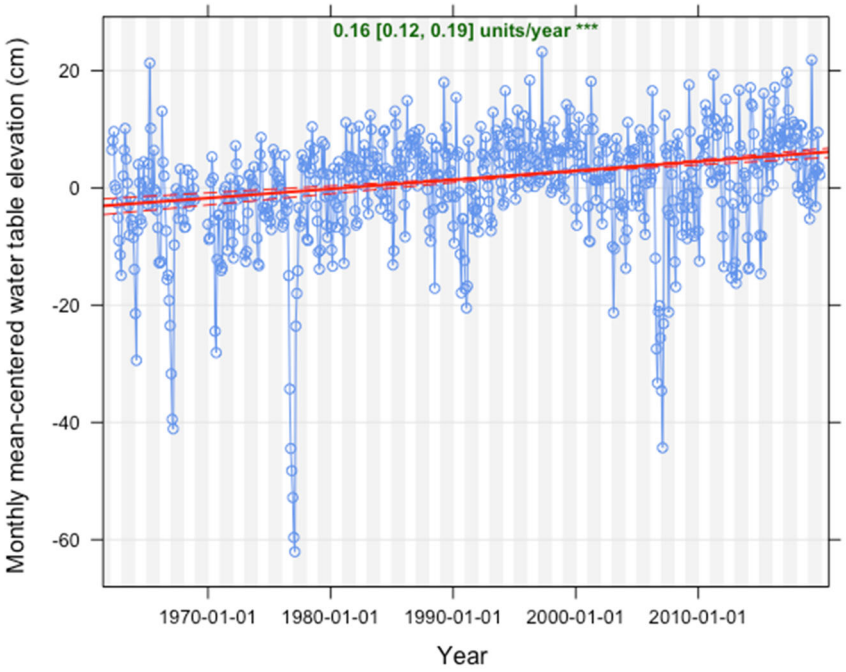

Figure 1d. Changes in monthly mean-centered water table elevation for the S5 bog. The linear trend was statistically significant ($p < 0.001$). The values at the top of the figure denote the slope of the line (cm/year) and the 95% confidence interval (cm).

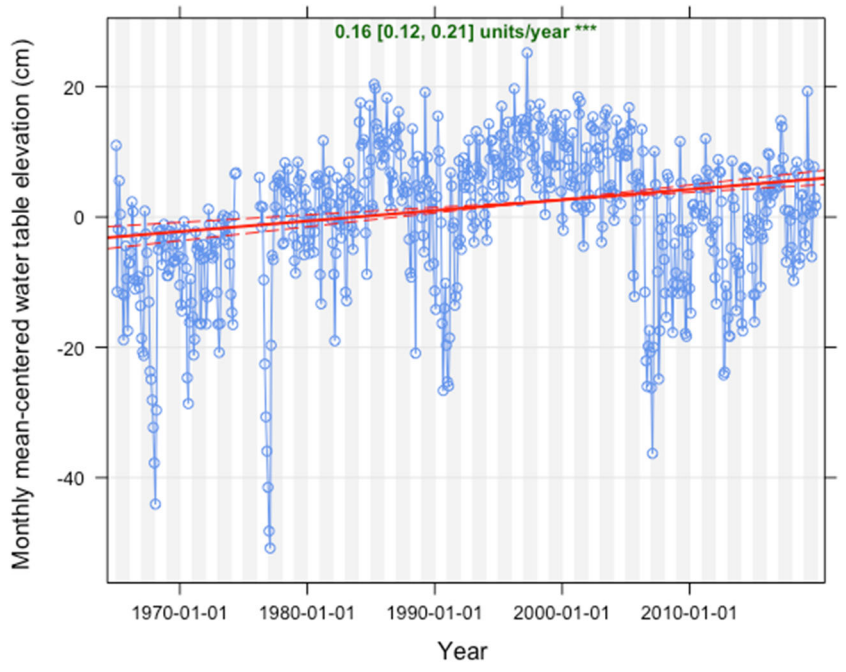

Figure 1e. Changes in monthly mean-centered water table elevation for the S6 bog. The linear trend was statistically significant ($p < 0.001$). The values at the top of the figure denote the slope of the line (cm/year) and the 95% confidence interval (cm).

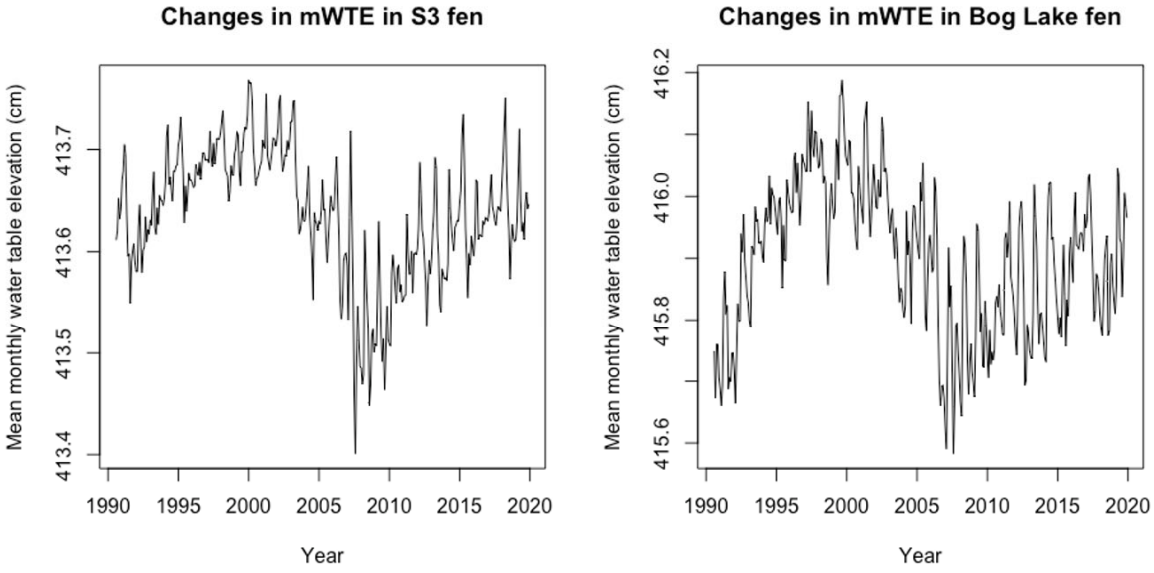

Figure 2. Trends in mean monthly water table elevation (mWTE) in the S3 fen and Bog Lake Peatland. Fens were excluded from nonparametric analyses due to data being non-monotonic.

Variability in monthly water table elevations

The Bog Lake Peatland had a higher coefficient of variation than all other peatlands except for the S1 bog (**Table 2**). The variability of the S3 fen was lower than the bogs.

1961-2019		1990-2019	
Peatland	**Coefficient of variation**	**Peatland**	**Coefficient of variation**
S1 bog	0.00034	S1 bog	0.00024
S2 bog	0.00024	S2 bog	0.00022
S3 fen	0.00016	S3 fen	0.00015
S4 bog	0.00018	S4 bog	0.00018
S5 bog	0.00024	S5 bog	0.00021
S6 bog	0.00026	S6 bog	0.00024
Bog Lake Peatland	0.00029	Bog Lake Peatland	0.00029

Table 2. Coefficients of variation (standard deviation divided by mean) for each peatland over the full period of record, as well as the 1990-2019 period. A higher coefficient of variation denotes higher variability.

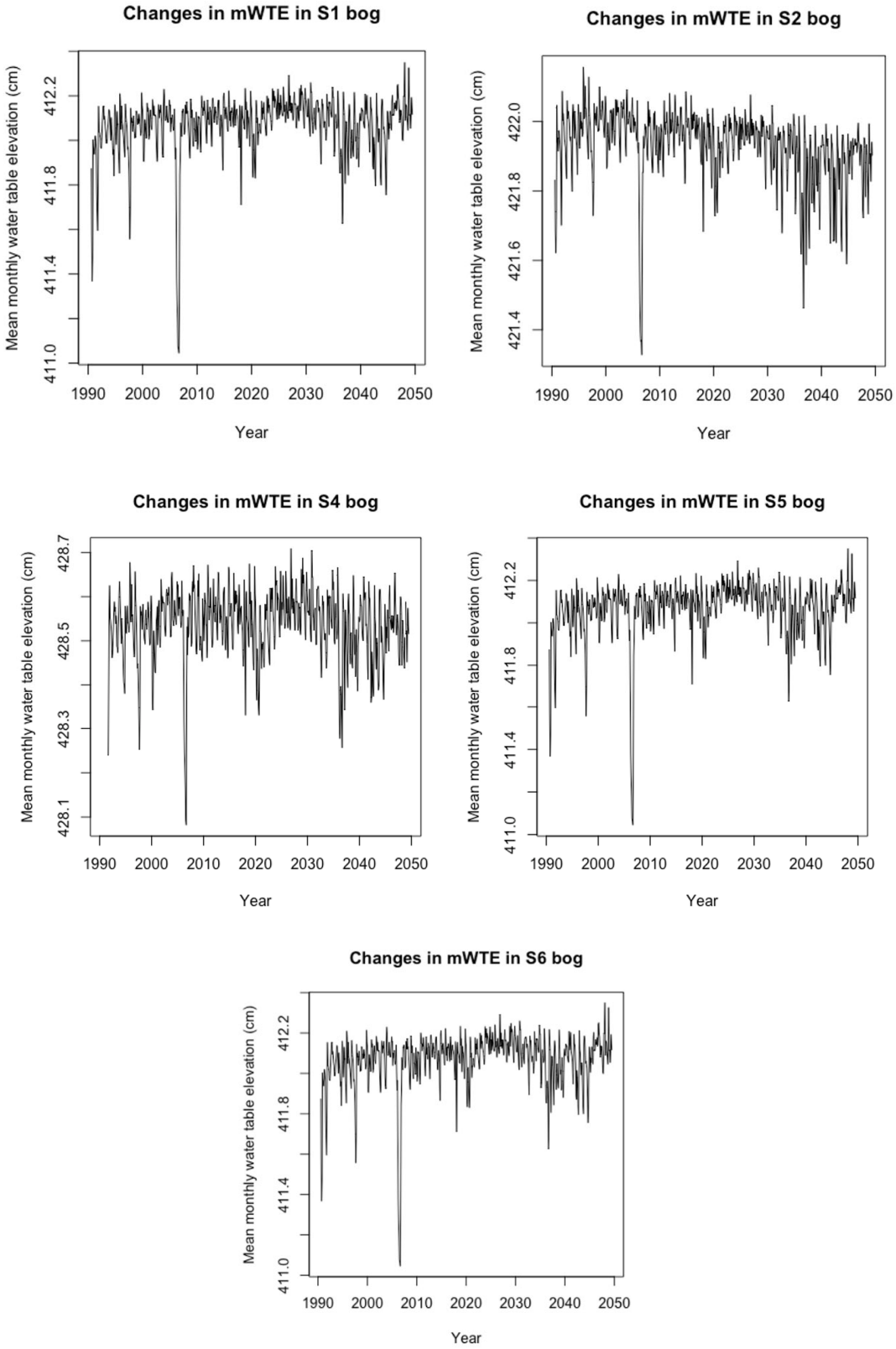

Figure 3. Trends in mean monthly water table elevation (mWTE) in the bogs over the same time period (1990-2019) as the fens.

Nonparametric regression with Theil-Sen estimator

Linear trends in monthly mean-centered WTE were significant for all except the S4 bog (**Figure 1; Table 3**). Fens were excluded from nonparametric analysis after initial exploratory analyses showed that trends were not monotonic, which violates a key assumption of the Theil-Sen estimator. The Theil-Sen estimator was applied to monthly mean-centered WTE to standardize across the landscape; thus, the Theil-Sen figures demonstrate deviations from the mean of all monthly water table observations during the period of record for each peatland. (**Figure 1**).

	Spring	Summer	Autumn	Winter	Deseasoned
S1 Bog					
Slope	0.13	0.10	0.10	0.10	0.10
Intercept	5.0	1.7	1.8	3.8	0.63
Significance	***	***	**	*	***
S2 Bog					
Slope	-0.17	-0.19	-0.20	-0.21	-0.20
Intercept	7.7	6.9	7.7	1.8	6.0
Significance	***	***	***	***	***
S4 Bog					
Slope	0.024	-0.015	-0.033	-0.047	-0.024
Intercept	4.4	2.6	2.2	-2.5	1.42
Significance	0.42	0.42	0.14	0.083	*
S5 Bog					
Slope	0.20	0.15	0.14	0.13	0.157
Intercept	1.8	-0.23	-0.82	-6.5	-2.3
Significance	***	***	***	***	***
S6 Bog					
Slope	0.20	0.17	0.12	0.16	0.16
Intercept	1.3	-1.6	-1.7	-7.3	-2.3
Significance	***	***	*	**	***

Table 3. Slopes, intercepts, and significance levels of Theil-Sen estimator for all bogs. Fens were notably non-monotonic and were not included in the Theil-Sen analysis. Slopes are in units of centimeters per year. Intercepts are in units of centimeters. Significance levels are denoted as $p < 0.001 = ***$, $p < 0.01 = **$, $p < 0.05 = *$.

Precipitation trends

We found no linear increases or decreases over time in monthly precipitation at the S5 or S2 stations between 1961 and 2019 (**Figure 4**).

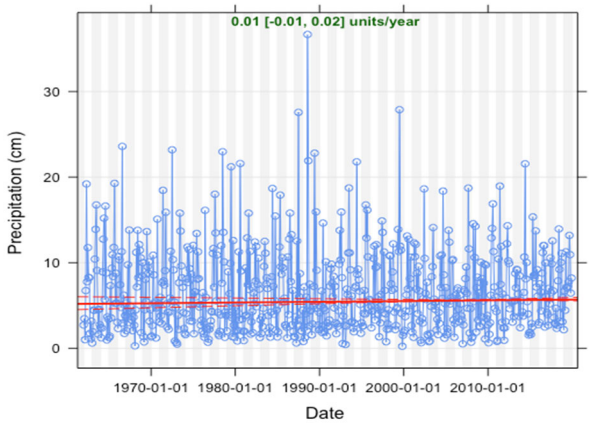

Figure 4a. Linear trends in monthly precipitation for the S5 meteorological station was not significant ($p > 0.05$). Values above each figure denote slope (cm) and 95% confidence intervals (cm).

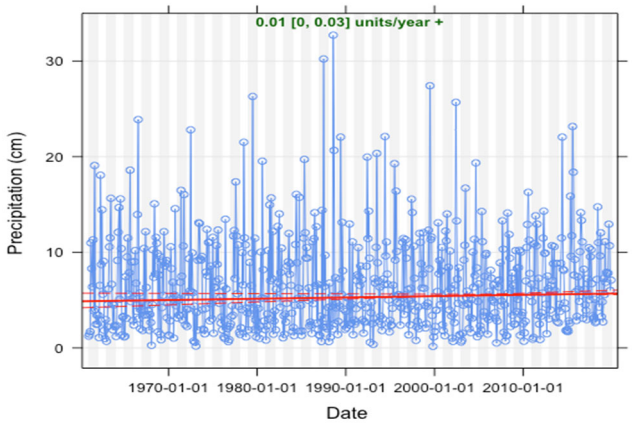

Figure 4b. Linear trends in monthly precipitation for the S2 meteorological station was not significant ($p > 0.05$). Values above each figure denote slope (cm) and 95% confidence intervals (cm).

DISCUSSION

Our results demonstrate the variability and diversity of water table elevation during similar climate conditions in peatlands, as well as the non-linearity of peatland responses to monthly precipitation in northern Minnesota peatlands. The magnitude of change in water table elevations differed among individual watersheds and were not consistent within peatland type. However, these trends were significantly different through time in general.

The responsiveness of water tables in bogs versus fens is an intrinsic hydrologic characteristic of these ecosystems. Fens are connected to local aquifers and groundwater inflow, while bogs are perched above aquifers and only receive precipitation inputs.[1, 2, 4, 9] However, the Bog Lake Fen had the highest coefficient of variation than all peatlands except for the S1 bog, which contradicts our initial hypothesis (**Figure 1, 2, 3; Table 2**). The lack of connection to local aquifers in bogs should increase the magnitude of water table responses to precipitation fluctuations, but this prediction is not clear from this analysis alone. The bogs contain more outliers than the fens, and trends in the fens appear to be more cyclical. The two peatland types are different, but the variability between bogs and fens did not support our initial hypothesis that bogs would be more variable than fens. The differences between the two fens, due to the harvesting of the S3 fen, may have resulted in the lack of clear differences in variability between the two peatland types. Ideally, both fens would receive the same experimental treatments to allow for the direct comparison to bogs; however, the difference between these two fens complicates the direct comparison to the bogs.

The analysis of individual peatlands revealed unique and inconsistent water table trends both within and between peatland types. For example, the mWTE did not significantly change in the S4 bog, in contrast to either a positive or negative trend in other watersheds (**Figure 1, 3**). When seasonality was removed, trends within all peatlands were significant except for the S4 bog, although the trends were not all the same direction (**Table 3**). The water table may be influenced by internal feedbacks, such as fluctuations in ET from vegetation.[24] External forcings, such as the harvesting activities performed in the S1 bog and S3 fen, also play a major role in the response of peatland water tables.[25] Therefore, the long-term trends of mWTE are site-specific and nonlinear.[24, 26]

Long-term water table dynamics were also not consistent within a peatland type, and bogs were more variable than the fens. When the two fens are viewed from 1990 on, the trend within the S3 fen mirrors that of the Bog Lake Peatland (**Figure 2**). The Bog Lake Peatland is mainly vegetated with *Sphagnum* moss and sedges, as well as some stunted tamarack. This peatland is a poor fen with a mean pH of 4.1 (1992-2019), and also lacks a surface water outlet (**Table 1**). On the other hand, the S3 rich fen is vegetated with willow, speckled alder, black spruce, tamarack, and paper birch. The entire fen was clearcut and the harvesting slash burned in the winter of 1972 to 1973.[4] No water table response to the harvesting was observed.[25] The S3 fen, with a pH of 6.9 ± 0.1, is also less acidic than the Bog Lake Peatland and also has a surface water outlet (**Table 1**).[4] Even with differences in vegetation, chemistry, and land management practices over the 1961 to 2019 period, water table responses were similar in both fens from 1990 to 2019. The connection of fens to surrounding aquifers acts as a stabilizing factor in long-term water table elevations.[4] Large-scale commercial harvesting, even when conducted in the winter, has the potential to change the bulk density and hydraulic conductivity of the underlying peat through compression of the organic soil and removal of tree roots, which subsequently affects soil structure.[9] However, these results show that water tables in both fens did not demonstrate a significant response to harvesting activities. The hydrological properties (*i.e.* connection to aquifer) of fens may allow for some magnitude of

resilience to change following large-scale harvesting operations. Semi-cyclical mWTE fluctuations occurred in both fens. These trends may represent the stabilization of water tables via connection to local aquifers, which provide a consistent input of water.[27]

Water table elevations were inconsistent within the two peatland types and our analyses demonstrated no clear similarities to precipitation trends (**Table 2**). The S1, S5, and S6 bogs experienced net increases in mWTE, and S2 and S4 experienced net decreases in mWTE (**Figure 2**). The trend in S4 mean-centered WTE, however, was only significant when the seasonal component was removed, and the slope coefficient was an order of magnitude smaller than the other peatlands (**Table 3**). Each bog had unique water table fluctuations through time, even though there was no significant linear trend in precipitation (**Figure 1, 4**). For example, the S2 bog had a significant negative slope in mWTE when seasonality was considered, showing that the water table has significantly fallen since 1961 (**Table 2**). The five bogs are similar in composition; the canopies consist mainly of black spruce and tamarack, and the understories are dominated by Ericaceous plants and *Sphagnum* moss. The net decrease in mWTE in the S2 bog may suggest that ET has potentially increased since 1961 since vegetation is similar across the bogs, but previous studies have found that variations in peatland water tables may not control ET. [28] It is critical to note that this analysis of precipitation only examined linear trends and did not consider factors such as snowmelt and inter-annual variability. Further detailed analysis of changes in the form of precipitation, inter- and intra-annual variability, and timing of precipitation is required to make further conclusions about the relationship between water tables and precipitation.

Regardless, the long-term relationship between mWTE and precipitation in the bogs is inconsistent among the sites. The variability of water table elevations in bogs poses potential difficulties in modeling these ecosystems or creating adaptive management plans. The bogs analyzed in this study were similar in composition, history, and location but each had unique a response despite the fact that all peatlands experienced the same amount of precipitation. This suggests that the responses of bogs to precipitation over long time-scales are extremely site-specific and difficult to predict.[2, 3, 6, 12] Understanding the diversity of peatland water table responses to warming air temperature and increasing ET through analysis of historical datasets is essential to representing peatlands in Earth Systems Models, which in turn, provide projections of future conditions. Regardless, in the context of management, this complexity of peatlands water table responses, especially differences between bogs and fens, suggests the need for site-specific knowledge, instead of generalized regional models.

Water table dynamics in peatlands are also complicated by microtopography, which is characterized by hummocks and hollows. These fine-scale variations lead to spatially complex water table dynamics that can be difficult to parameterize.[29-31] Changes in water table levels may lead to altered fine-root growth, which is strongly influenced by decreased water table elevations.[32] Black spruce and tamarack are both shallow-rooted species. Accordingly, longer durations of lowered water tables may increase drought stress of the overstory trees. These feedbacks would subsequently change rates of ET. Understanding these dynamics is especially crucial in the context of peatland carbon dynamics, since water tables and carbon cycling are closely coupled. Not only do fens and bogs possibly respond differently to precipitation and disturbances (*e.g.* harvesting activities), but individual bogs demonstrated different trends in mWTE between 1961 and 2019. It is important to note, however, that differences in drainage area, trees (size, age, and basal area), and elevation above surrounding aquifers may have caused these differences.

Changes in water table elevation may also alter potential greenhouse gas (GHG) emissions from peatlands.[10, 27, 33] For example, water table drawdowns can lead to increased tree growth and carbon dioxide emissions due to enhanced decomposition. On the other hand, high water tables promote methanogenesis and methane emissions from peatland soils.[10, 29] While carbon cycle responses at the Marcell Experimental Forest are beyond the scope of this study, this study identifies uncertainties related to potential ecosystem-level responses in peatlands to changes in water table elevation.

The nearly sixty-year temporal span of these data provides preliminary insights on the long-term precipitation patterns in northern Minnesota. The IPCC Fifth Assessment Report predicts that precipitation will increase in the long term in northern latitudes.[34] In addition, peatlands are expected to be extremely responsive to an increasing global temperature, which may lead to increased ET and decreased mWTE.[29, 33, 34] The unique responses among fens and bogs in northern Minnesota represent the need for additional research and monitoring in these systems. The highly localized responses among fens and bogs have implications for carbon cycle models, which may be over or underestimating outputs depending on ecosystem representation (or lack thereof) and model parameters.[35, 36] Additionally, these highly localized responses have implications for modeling or predicting future forest composition and structure. The development of regional or state-wide forest management plans may be unable to fully account for the many possible peatland water table responses under a changing climate and continue to highlight the importance of evaluating individual sites and stands when considering forest management activities in peatland forest ecosystems.

While the simple linear modeling presented in this research serves as a foundational first step in this study, further consideration of these data could include: 1) making direct comparisons between monthly precipitation and water table data; 2) using the precipitation data to parse periods of time so that the authors can determine whether sites are behaving similarly to one another

during different climatic conditions. Across all of these approaches, the authors should attempt to analyze for significant differences between bogs and fens as well as disturbed and undisturbed sites.

CONCLUSIONS

This study demonstrated the complexity of peatland hydrological dynamics and the uncertainties of the long-term relationship between mWTE and precipitation.[37] Water table elevations differed between seasons both within and between peatlands, and bogs were more variable than fens (**Table 3**). In addition, bogs and fens had significantly different trends in mWTE (**Figure 1, 2, 3**). The non-linearity of water table responses to rainfall variability is likely due to complex physical and biophysical flowpaths and feedbacks. Precipitation serves as only one control on mWTE, in addition to temperature fluctuations, ET, and other processes. Therefore, these results represent a small portion of the complex responses of peatlands over time. However, the results of this study revealed site-specific responses of each peatland to changes in moisture and the inconsistency of trends within the same peatland type. This site specificity has implications for the representation of peatlands in models. The management history, geomorphic setting, subsurface heterogeneity, connectivity to surrounding uplands, and composition of each peatland likely all influence the response of a site to changes in precipitation, which can result in uncertainty of how water tables will respond with air warming, increasing ET, and other manifestations of climate change.[37, 38, 39]

Given our current limited understanding of forest ecosystem successional development pathways of peatland forests in Minnesota, there is still much to learn. This learning process becomes more complicated as climate change continues to influence ecosystem processes in peatlands. This complexity is demonstrated by our results which show inconsistent results between fens and bogs and also the variable response among the different bogs. This research highlights the need for natural resource managers to utilize an adaptive management framework, which relies on continual assessment and monitoring. Data from management at the southern edge of the boreal forest will provide critical information as these changes move further north. Adaptive forest management would allow for flexible decision-making that accounts for the site-specific behavior of peatland ecosystems. The complexity of peatland responses to climate requires the need for ecologically-sound management decisions in these systems, as well as a detailed understanding of local hydrodynamics and the sensitivity of the landscape to change.

ACKNOWLEDGEMENTS

The authors thank the staff at the Marcell Experimental Forest for the collection and compilation of the precipitation and water table data.

REFERENCES

1. Macrae, M. L., Devito, K. J., Strack, M., & Waddington, J. M. (2013) Effect of water table drawdown on peatland nutrient dynamics: Implications for climate change. *Biogeochemistry*, *112*(1), 661–676. *https://doi.org/10.1007/s10533-012-9730-3*
2. Ise, T., Dunn, A., Wofsy, S., Moorcraft, P. (2008) High sensitivity of peat decomposition to climate change through water-table feedback. *Nature Geosci* 1, 763–766. *https://doi.org/10.1038/ngeo331*
3. Strack, M., Waddington, J. M., & Tuittila, E.-S. (2004) Effect of water table drawdown on northern peatland methane dynamics: Implications for climate change. *Global Biogeochemical Cycles*, *18*(4). *https://doi.org/10.1029/2003GB002209*
4. Sebestyen, S. D., Dorrance, C., Olson, D. M., Verry, E. S., Kolka, R. K., Elling, A. E., & Kyllander, R. (2011) Long-term monitoring sites and trends at the Marcell Experimental Forest. In Kolka, R. K., Sebestyen, S. D., Verry, E. S., & Brooks, K. N. (Eds.), *Peatland biogeochemistry and watershed hydrology at the Marcell Experimental Forest* (pp. 15-71). Boca Raton, FL: CRC Press.
5. Babst, F., Bouriaud, O., Papale, D., Gielen, B., Janssens, I. A., Nikinmaa, E., Ibrom, A., Wu, J., Bernhofer, C., Köstner, B., Grünwald, T., Seufert, G., Ciais, P., & Frank, D. (2014) Above-ground woody carbon sequestration measured from tree rings is coherent with net ecosystem productivity at five eddy-covariance sites. *New Phytologist*, 201(4), 1289–1303. *https://doi.org/10.1111/nph.12589*
6. Grant, R. F. (2004) Modeling topographic effects on net ecosystem productivity of boreal black spruce forests. *Tree Physiology,* 24(1), 1–18. https://doi.org/10.1093/treephys/24.1.1
7. Laiho, R., & Prescott, C. E. (1999) The contribution of coarse woody debris to carbon, nitrogen, and phosphorus cycles in three Rocky Mountain coniferous forests. *Canadian Journal of Forest Research*, 29(10), 1592–1603. *https://doi.org/10.1139/x99-132*
8. Strack, M., Waddington, J. M., Bourbonniere, R. A., Buckton, E. L., Shaw, K., Whittington, P., & Price, J. S. (2008) Effect of water table drawdown on peatland dissolved organic carbon export and dynamics. *Hydrological Processes*, *22*(17), 3373–3385. *https://doi.org/10.1002/hyp.6931*
9. Whittington, P. N., & Price, J. S. (2006) The effects of water table draw-down (as a surrogate for climate change) on the hydrology of a fen peatland, Canada. *Hydrological Processes*, *20*(17), 3589–3600. *https://doi.org/10.1002/hyp.6376*
10. Koven, C. D., Ringeval, B., Friedlingstein, P., Ciais, P., Cadule, P., Khvorostyanov, D., Krinner, G., & Tarnocai, C. (2011) Permafrost carbon-climate feedbacks accelerate global warming. *Proceedings of the National Academy of Sciences*, *108*(36), 14769–14774. *https://doi.org/10.1073/pnas.1103910108*

11. Cleland, D.T., Avers, P.E., McNab, W.H., Jensen, M.E., Bailey, R.G., King, T., Russell, W.E. (1997) National Hierarchical Framework of Ecological Units. Published in, Boyce, M. S.; Haney, A., ed. 1997. *Ecosystem Management Applications for Sustainable Forest and Wildlife Resources*. Yale University Press, New Haven, CT. pp. 181-200.

12. Dymond, S. F., D'Amato, A. W., Kolka, R. K., Bolstad, P. V., Sebestyen, S. D., Gill, K., & Curzon, M. T. (2019) Climatic controls on peatland black spruce growth in relation to water table variation and precipitation. *Ecohydrology*, 12(7), e2137. *https://doi.org/10.1002/eco.2137*

13. Bisbee, K. E., Gower, S. T., Norman, J. M., & Nordheim, E. V. (2001) Environmental controls on ground cover species composition and productivity in a boreal black spruce forest. *Oecologia*, 129(2), 261–270. *https://doi.org/10.1007/s004420100719*

14. McPartland, M. Y., Kane, E. S., Falkowski, M. J., Kolka, R., Turetsky, M. R., Palik, B., & Montgomery, R. A. (2019) The response of boreal peatland community composition and NDVI to hydrologic change, warming and elevated carbon dioxide. *Global Change Biology. https://doi.org/10.1111/gcb.14465*

15. Iversen, C. M., Childs, J., Norby, R. J., Ontl, T. A., Kolka, R. K., Brice, D. J., McFarlane, K. J., & Hanson, P. J. (2017) Fine-root growth in a forested bog is seasonally dynamic, but shallowly distributed in nutrient-poor peat, *Plant and Soil*, 1-21. *https://doi.org/10.1007/s11104-017-3231-z*

16. Aaseng, N., Almendinger, J., Rusterholz, K., Wovcha, D., Klein, T.R., (2003) Field guide to the native plant communities of Minnesota: the Laurentian Mixed Forest Province. Minnesota Department of Natural Resources, Saint Paul, Minnesota.

17. Johnston, W.F., (1977) Manager's handbook for black spruce in the north-central states. *Gen. Tech. Rep.* NC-34 18.

18. Hillard, S., Bergstrand, K. Deckard, D. Minnesota's Forest resources (2017) Department of Natural resources; Division of Forestry, 92pp.

19. Sebestyen, S.D., E.S. Verry, A.E. Elling, R.L. Kyllander, D.T. Roman, J.M. Burdick, N.K. Lany, and R.K. Kolka. (2020) Marcell Experimental Forest daily precipitation, 1961 - ongoing ver 1. *Environmental Data Initiative*. http*s://doi.org/10.6073/pasta/75646a3bd41ba3219d0e578e8374eef7*

20. Sebestyen, S.D., E.S. Verry, A.E. Elling, R.L. Kyllander, D.T. Roman, J.M. Burdick, N.K. Lany, and R.K. Kolka. (2020) Marcell Experimental Forest daily peatland water table elevation, 1961 - ongoing ver 1. *Environmental Data Initiative. https://doi.org/10.6073/pasta/6e9348a1c691c10271c9373bd31da67f*

21. RStudio Team (2020) RStudio: Integrated Development for R. RStudio, PBC, Boston, MA URL http://www.rstudio.com/.

22. Carslaw, D.C. and K. Ropkins, (2012) openair — an R package for air quality data analysis. *Environmental Modelling & Software.* Volume 27-28, pp. 52–61.

23. Carslaw, D.C. (2015) The openair manual — open-source tools for analysing air pollution data. Manual for version 1.1-4, King's College London.

24. Waddington, J. M., Morris, P. J., Kettridge, N., Granath, G., Thompson, D. K. and Moore, P. A. (2015) Hydrological feedbacks in northern peatlands, *Ecohydrology.*, 8, pages 113– 127, *doi: 10.1002/eco.1493*

25. Sebestyen, S. D., Verry, E. S., & Brooks, K. N. (2011) Hydrological responses to forest cover changes on uplands and peatlands. In Kolka, R. K., Sebestyen, S. D., Verry, E. S., & Brooks, K. N. (Eds.), *Peatland biogeochemistry and watershed hydrology at the Marcell Experimental Forest* (pp. 433-458). Boca Raton, FL: CRC Press.

26. Sivakumar, B. (2000) Chaos theory in hydrology: Important issues and interpretations. Journal of Hydrology, 227(1), 1–20. *https://doi.org/10.1016/S0022-1694(99)00186-9*

27. Bridgham, S. D., Pastor, J., Dewey, B., Weltzin, J. F., & Updegraff, K. (2008) Rapid Carbon Response of Peatlands to Climate Change. *Ecology*, 89(11), 3041–3048. *https://doi.org/10.1890/08-0279.1*

28. Moore, P. A., Pypker, T. G., & Waddington, J. M. (2013). Effect of long-term water table manipulation on peatland evapotranspiration. *Agricultural and Forest Meteorology*, *178–179*, 106–119.

29. Shi, X., Thornton, P. E., Ricciuto, D. M., Hanson, P. J., Mao, J., Sebestyen, S. D., Griffiths, N. A., & Bisht, G. (2015) Representing northern peatland microtopography and hydrology within the Community Land Model. *Biogeosciences*, *12*(21), 6463–6477. *https://doi.org/10.5194/bg-12-6463-2015*

30. Graham, J. D., Glenn, N. F., Spaete, L. P., & Hanson, P. J. (2020) Characterizing peatland microtopography using gradient and microform-based approaches, *Ecosystems. https://doi.org/10.1007/s10021-020-00481-z*

31. Verry, E. S. (1984) Microtopography and water table fluctuation in a Sphagnum mire, *Proceedings of the 7th International Peat Congress*, Dublin, Ireland, edited, pp. 11-31, The Irish National Peat Committee / The International Peat Society.

32. Malhotra, A., Brice, D. J., Childs, J., Graham, J. D., Hobbie, E. A., Stel, H. V., Feron, S. C., Hanson, P. J., & Iversen, C. M. (2020) Peatland warming strongly increases fine-root growth. *Proceedings of the National Academy of Sciences. https://doi.org/10.1073/pnas.2003361117*

33. Jiang, J., Huang, Y., Ma, S., Stacy, M., Zheng, S., Ricciuto, D., Hanson, P., & Luo, Y. (2018) Forecasting responses of a northern peatland carbon cycle to elevated CO2 and a gradient of experimental warming. *Journal of Geophysical Research: Biogeosciences*, 123(3), 1057–1071. *https://doi.org/10.1002/2017JG004040*

34. Collins, M., Knutti, R., Arblaster, J., Dufresne, J-L., Fichefet, T., Friedlingstein, P., Gao, X., Gutowski, W.J., Johns, T., Krinner, G., Shongwe, M., Tebaldi, C., Weaver, A.J., Wehner, M. (2013) Long-term Climate Change: Projections, Commitments and Irreversibility. In: Climate Change 2013: The Physical Science Basis. Contribution of Working Group I to

the Fifth Assessment Report of the Intergovernmental Panel on Climate Change [Stocker, T.F., D. Qin, G.-K. Plattner, M. Tignor, S.K. Allen, J. Boschung, A. Nauels, Y. Xia, V. Bex and P.M. Midgley (eds.)]. Cambridge University Press, Cambridge, United Kingdom and New York, NY, USA.

35. Ricciuto, D. M., Xu, X., Shi, X., Wang, Y., Song, X., Schadt, C. W., Hanson, P. J. (in press). An integrative model for soil biogeochemistry and methane processes: I. Model structure and sensitivity analysis. *Journal of Geophysical Research, G, Biogeosciences*.

36. Feng, X., Deventer, M. J., Lonchar, R., Ng, G. H. C., Sebestyen, S. D., Roman, D. T., Kolka, R. K. (2020) Climate sensitivity of peatland methane emissions mediated by seasonal hydrologic dynamics. *Geophysical Research Letters, 47*(17), e2020GL088875. https://doi.org/10.1029/2020gl088875

37. Parsekian, A. D., Slater, L., Ntarlagiannis, D., Nolan, J., Sebestyen, S. D., Kolka, R. K., & Hanson, P. J. (2012) Uncertainty in peat volume and soil carbon estimated using ground-penetrating radar and probing, *Soil Sci. Soc. Am. J*., 76(5), 1911-1918. *https://doi.org/10.2136/sssaj2012.0040*

38. Hill, B. H., Jicha, T. M., Lehto, L. L. P., Elonen, C. M., Sebestyen, S. D., & Kolka, R. K. (2016) Comparisons of soil nitrogen mass balances for an ombrotrophic bog and a minerotrophic fen in northern Minnesota, *Sc. Total Environ.*, 550, 880-892. *https://doi.org/10.1016/j.scitotenv.2016.01.178*

39. Verry, E. S., & Janssens, J. (2011) Geology, vegetation, and hydrology of the S2 bog at the MEF: 12,000 years in northern Minnesota, in Peatland biogeochemistry and watershed hydrology at the Marcell Experimental Forest, edited by Kolka, R. K., et al., pp. 93-134, CRC Press, Boca Raton, FL.

ABOUT STUDENT AUTHOR

Anna Stockstad graduated from the University of Minnesota in May 2020 with a Bachelor of Science in Forest and Natural Resource Management and minors in environmental science and wildlife biology. She is currently a Master of Science student in the Natural Resource Science and Management program at the University of Minnesota and researching forest soil operability and biogeochemistry.

PRESS SUMMARY

Changes in water tables in northern peatlands strongly influence the health and productivity of these ecosystems. Peatlands (bogs and fens) cover ten percent of the surface area in Minnesota, USA, and thus are a critical part of the landscape. Long-term data (1961 to 2019) from the Marcell Experimental Forest were used to analyze the trends in water tables in northern peatlands. Responses were not consistent across peatland type, and water table trends were different between bogs and fens as a whole. Even though precipitation has not significantly changed since 1961, water tables in peatlands at the Marcell Experimental Forest have varied through time. These results show that water table trends within peatlands, which provide crucial ecosystem services, are likely site-specific and variable. These findings highlight a need for site-specific management plans and long-term hydrological modelling.

Treatment Outcomes in a Partial Hospital Program for Patients with Social Anxiety Disorder: The Effects of Comorbid Major Depression

Allison Graham[a,b], Douglas R. Terrill[a], Simone I. Boyd[a], Isabel Benjamin[a], Madeline Ward[a], & Mark Zimmerman[a,c]*

[a]*Rhode Island Hospital Department of Psychiatry, Providence, RI*
[b]*Department of Cognitive, Linguistic, and Psychological Sciences, Brown University, Providence, RI*
[c]*Department of Psychiatry and Human Behavior, Brown Alpert Medical School, Providence, RI*

https://doi.org/10.33697/ajur.2020.033

*Student: allison_graham@alumni.brown.edu**
Mentor: mzimmerman@lifespan.org

ABSTRACT
Although previous studies have examined the impact of comorbid major depressive disorder (MDD) on social anxiety disorder (SAD), the results have been somewhat mixed. Furthermore, most studies have been conducted in inpatient or outpatient settings. Given the large body of literature that suggests that this particular comorbidity can have negative effects on treatment efficacy and outcomes, it is important to continue to explore its impact. The present study aims to clarify contradictions in the literature and expands on previous studies by examining patients in a partial hospitalization setting. Patients at Rhode Island Hospital with a diagnosis of SAD were compared to those with comorbid SAD and MDD on pre-treatment and post-treatment measures of anxiety and depression. The results indicated that while the comorbid group showed significantly less improvement post-treatment on anxiety symptoms and constructs related to remission from depression, they did not show significantly less improvement on depression symptoms. The implications of these results for clinical practice are discussed.

KEYWORDS
Social Anxiety Disorder; Major Depressive Disorder; Comorbid Anxiety Disorders; Comorbid Mood Disorders; Treatment Outcomes; Partial Hospitalization Program

INTRODUCTION

Social anxiety disorder (SAD) is one of the most common mental disorders in the U.S., with a prevalence (12.1%) behind only major depressive disorder (MDD; 16.6%), alcohol use disorder (13.2%), and specific phobias (12.5%).[1] According to the 2001-2003 National Comorbidity Survey, nearly one in 10 individuals in the U.S. suffer from SAD during their lifetime.[2] Not only is SAD common, the disorder can have debilitating effects. Roughly one-third of people diagnosed with SAD in the U.S. report severe interpersonal, occupational, or psychosocial impairment.[2] Over 90% of those diagnosed with SAD report some level of impairment in one or more of these domains.[3] The pervasive, chronic, and disruptive nature of the disorder highlights a need for effective treatments.

A high rate of psychiatric comorbidity among those with SAD further increases the complexity and resulting impairment of this disorder. Prevalence estimates of comorbid disorders with SAD are as high as 90%, with major depressive disorder (MDD) being the most common comorbid diagnosis, estimated in 30-75% of individuals with SAD.[4] A diagnosis of SAD has even been demonstrated to predict subsequent MDD,[5] further highlighting the relationship between these disorders. This comorbidity results in much greater impairment across various domains than either disorder alone. Patients with comorbid SAD and MDD often experience more severe social anxiety symptoms,[4] greater psychosocial impairment, longer depressive episodes, increased suicidal ideation, more time out of work, and greater likelihood of substance abuse.[6] Greater impairment associated with this comorbidity may significantly affect the clinical course, underscoring a need for more research on treatment outcomes among this population.

Several treatments have been found to be efficacious in treating SAD or MDD. Cognitive Behavioral Therapy (CBT) is the most widely studied psychosocial approach to treating these disorders and produces consistently positive results in both group and individual settings.[7–10] For patients with SAD, CBT shows nearly twice the response rate of placebo groups (50-56% vs. 32%) and remission rates between 8% and 36%, indicating moderate short-term and long-term efficacy.[10] Other psychosocial treatments that have demonstrated similar efficacy in treating these disorders include interpersonal therapy, psychodynamic therapy, and mindfulness-based treatments.[10] Patients with either diagnosis have been shown to improve as a result of mindfulness-based stress

reduction programs (MBSR),[11–13] mindfulness-based cognitive therapy (MBCT),[14–16] and Acceptance and Commitment Therapy (ACT).[17–20] These results illustrate that a number of different therapies can successfully treat individuals with SAD or MDD.

While certain treatments are effective in treating SAD and MDD individually, there are mixed results on treatment outcomes among individuals with comorbid SAD and MDD. Some research has shown that the presence of this comorbidity does not produce different treatment outcomes than the presence of SAD or MDD alone.[21] For instance, one study found that comorbid SAD did not interfere with CBT outcomes in depressed patients.[22] Another preliminary study found that 16 sessions of ACT improved both symptoms and functioning in adults with SAD and MDD in an outpatient psychiatric setting.[23] However, it is unclear whether these gains would be comparable to those obtained by patients with a single SAD diagnosis undergoing the same therapy. Conversely, some research has found poorer treatment outcomes for those with comorbid SAD and MDD. One study demonstrated that SAD patients with severe depressive symptoms, while not meeting clinical criteria for MDD, exhibited diminished response to treatment and increased treatment drop-out rates when compared to SAD patients with less severe depressive symptoms.[24] Social anxiety symptoms in depressed patients treated with CBT and cognitive-behavioral group therapy (CBGT) have also been shown to increase during one-year follow-up periods.[25] Other research on the efficacy of CBT has found smaller magnitudes of improvement in those with comorbid SAD and MDD than those with SAD alone.[21] Given this conflicting evidence, further research into treatment outcomes for comorbid SAD and MDD is needed to clarify the response of these individuals to psychological treatment.

The majority of research evaluating treatment outcomes for patients with SAD or comorbid SAD and MDD has been conducted within inpatient and outpatient treatment settings.[26–27] Partial hospitalization programs fall between the differing intensities of these settings. While some research has shown CBT to be effective for either SAD or MDD in a partial hospital setting, there has been limited research conducted in this setting overall.[28-29] The authors are not aware of any research evaluating differences in treatment outcomes in a partial hospital setting for individuals with SAD alone and individuals with comorbid SAD and MDD. The current study from the Rhode Island Hospital Methods to Improve Diagnostic and Assessment Services (MIDAS) Project aims to compare treatment outcomes between patients with a diagnosis of SAD in the absence of MDD and patients with comorbid SAD and MDD. While research on this topic is mixed, it was hypothesized that treatment outcomes would be poorer across a number of domains for those with comorbid SAD and MDD than those with SAD in the absence of MDD. Specifically, due to literature that has linked this comorbidity with poor treatment outcomes,[21, 24, 25] it was expected that individuals with comorbid SAD and MDD would demonstrate less improvement during treatment, and upon discharge would exhibit more impairment in everyday life and greater severity of anxiety and depression when compared to individuals with SAD in the absence of MDD.

METHODS AND PROCEDURES

The Rhode Island Hospital institutional review committee approved the following research protocol, and all patients provided informed, written consent.

Site

Data was collected from individuals referred to the Rhode Island Hospital partial hospitalization program for first time treatment. The program treats patients five days per week, and patients attend four group therapies throughout the day, as well as daily individual meetings with a therapist and psychiatrist. Patients return home after each day in the program. Both group and individual therapies are largely based in Acceptance and Commitment Therapy. Patients undergo mindfulness training during treatment, and the program also offers a volunteer, therapist-led meditation group. Duration of treatment is most often based on treatment responses, thus, patients who improve more quickly discharge from the program after fewer days of treatment than those who do not. The average duration of treatment is just over eight days.

Participants

Between April 2014 and January 2020, 4,634 individuals presented for treatment to the Rhode Island Hospital Department of Psychiatry Partial Hospital Program. For patients who were treated in the program more than once, we included data only from their first admission. Patients were excluded if they had missing data on measures of depression or anxiety at baseline or discharge (n = 2,547). Patients were also excluded if they did not have a current diagnosis of social anxiety disorder (n = 1,617), leaving a sample of 470 patients. Diagnoses were made on patients' first day of attendance in the program, either by a trained clinical interviewer who administered the Structured Clinical Interview for DSM-IV[30] (n = 292), or by a board-certified psychiatrist (n = 178).

As the focus of this investigation concerned the impact of MDD on treatment outcomes in patients with a diagnosis of SAD, an MDD only comparison group was not included. Furthermore, our choice of a SAD comparison group was based on previous findings that a diagnosis of SAD precedes a diagnosis of MDD in 69% of comorbid cases, even predicting later development of

MDD.[5] Because patients with a SAD/MDD comorbidity are more likely to have been diagnosed with SAD first, comparing comorbid patients to those with SAD alone was most intuitive.

Measures

Clinically Useful Anxiety Outcome Scale: The Clinically Useful Anxiety Outcome Scale (CUXOS)[31] is a 25-item self-report measure of anxiety symptom severity. Patients are asked to rate the frequency of anxiety symptoms on an ordinal scale with the prompt "in the past week, including today…" (for the intake scale) and "during the past day…" (for the daily scale). Possible responses include (0) not at all, (1) a little bit, (2) a moderate amount, (3) quite a bit, and (4) almost always. The daily version of the CUXOS has demonstrated good internal consistency (Cronbach's alpha at intake = 0.93; Cronbach's alpha at follow-up = 0.95), test-retest reliability (r = 0.95 and 0.96, at intake and follow-up respectively), and was more correlated with measures of anxiety than with scales measuring other symptoms such as depression.[32] First and last day scores were used from the CUXOS to represent pre- and post-treatment anxiety symptom severity.

Clinically Useful Depression Outcome Scale: The Clinically Useful Depression Outcome Scale (CUDOS)[33] is an 18-item self-report measure of depression symptom severity. Patients are asked to rate the severity of depression symptoms "in the past week, including today…" (for the intake scale) and "during the past day…" (for the daily scale). Possible responses include (0) not at all, (1) a little bit, (2) a moderate amount, (3) quite a bit, and (4) almost always. The daily version of the CUDOS has been found to exhibit high internal consistency (Cronbach's alpha at intake = 0.82, Cronbach's alpha at follow-up = 0.93), test-retest reliability, (r = 0.91 at intake, r = 0.98 at follow-up) and high correlation with other measures of depressive symptoms.[34] First and last day scores were used from the CUDOS to represent pre- and post-treatment depression levels in this study.

Remission from Depression Questionnaire: The Remission from Depression Questionnaire (RDQ)[35] is a 60-item measure designed to capture a broad array of domains considered by patients to be relevant to constructs of depression remission. These domains include symptoms (25 items), coping ability (five items), positive mental health (12 items), functioning (10 items), and wellbeing and life satisfaction (eight items). This scale has demonstrated good internal consistency (overall Cronbach's alpha = 0.97, Cronbach's alpha for each subscale > 0.80), test-retest reliability (r = 0.85 for overall scale, and r > 0.64 for each subscale), and was significantly correlated with measures of depression, anxiety, psychosocial impairment, and quality of life.[35] As the CUDOS and CUXOS are more comprehensive measures of depression and anxiety symptom severity, the RDQ symptom subscale was not included in analysis.

Analytic Strategy

Patients included in analysis were divided into two groups: those with a current diagnosis of social anxiety disorder (SAD) in the absence of major depressive disorder (MDD) (n = 161), and those with comorbid SAD and MDD (n = 309). Demographic and clinical information were compared between groups, using Chi-square tests for categorical variables and t-tests for continuous variables. A series of one-way analysis of covariance models (ANCOVAs) were conducted to determine differences in measures of symptom and functioning change during treatment between groups, while controlling for score of pre-treatment measures. Levene's test and normality checks were carried out and the assumptions met.

RESULTS

Demographics

This sample was predominately white, identified as female, and had completed at least a high school education. Patients were between 18 and 80 years old (M = 33.3, SD = 13.4), and patients in the comorbid SAD and MDD group were significantly older (34.49 $\pm$ 13.82 vs. 31.03 $\pm$ 12.26, p = .008). Full demographic results for each group can be found in **Table 1**.

Demographic Characteristic	SAD (n = 161)		SAD/MDD (n = 309)		Group test	
	N	***%***	***N***	***%***	***x***	***P***
Gender					1.84	.40
Female	107	66.5	207	67.0		
Male	44	27.3	91	28.5		
Trans, Nonbinary	10	6.2	11	3.6		
Race/Ethnicity					5.01	.42
White	122	75.8	247	79.9		
Black	12	7.5	23	7.4		

Hispanic	11	6.8	22	7.1		
Asian	8	5.0	7	2.3		
Other	7	4.3	10	3.2		
Relationship Status					8.19	.15
Married	24	14.9	66	21.4		
Single	98	60.9	152	49.2		
Cohabiting	15	9.3	36	11.7		
Divorced/Separated	17	10.6	38	12.3		
Widowed	1	0.6	8	2.6		
Education					3.53	.90
High School Degree	151	93.8	289	93.5		
4-Year College Degree	49	30.4	82	26.5		
Graduate Degree	11	6.8	24	7.8		
	M	***SD***	***M***	***SD***	***t***	
Age	31.03	12.26	34.49	13.82	-2.67	.008

Table 1. Demographic and Diagnostic Characteristics in Outpatient and Partial Hospital Samples

Clinical Differences

At baseline, patients in the comorbid group had significantly higher depression severity, fewer coping skills, lower functioning, poorer well-being, and less positive mental health than the SAD group. Conversely, there was no difference in baseline anxiety severity between the two groups. Full clinical differences between groups at baseline can be found in **Table 2**.

Measure	**SAD**			**SAD/MDD**			
	N	***M***	***SD***	***N***	***M***	***SD***	***T-Value***
CUDOS	161	38.91	13.52	309	44.63	10.55	-5.05*
CUXOS	161	40.43	16.84	309	41.60	16.32	-0.72
Coping Skills	141	3.24	2.19	277	2.39	2.04	3.93*
Functioning	140	7.94	4.42	276	6.51	3.81	3.42*
Well-Being	140	3.89	3.63	276	2.58	3.02	3.91*
Positive Mental Health	140	7.31	5.40	277	4.29	4.08	6.39*

Table 2. Baseline Characteristics Between SAD and SAD/MDD Groups. *$p < .05$

At discharge, however, the comorbid group had significantly higher anxiety severity than the SAD group. Once again, the comorbid group also had significantly higher depression severity, fewer coping skills, lower functioning, poorer well-being, and less positive mental health than the SAD group. Full clinical differences between groups at discharge can be found in **Table 3**.

Measure	**SAD**			**SAD/MDD**			
	N	***M***	***SD***	***N***	***M***	***SD***	***T-Value***
CUDOS	161	16.52	14.09	309	21.46	14.76	-3.50*
CUXOS	161	21.01	17.40	309	25.15	18.19	-2.38*
Coping Skills	102	6.13	2.59	209	4.59	2.48	5.05*
Functioning	102	12.96	4.65	209	10.81	4.76	5.20*
Well-Being	102	9.01	4.33	209	6.72	4.46	3.77*
Positive Mental Health	102	14.44	5.53	209	10.81	5.88	4.29*

Table 3. Discharge Clinical Characteristics Between SAD and SAD/MDD Groups. *$p < .05$

Treatment Outcomes

Number of days in treatment did not differ between groups (7.78 ± 5.05 vs. 8.49 ± 5.29, $p = .16$). Both the observed and adjusted means showed that the comorbid group was more impaired at discharge across all measures. At treatment termination, the comorbid group showed significantly less improvement in anxiety severity ($F(1, 467) = 5.52$, $p = .02$), coping skills ($F(1, 278) = 16.44$, $p < .01$) functioning ($F(1, 278) = 4.43$, $p = .04$), positive mental health ($F(1, 278) = 10.63$, $p = .001$), and well-being and life satisfaction ($F(1, 278) = 6.54$, $p = .01$) than the SAD group. The comorbid group did not significantly differ from the SAD group in terms of improvement in depressive symptom severity ($F(1, 467) = 3.62$, $p = .07$). Although the comorbid group exhibited less improvement in anxiety symptoms and across RDQ domains relative to the SAD group, both groups improved greatly across all measures during treatment.

DISCUSSION

Consistent with literature that has found poorer treatment outcomes among those with comorbid SAD and MDD, our results suggest that comorbid patients exhibited less improvement in anxiety symptoms, coping skills, functioning, positive mental health, and well-being and life satisfaction than patients with SAD alone. On the other hand, our hypothesis that the comorbid group would show less improvement in depressive severity was not supported, with neither group showing significantly greater improvement in depressive symptoms.

These results are in line with literature that has found diminished treatment responses and smaller magnitudes of improvement among patients with comorbid SAD and MDD.[21, 24] The finding that anxiety symptoms improved comparatively less than depressive symptoms among comorbid patients is likewise supported by previous studies. In examining treatment outcomes among depressed patients with comorbid anxiety disorders, one study found that comorbid SAD uniquely produced greater reductions in depressive symptoms during treatment as well as elevated social anxiety symptoms during and after treatment.[22] Another study also described increased social anxiety symptoms in patients with comorbid SAD and MDD following treatment.[25] Insofar as our study supports these conclusions, our results indicate that anxiety symptoms should be a point of increased focus for clinicians when treating SAD patients with comorbid MDD.

It is also of note that while the amount of improvement in depressive symptom severity during treatment did not differ between the two groups, the comorbid group did show significantly less improvement in depression-adjacent constructs measured by the RDQ. Given that these constructs have been rated by patients as important in determining remission from depression,[34] this indicates that those in the comorbid group derived less benefit from treatment than those in the SAD only group, even if the depressive symptoms themselves are not improving at significantly different rates.

Future research could expand upon our findings in a number of ways. Research building on differences found in this study between anxiety and depressive symptom improvement among those with comorbid SAD and MDD is warranted. Moscovich *et al.* reported that changes in social anxiety symptoms during CBGT account for 91% of changes in depressive symptoms, whereas changes in depression account for only 6% of changes in social anxiety symptoms.[36] Thus, targeting social anxiety symptoms in patients with this comorbidity will likely simultaneously reduce depression. Other research enumerates which aspects of social anxiety may require more focus in therapy among patients with SAD/MDD. For instance, social avoidance has been shown to be augmented in comorbid patients both during and up to 32 months after treatment.[22] Given Moscovitch *et al.*'s conclusions that changes in social anxiety mediate changes in depression among comorbid patients,[36] future studies should examine symptom-level changes during treatment in order to assess which cognitive or behavioral areas exhibit differential improvement between these two disorders. Such research could reveal more precisely which specific social anxiety symptoms are associated with these changes in depression.

In addition, some research has suggested that gains made in therapy are typically not maintained over a one-year follow-up period in SAD patients with current MDD.[25] Furthermore, current MDD predicted the post-treatment loss of gains better than the presence of other comorbid anxiety disorders or social anxiety severity at intake.[25] Other researchers have found that depressive symptom severity, but not social anxiety symptom severity, at intake is related to poorer treatment response and higher drop-out rates.[24] Due to these findings, future studies in partial hospital settings should examine whether improvements made during treatment are maintained after discharge.

Along similar lines, future research should explore treatment outcomes as a function of the duration of treatment. Research on the efficacy of acute partial hospital treatment is extremely limited and previous findings on the outcomes of shorter treatment durations are conflicted. Although most research has found acute treatment (5-8 days) in partial hospital settings to be comparable to inpatient treatment or longer partial hospital stays in treating psychiatric disorders,[37, 38, 39] other research has suggested that shorter stays may have negative impacts on readmission rates[40] and suicide risk[41] among depressed patients.

Data for the current study was collected in an in-person treatment format prior to the Covid-19 pandemic. It may be important to explore effects of the Covid-19 pandemic on psychiatric populations receiving care virtually in partial hospital programs. Patients with higher baseline symptom severity and greater numbers of psychiatric comorbidities, such as those typically treated in partial hospital programs, may experience more severe and persistent effects than others. However, a virtual treatment format requires less patient interaction, which may be beneficial to patients with a diagnosis of SAD. The impact of the pandemic on mental health may be long-lasting, and has magnified healthcare and economic disparities, disproportionately affecting ethnic and other minority populations.[42] Exploration of treatment outcomes as a result of adaptations made to mental health care in the last year are warranted.

The current study has some important limitations. This study was conducted in a single clinical location in which the majority of patients were white, female, and had health insurance. Replication of this study in different treatment settings and a sample with different demographic characteristics is warranted. In addition, the CUXOS items are designed to assess general anxiety symptoms rather than specific social anxiety symptoms. Future extensions of this study may benefit from measures designed specifically to assess social anxiety. This study also chose to focus on differences in treatment outcomes exclusively among SAD patients with and without MDD. As SAD typically predates development of MDD in patients with both disorders, this study examined how comorbid MDD impacts treatment for patients with SAD, rather than the other way around. However, this line of research would benefit from the inclusion of an MDD group in the future, to determine if results would differ.

CONCLUSIONS

Despite these limitations, our research makes several contributions to existing literature. By exploring treatment outcomes in a partial hospital setting, this study expands upon and supports studies that have found poorer treatment outcomes among comorbid patients within inpatient and outpatient settings. In addition, this is the first study that we are aware of that examines these differences in a partial hospital setting. Furthermore, our results align with past findings regarding increased anxiety symptoms among comorbid patients, clarifying points for future research and indicating potential areas for clinician focus. Our research confirms that a comorbid diagnosis of SAD and MDD may present unique challenges that should be properly addressed in treatment and encourages further exploration of these challenges.

REFERENCES

1. Kessler, R. C., Berglund, P., Demler, O., Jin, R., Merikangas, K. R., and Walters, E. E. (2005) Lifetime prevalence and age-of-onset distributions of DSM-IV disorders in the national comorbidity survey replication, *Arch Gen Psychiatry* 63, 593–602. *https://doi.org/10.1001/archpsyc.62.6.593*

2. Stein, D.J., Lim, C.C.W., Roest, A.M., de Jonge, P., Aguilar-Gaxiola, S., Al-Hamzawi, A., Alonso, J., Benjet, C., Bromet, E. J., Bruffaerts, R., de Girolamo, G., Florescu, S., Gureje, O., Haro, J. M., Harris, M. G., He, Y., Hinkov, H., Horiguchi, I., Hu, C., Karam, A., Karam, E. G., Lee, S., Lepine, J.-P., Navarro-Mateu, F., Pennell, B.-E., Piazza, M., Posada-Villa, J., ten Have, M., Torres, Y., Viana, M. C., Wojtyniak, B., Xavier, M., Kessler, R.C., Scott, K. M., and WHO world Mental Health Survey Collaborators (2017) The cross-national epidemiology of social anxiety disorder: Data from the World Mental Health Survey Initiative, *BMC Med* 15, n.p. *https://doi.org/10.1186/s12916-017-0889-2*

3. Ruscio, A.M., Brown, T.A., Chiu, W.T., Sareen, J., Stein, M.B., & Kessler, R.C. (2008). Social fears and social phobia in the USA: Results from the National Comorbidity Survey Replication, *Psychol Med* 38, 15–28. *https://doi.org/10.1017/S0033291707001699*

4. Koyuncu, A., Ince, E., Ertekin, E., and Tükel, R. (2019) Comorbidity in social anxiety disorder: Diagnostic and therapeutic challenges, *Drugs Context* 8, 1–13. *https://doi.org/10.7573/dic.212573*

5. Bittner, A., Goodwin, R. D., Wittchen, H.-U., Beesdo, K., Höfler, M., & Lieb, R. (2004) What characteristics of primary anxiety disorders predict subsequent major depressive disorder?, *J Clin Psychiatry* 65, 618–626. *https://doi.org/10.4088/jcp.v65n0505*

6. Dalrymple, K. L. and Zimmerman, M. (2007) Does comorbid social anxiety disorder impact the clinical presentation of principal major depressive disorder? *J Affect Disord* 100, 241–247. *https://doi.org/10.1016/j.jad.2006.10.014*

7. Heimberg, R. G. (2002) Cognitive-behavioral therapy for social anxiety disorder: Current status and future directions, *Biol Psychiatry* 51, 101–108. *https://doi.org/10.1016/s0006-3223(01)01183-0*

8. Hofmann, S. G., Asnaani, A., Vonk, I. J. J., Sawyer, A. T., and Fang, A. (2012) The efficacy of cognitive behavioral therapy: A review of meta-analyses, *Cognit Ther Res* 36, 427–440. *https://doi.org/10.1007/s10608-012-9476-1*

9. Scaini, S., Belotti, R., Ogliari, A. and Battaglia, M. (2016) A comprehensive meta-analysis of cognitive behavioral interventions for social anxiety disorder in children and adolescents, *J Anxiety Disord* 42, 105–112. *https://doi.org/10.1016/j.janxdis.2016.05.008*.

10. Leichsenring, F. and Leweke, F. (2017) Social anxiety disorder, *N Engl J Med* 376, 2255-2264. *https://doi.org/10.1056/NEJMcp1614701*

11. Goldin, P. R. and Gross, J. J. (2010) Effects of mindfulness-based stress reduction (MBSR) on emotion regulation in social anxiety disorder, *Emotion* 10, 83–91. *https://doi.org/10.1037/a0018441*

12. Hjeltnes, A., Molde, H., Schanche, E., Vøllestad, J., Lillebostad Svendsen, J., Moltu, C., and Binder, P.-E. (2017) An open trial of mindfulness-based stress reduction for young adults with social anxiety disorder, *Scand J Psychol* 58, 80–90. *https://doi.org/10.1111/sjop.12342*

13. Chi, X., Bo, A., Liu, T., Zhang, P., and Chi, I. (2018) Effects of mindfulness-based stress reduction on depression in adolescents and young adults: A systematic review and meta-analysis, *Front Psychol* 9, n.p. *https://doi.org/10.3389/fpsyg.2018.01034*

14. Strege, M. V., Swain, D., Bochicchio, L., Valdespino, A., and Richey, J. A. (2018) A pilot study of the effects of mindfulness-based cognitive therapy on positive affect and social anxiety symptoms, *Front Psychol* 9, n.p. *https://doi.org/10.3389/fpsyg.2018.00866*

15. Piet, J., Hougaard, E., Hecksher, M. S., and Rosenberg, N. K. (2010) A randomized pilot study of mindfulness-based cognitive therapy and group cognitive-behavioral therapy for young adults with social phobia, *Scand J Psychol* 51, 403–410. *https://doi.org/10.1111/j.1467-9450.2009.00801.x*

16. Goldberg, S. B., Tucker, R. P., Greene, P. A., Davidson, R. J., Kearney, D. J., and Simpson, T. L. (2019) Mindfulness-based cognitive therapy for the treatment of current depressive symptoms: A meta-analysis, *Cogn Behav Ther* 48, 445–462. *https://doi.org/10.1080/16506073.2018.1556330*

17. Roohi, R., Soltani, A. A., Meimand, Z. Z., and Nematollahi, V. R. (2019) The effect of acceptance and commitment therapy (ACT) on increasing the self-compassion, distress tolerance, and emotion regulation in students with social anxiety disorder, *Journal Child Ment Health* 6, 173–187. *https://doi.org/10.29252/jcmh.6.3.16*

18. Dalrymple, K. L. and Herbert, J. D. (2007) Acceptance and commitment therapy for generalized social anxiety disorder, *Behav Modif* 31, 543–568. *https://doi.org/10.1177/0145445507302037*

19. Ivanova, E., Lindner, P., Ly, K. H., Dahlin, M., Vernmark, K., Andersson, G., and Carlbring, P. (2016) Guided and unguided acceptance and commitment therapy for social anxiety disorder and/or panic disorder provided via the Internet and a smartphone application: A randomized controlled trial, *J Anxiety Disord* 44, 27–35. *https://doi.org/10.1016/j.janxdis.2016.09.012*

20. Bai, Z., Luo, S., Zhang, L., Wu, S., and Chi, I. (2020) Acceptance and commitment therapy (ACT) to reduce depression: A systematic review and meta-analysis, *J Affect Disord* 260, 728–737. *https://doi.org/10.1016/j.jad.2019.09.040*

21. Bauer, I., Wilansky-Traynor, P., and Rector, N. A. (2012) Cognitive-behavioral therapy for anxiety disorders with comorbid depression: A review, *Intl J Cog Ther* 5, 118–156. *https://doi.org/10.1521/ijct.2012.5.2.118*

22. Vittengl, J. R., Clark, L. A., Smits, J. A. J., Thase, M. E., and Jarrett, R. B. (2019) Do comorbid social and other anxiety disorders predict outcomes during and after cognitive therapy for depression?, *J Affect Disord* 242, 150–158. *https://doi.org/10.1016/j.jad.2018.08.053*

23. Dalrymple, K. L., Morgan, T. A., Lipschitz, J. M., Martinez, J. H., Tepe, E., and Zimmerman, M. (2014) An integrated, acceptance-based behavioral approach for depression with social anxiety: Preliminary results, *Behav Modif* 38, 516–548. *https://doi.org/10.1177/0145445513518422*

24. Ledley, D.R., Huppert, J.D., Foa, E.B., Davidson, J.R., Keefe, F.J., and Potts, N.L (2005) Impact of depressive symptoms on the treatment of generalized social anxiety disorder, *Depress Anxiety* 22, 161–167. *https://doi.org/10.1002/da.20121*

25. Marom, S., Gilboa-Schechtman, E., Aderka, I.M., Weizman, A., and Hermesh, H. (2009) Impact of depression on treatment effectiveness and gains maintenance in social phobia: a naturalistic study of cognitive behavior group therapy, *Depress Anxiety* 26, 289–300. *https://doi.org/10.1002/da.20390*

26. McLean, P. D. and Hakstian, A. R. (1979) Clinical depression: Comparative efficacy of outpatient treatments, *J Consult Clin Psychol* 47, 818–836. *https://doi.org/10.1037/0022-006X.47.5.818*

27. Cuijpers, P., Clignet, F., van Meijel, B., van Straten, A., Li, J., and Andersson, G. (2011) Psychological treatment of depression in inpatients: A systematic review and meta-analysis, *Clin Psychol Rev* 31, 353–360. *https://doi.org/10.1016/j.cpr.2011.01.002*

28. Beard, C., Stein, A. T., Hearon, B. A., Lee, J., Hsu, K. J., and Björgvinsson, T. (2016) Predictors of depression treatment response in an intensive CBT partial hospital, *J Clin Psychol* 72, 297–310. *https://doi.org/10.1002/jclp.22269*

29. Peckham, A. D., Forgeard, M., Hsu, K. J., Beard, C., and Björgvinsson, T. (2019) Turning the UPPS down: Urgency predicts treatment outcome in a partial hospitalization program, *Compr Psychiatry* 88, 70–76. *https://doi.org/10.1016/j.comppsych.2018.11.005*

30. First M.B. (1997) *A guide for the Structured Clinical Interview for DSM-IV axis 1 disorders SCID-1: Clinician version,* American Psychiatric Press, Washington D.C.

31. Zimmerman, M., Chelminski, I., Young, D., and Dalrymple, K. (2010) A clinically useful anxiety outcome scale, *J Clin Psychiatry* 71, 534–542. *http://doi.org/10.4088/JCP.09m05264blu*

32. Zimmerman, M., Kiefer, R., Kerr, S., and Balling, C. (2019) Reliability and validity of a self-report scale for daily assessments of the severity of anxiety symptoms, *Compr Psychiatry* 90, 37–42. *https://doi.org/10.1016/j.comppsych.2018.12.014*

33. Zimmerman, M., Chelminski, I., McGlinchey, J. B., and Posternak, M. A. (2008) A clinically useful depression outcome scale, *Compr Psychiatry* 49, 131–140. *https://doi.org/10.1016/j.comppsych.2007.10.006*

34. Zimmerman, M., Harris, L., Martin, J., and McGonigal, P. (2018) Reliability and validity of a self-report scale for daily assessments of the severity of depressive symptoms, *Psychiatry Res* 270, 581–586. *https://doi.org/10.1016/j.psychres.2018.10.007*

35. Zimmerman, M., Martinez, J. H., Attiullah, N., Friedman, M., Toba, C., Boerescu, D. A., and Ragheb, M. (2013) A new type of scale for determining remission from depression: The Remission from Depression Questionnaire, *J Psychiatr Res* 47, 78–82. *https://doi.org/10.1016/j.jpsychires.2012.09.006*
36. Moscovitch, D. A., Hofmann, S. G., Suvak, M. K., and In-Albon, T. (2005) Mediation of changes in anxiety and depression during treatment of social phobia, *J Consult Clin Psychol* 73, 945–952. *https://doi.org/10.1037/0022-006X.73.5.945*
37. Morgan, T. A., Dalrymple, K., D'Avanzato, C., Zimage, S., Balling, C., Ward, M., & Zimmerman, M. (2020) Conducting outcomes research in a clinical practice setting: The effectiveness and acceptability of acceptance and commitment therapy (ACT) in a partial hospital program, *Behav Ther. https://doi.org/10.1016/j.beth.2020.08.004*
38. Lieberman, P. B., Villalba, R., & Farris, S. G. (2017) Outcomes of acute partial hospital treatment. *J Psychiatr Pract* 23, 401-408. *https://doi.org/10.1097/pra.0000000000000271*
39. Larivière, N., Desrosiers, J., Tousignant, M., & Boyer, R. (2011) Multifaceted impact evaluation of a day hospital compared to hospitalization on symptoms, social participation, service satisfaction and costs associated to service use, *Int J Psychiatry Clin Pract* 15, 228-240. *https://doi.org/10.3109/13651501.2011.572170*
40. Figueroa, R., Harman, J., & Engberg, J. (2004) Use of claims data to examine the impact of length of inpatient psychiatric stay on readmission rate, *Psychiatr Serv* 55, 560-565. *https://doi.org/10.1176/appi.ps.55.5.560*
41. Desai, R. A., Dausey, D. J., & Rosenheck, R. A. (2005) Mental health service delivery and suicide risk: The role of individual patient and facility factors, *Am J Psychiatry* 162, 311-318. *https://doi.org/10.1176/appi.ajp.162.2.311*
42. Moreno, C., Wykes, T., Galderisi, S., Nordentoft, M., Crossley, N., Jones, N., . . . Arango, C. (2020) How mental health care should change as a consequence of the COVID-19 pandemic, *Lancet Psychiatry* 7, 813-824. *https://doi.org/10.1016/s2215-0366(20)30307-2*

ABOUT STUDENT AUTHOR

Allison Graham graduated magna cum laude from Brown University in 2020. She plans on pursuing a PhD in clinical psychology and a career as a licensed psychologist.

PRESS SUMMARY

Although previous studies have examined the impact of comorbid major depressive disorder (MDD) on social anxiety disorder (SAD), the results have been somewhat mixed. Most studies have found that comorbid MDD negatively impacts patients with SAD both in terms of everyday impairment and in terms of treatment efficacy and outcomes. This study confirms these findings, while examining this comorbidity in an under-studied setting (partial hospitalization program). Patients at Rhode Island Hospital with a diagnosis of SAD were compared to those with comorbid SAD and MDD on pre-treatment and post-treatment measures of anxiety and depression. As predicted, the comorbid groups showed significantly less improvement on anxiety symptoms and several constructs related to remission from depression. However, there were no significant differences on improvement in depressive symptoms. These findings corroborate previous studies which have suggested that anxiety symptoms may need to be a point of focus for patients with this comorbidity.

Evaluation of Physical Activity Participation, Self-Efficacy and Outcome Expectancy for Employees Participating in Exercise Is Medicine® On Campus Program

Maximilian Gastelum-Morales, Lisa J. Leininger[a], Joanna L. Morrissey[b], Ryan Luke[a], & Mark DeBeliso[c]*

[a]Department of Kinesiology, California State University, Monterey Bay, Marina, CA
[b]Department of Psychology, University of Wisconsin, Green Bay, Green Bay, WI
[c]Department of Kinesiology and Outdoor Recreation, Southern Utah University, Cedar City, UT, United States

https://doi.org/10.33697/ajur.2020.034

Student: Mgastelum-morales@csumb.edu
Mentor: Lleininger@csumb.edu

ABSTRACT
Exercise Is Medicine® On Campus (EIM-OC) is a worldwide initiative from the American College of Sports Medicine (ACSM) to promote physical activity (PA) at universities. California State University, Monterey Bay (CSUMB) implemented this initiative in Fall 2019 with offerings to students and employees. For employees, an "Introduction to Resistance Training Class" was offered. Participants attended classes two times per week, with the sessions lasting approximately fifty minutes. The purpose of this study was to evaluate the EIM-OC employee Introduction to Resistance Training class for its effectiveness on increasing PA, self-efficacy, and outcome expectancy. The research design was pre-post, with participants completing online questionnaires before and after the course. The Godin Leisure Time Physical Activity Questionnaire (LTPQ), Resistance Training Self-Efficacy and Outcome Expectancy Questionnaire, and Self-Efficacy and the Maintenance of Exercise Participation in Older Adults Questionnaire were included. The training class had a total of 14 female participants, 12 of which completed the pre- and post-questionnaires. There was a significant increase ($t=-3.2$, $df=11$, $p=.004$) in resistance training self-efficacy score following the course ($M=3.52\pm1.03$ versus $M=4.31\pm.56$). Resistance training outcome expectancy score was also statistically significant ($t=-2.54$, $df=11$, $p=.01$) following the course ($M=4.48\pm.53$ versus $M=4.71\pm.37$). There were increases in strenuous exercise days, physical activity scores, and future resistance training self-efficacy, although they were not statistically significant. The results of this study indicate that employee exercise classes, as part of the EIM-OC initiative, can be effective in increasing resistance training self-efficacy, and outcome expectancy. These indicators are important for individuals to maintain lifelong PA therefore future programming and research on EIM-OC should continue.

KEYWORDS
Exercise Is Medicine®-On Campus; Resistance Training; Physical Activity; Exercise; Worksite Health Promotion Program; Self-Efficacy; Outcome Expectancy; Employees; California State University, Monterey Bay

INTRODUCTION

In the United States, individuals are dying prematurely due to lack of physical activity (PA) and an increase in non-communicable diseases.[1] As PA levels decline, there is an increased risk of hypertension, obesity, diabetes, and many cancers.[2] For example, in 2020, 1,806,590 new cancer cases and 606,520 cancer deaths are projected to occur in the United States.[3] However, research indicates that patients involved in greater levels of exercise have a lower relative risk of cancer mortality and a lower relative risk of cancer recurrence, and they experience fewer and/or less severe treatment-related adverse effects.[4] Furthermore, in healthy individuals, exercise can decrease the likelihood of succumbing to disease and illness. Considering physical inactivity across the globe, where only 26% of men and 19% of women report sufficient PA to meet the 150-minute per week moderate aerobic activity and two day per week muscle-strengthening guidelines, it is important to implement strategies and programs to foster individual involvement in their own physical health.[5]

Studies have observed self-efficacy and its relationship with health behavior change.[6] In social cognitive theory,[7] self-efficacy is an important precondition for adequate self-management behavior.[6] Increased self-efficacy levels have been shown to play a significant role in improving PA participatory patterns in adult females.[8] Alongside self-efficacy, outcome expectancy and self-regulation have been identified to be highly associated with exercise behavior. A study done as part of a worksite intervention

provided significant positive results for these three variables.[9] Therefore, examining these variables in a university worksite population will add to the body of knowledge of the effects of programming on health behaviors.

Worksite health promotion programs (WHPPs) are an important tool due to its capacity to change the burden of physical inactivity, and it can serve to remove one challenge for those employees who deem PA to be out of their reach due to accessibility, instruction, or motivation. WHPPs have been shown to improve nutritional health behavior and increase PA in working class adults.[10] Due to their numerous benefits, many universities have implemented WHPPs.[11] In previous years California State University, Monterey Bay (CSUMB) implemented WHPPs such as the "Workplace Walk Off Challenge" and offerings from the insurance partners and local hospital wellness programs.[12] WHPPs also play an integral part in exercise adherence for those employees who participate in them.[9] Furthermore, WHPPs have been used by companies to keep employees healthy in order to prevent any health complications that would impede them from continuing to work. There is evidence that WHPPs are associated with lower levels of absenteeism and health care costs, and fitness programs are associated with reduced health care costs.[13]

Exercise is Medicine® on Campus

Exercise Is Medicine® is a global health initiative launched by the American Medical Association and the ACSM in 2007. The initiative aimed to make PA a standard of the medical paradigm for the prevention and treatment of non-communicable diseases in healthcare systems. Branching from this global health initiative is the Exercise Is Medicine® On Campus (EIM-OC) initiative, which encourages colleges and universities to promote PA to make movement part of the daily campus culture for both students and employees. EIM-OC activities help improve the knowledge and promotion of PA on college campuses. This is done in a variety of ways, and many departments are often involved (Kinesiology or related departments, Student Health Services, Student Counseling Services, and Health Promotion and/or Wellness Departments).

Many different programs were successfully implemented and have provided effective strategies for improving PA across campuses worldwide under the EIM-OC initiative. Effective strategies utilized by different campuses for a successful implementation of an EIM-OC program included placing exercise stations across campus to promote PA during an EIM-OC week, [14,15] and using campus health centers to screen for inactivity in patients with the intention to refer them to an exercise practitioner that can help them with increasing their PA levels.[16] Another major characteristic of a successful EIM-OC program is the amount of student involvement, students can play different roles such as promotion, leadership, organization, planning, education, implementation, and data collection.[14-16] EIM-OC provides a strong framework due to the support and resources provided by the ACSM. EIM-OC allows campuses great flexibility to implement programming within their bandwidth and capabilities. However, fewer programs have included employees in their effort to increase PA on campus. Including employees is imperative if a campus wishes to truly have a culture of PA.

Exercise is Medicine® on Campus at CSUMB

CSUMB followed all steps necessary to register the campus and implement the EIM-OC program. This included creating a leadership team and completing the registration form. Concurrently, the leadership team developed campus support, and then implemented EIM-OC in a variety of ways, once registration was approved from the ACSM. During Fall 2019, the CSUMB EIM-OC Executive Committee planned initial programming for students and employees. Employee programming focused on in-person exercise classes, which included an "Introduction to Resistance Training (RT) class." The RT class focused on employees learning to lift with proper technique, were given instant feedback on their performance, and were encouraged to work at their own pace so that they develop healthy behaviors towards resistance training inside and outside of the class. Given that RT can help maintain health in all populations, a goal for the program was to collect data on key health behavior variables in order to evaluate the effectiveness of the class.

PA level, self-efficacy and outcome expectancy were variables measured in the study due to their strong correlation to exercise health behaviors. It has been observed that high levels of PA have a significant effect on life expectancy. Studies have also found that self-efficacy and outcome expectancy are key psychological constructs which play a key role in exercise adherence, maintenance, and outcomes regarding strength training specifically.[17] Self-efficacy is an individual's belief in oneself to execute situation-specific behavior and enhances an individual's behavioral persistence.[18-20] Outcome expectancy is thought to play an important role in motivation and is defined as a person's belief that a specific behavior will lead to certain positive and negative consequences related to one's physical health or affective outcomes, such as impacts on one's mood or mental state.[17,18,20]

The research questions for this study were: 1) are there increases in PA participation among employees participating in the exercise classes offered through the CSUMB EIM-OC initiative? and 2) are there increases in exercise self-efficacy and outcome expectancy among employees who participate in the exercise classes offered through the CSUMB EIM-OC initiative? The

purpose of this study was to evaluate the effectiveness of the EIM-OC employee Introduction to RT class, specifically related to PA participation, self-efficacy and outcome expectancy.

METHODS AND PROCEDURES

Program Description

Beginning in Fall 2019, EIM-OC the Introduction to RT class was made available to all campus employees (staff, faculty, administration). Space in the Kinesiology Department's exercise facility was limited; therefore, employees were required to sign up online through a link displayed on CSUMB's dashboard page. The Introduction to RT class was held on Tuesdays and Thursdays during lunch time hours (12pm to 12:50pm) for four weeks. Participants were introduced to a variety of RT exercises during the span of the course. Examples of exercises introduced included front squats, goblet squats, lunges, Romanian deadlifts, deadlift, bent over row, push-ups, military press, and dumbbell shoulder press. Participants primarily used free weights and learned to use proper exercise technique. Body weight exercises were also used to develop proper exercise technique in participants who showed the need. Equipment used included barbells, dumbbells, benches, rubber plates and clamps.

The class was led by a tenured Kinesiology professor who is a National Strength and Conditioning Association, Certified Strength and Conditioning Specialist. Undergraduate student leaders (n=6), majoring in Kinesiology, were trained beforehand to assist in the facilitation of the classes. Student leaders set up, demonstrated exercises, and coached form. Employees who participated in this study were given clear instructions and information on what to expect, bring, and wear for the class. The Institutional Review Board at CSUMB approved this research study and all authors and researchers completed the Collaborative Institutional Training Initiative where they became certified to work with human subjects in research. Informed consent was obtained for all those participating in the research study. All participants filled out a Physical Activity Readiness Questionnaire (PAR-Q) to assure no contraindications for exercise participation.

Participants

No exclusion or inclusion criteria were established and the course was available to all employees (faculty, staff and administration) at the university. A participant cap of 16 was set due to space limitations. Fourteen employees volunteered for the study, with 12 completing both pre and post surveys, and therefore were included in the statistical analysis. No incentives were given for attendance or completion of surveys. Average age of the participants was 40.7 years (SD±12.66). Of the 12 that completed both surveys, 10 were staff and two were faculty. All participants were female. Attendance was not mandatory, and participants were not required to participate in PA outside of the exercise intervention, but were encouraged to stay active. Out of the eight exercise sessions, five attended eight sessions, five attended six sessions, and two attended five sessions. Therefore, 41.6% of all participants completed all workout sessions, with 83% completing 6 or more sessions.

Protocol

Upon participant arrival to the class, a brief greeting was completed during which the exercises for the day were explained and demonstrated. After participants assembled into groups of two to three individuals, they began at a chosen station. Stations were set up in a circular fashion in order to increase supervision. Eight stations were available and prepped with the equipment for the session. Employees stayed at their station and student leaders circulated between the groups of employees, giving employees the opportunity to interact with each student leader during the session. Students provided verbal feedback to employees. Therefore, employees had significant guidance and support from the student leaders. Student leaders were responsible for arriving on time before each session and setting up. All six students were to attend all 8 sessions with exceptions made when necessary. Workouts were designed by the student leaders, and approved by the faculty lead. Exercises were chosen based on the recommendation of all major muscle groups being targeted during a given workout.

The research design was pre-post. Questionnaires were administered a week before the first class and two days following the last class in the four-week series. The online questionnaire included basic demographic information, the PAR-Q form, Godin Leisure Time Physical Activity Questionnaire,[21] Resistance Training Self-Efficacy and Outcome Expectancy Questionnaire,[22] and Self-Efficacy and the Maintenance of Exercise Participation in Older Adults Questionnaire.[23]

The Godin LTPQ includes a table in which participants indicate how many times on average they participated in the following intensity of exercise for more than 15 minutes during their free time in one week. Exercises intensities were broken into three categories: strenuous, moderate, mild/light. Scores were determined by taking the number for each category and multiplying it by a fixed variable, after which the scores for the three categories were added and interpreted through the questionnaire key where participants could be placed in three categories (active, moderately active, and insufficiently active/sedentary).

The Resistance Training Self-Efficacy & Outcome Expectancy Questionnaire includes nine questions which are divided into two sections (Self-Efficacy and Outcome Expectancy). Four questions are regarding Self-Efficacy and five questions are regarding

outcome expectancy. Answers for the questions were based on a five-point scale (one= strongly disagree and five= strongly agree). Scores were calculated by adding the answers and dividing them by the corresponding amount of questions. High levels of self-efficacy yielded a larger number, while lower yields indicated lower self-efficacy. Internal consistency for self-efficacy was **α** = .83, with internal consistency for outcome expectancy **α** = .75.[22]

The Self-Efficacy & Maintenance of Exercise Participation in Older Adults Questionnaire included a set of eight questions which were scored based on a percentage scale which started at zero and ended at one-hundred (0%= not at all confident, 50%= moderately confident, and 100%= Highly confident). Scores were derived by adding the scores and dividing by eight, high levels of self-efficacy yielded a larger number, while lower yields indicated lower self-efficacy. Internal consistency for this questionnaire was **α** = .85. While this questionnaire was originally designed for older populations, it has since been validated with other populations, including adults under the age of 65.[24]

Statistical Analysis

Paired-samples t-tests were performed for LTPQ score, strenuous days of PA, moderate days of PA, and light days of PA per week. Paired samples t-tests were also performed for resistance training self-efficacy, resistance training outcome expectancy, and resistance training future self-efficacy. All statistical analysis was done on SPSS version 25. Significance was set at **α** = 0.05.

RESULTS

Resistance training self-efficacy score was statistically significant (t=-3.2, df=11, p=.004) from pre (M=3.5±1.03) to post (M=4.31±.56) RT class. Resistance training outcome expectancy score was also statistically significant (t=-2.54, df=11, p=.01) pre (M=4.48±.53) to post (M=4.71±.37) RT class. See Figures 1 & 2.

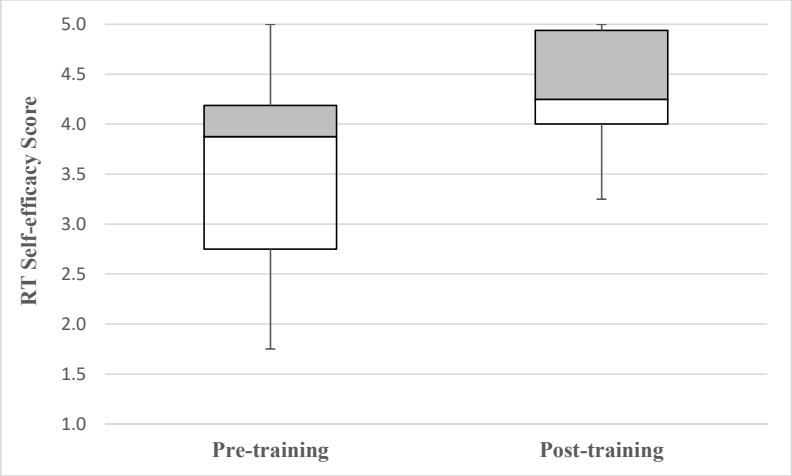

Figure 1. Resistance training self-efficacy score pre and post training. p<0.05

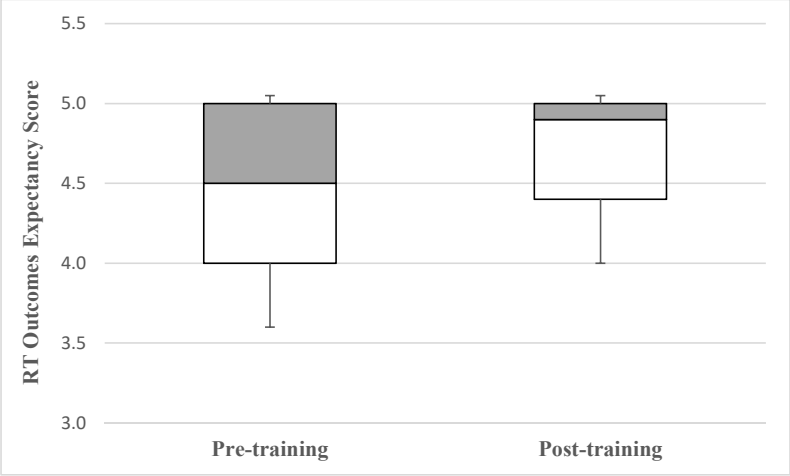

Figure 2. Resistance training outcome expectancy score pre and post training. p<0.05

Future resistance training self-efficacy was not statistically significant (t=-.06, df=11, p=.48), although there was an increase from pre (M=89.06±12.58) to post (M=89.27±15.13) training. See Figure 3.

Figure 3. Future resistance training self-efficacy score.

LTPQ PA Score was not statistically significant, but also increased (t=-.54, df=11, p=.30) from pre (M=44.08±27.9) to post (M=46.58±21.73). Days of strenuous PA per week were not statistically significant, but increased (t=-9.59, df=11, p=.18) from pre (M=1.67±1.87) to post (M=2.08±1.73). Days of moderate PA per week were not statistically significant and unchanged (t=.00, df=11, p=.50) from pre (M=3.42±2.15) to post (M=3.42±1.37). Days of light PA per week were not statistically significant (t=1.0, df=11, p=.16) from pre (M=4.0±2.0) to post (M=3.58±2.23).
See Figure 4.

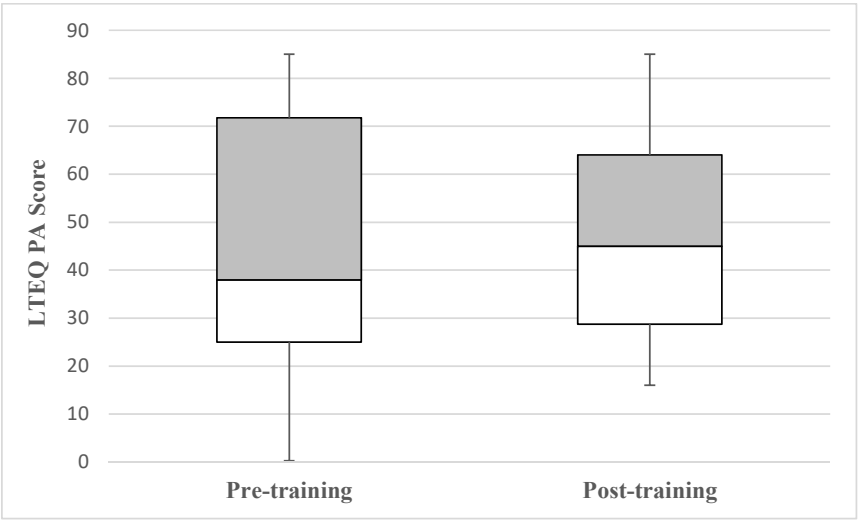

Figure 4. LTPQ score pre versus post training.

Given the appearance of the box plots, Wilcoxon signed-rank tests were conducted for each of the dependent variables. The results of the Wilcoxon analysis were consistent with the paired samples t-tests for each dependent variable.

DISCUSSION

The purpose of this study was to evaluate the effectiveness of the EIM-OC employee Introduction to RT class. This course was implemented as part of the EIM-OC initiative at CSUMB. This study focused on the effects of an employee RT class on PA participation, resistance training self-efficacy and outcome expectancy.

Results of this study indicated that the program's intervention was effective in influencing health behavior variables. Significant changes in self-efficacy and outcome expectancy were observed. In addition, increasing trends in PA score, PA days (light, moderate, and strenuous) and future RT self-efficacy were observed. While university employees are a small sample of the population, the effectiveness of WHPPs can prove effective in maintaining their health to avoid any unwanted health emergencies or complications associated with the decline in PA.[25]

This study provided evidence to the effectiveness of the EIM-OC employee Introduction to RT class, WHPPs and the EIM-OC program at CSUMB in improving key psychological constructs that play a role in exercise adherence. Previous studies that have tracked self-efficacy and outcome expectancy have found that through an exercise intervention they can be positively influence.[7,8] Studies have also shown that improved self-efficacy in adults correlates to gait speed which is an important predictor of current and future functional status.[26] This study provides evidence that exercise interventions can impact self-efficacy, which in of itself has been a proven predictor of health quality. Furthermore, it is adding literature to the growing body of knowledge regarding EIM-OC. As of this study's publication, most EIM-OC programs focus on student programming. However, to truly make physical activity at part of the campus culture, employees should be included. The program at CSUMB differs from many other EIM-OC programs because it is invested in developing exercise interventions for employees. Therefore, this EIM-OC program provides a framework to implement a worksite health promotion program.

While this study required plenty of planning, background knowledge and training, it was feasible with a team of individuals who have proper experience in research and implementing WHPPs. Proper steps were taken to ensure that employees in the study were safe and properly informed of their options.

The employees participating in the study went through a four-week intervention in which they were provided with two days of guided exercise instruction. Each day incorporated exercises which stressed all major muscle groups. No incentives were given for attendance, but it was recommended that participating employees attend both days. A support system made up of student leaders and a certified professional served to guide, motivate, and encourage participating employees.

Limitations

There are some study limitations to note. A participant cap was set at 16, due to limited space within the exercise science lab. Due to class limitations, the sample size (n=12) was small. Additionally, the participants were all female and mostly staff members. Therefore, these results may not be generalizable to the larger campus population or more diverse groups of employees who participate in future studies.

The questionnaires used required participants to self-report data which could have impacted the validity of the results. For example, given the pre- and post-structure of filling out questionnaires, participants might have an inaccurate recollection of their daily activity over the four weeks of the study. With attendance not mandatory, employees may not have attended all classes potentially impacting the results of the study.

The participants who volunteered for this study were also already considered active. Of the 14 individuals who began the study, 11 were rated as "Active" according to the LTPAQ, while three were considered "Insufficiently Active." Following the RT course, of the 12 participants who completed the study, 10 were scored as "Active" and two were scored as "Moderately Active." No participants were scored as "Insufficiently Active" following the course. Additionally, this study did not have a control group, which could have helped demonstrate that the three variables being measured could have been impacted by other factors.

Implications and Areas of Future Research

Future EIM-OC employee Introduction to RT classes should aim to increase participation among employees, especially related to recruiting males. Issues facing EIM-OC during this pilot study were having a small sample size, lack of accountability by the participants, coupled with a short intervention period of four weeks. This study also only had one population which was involved, adult females. Participants in this study participated out of their own interest. Participants were encouraged to attend both classes each week, but there were no repercussions if they did not make one of the sessions. The choice to participate in the study was also based on personal preference. There were participants who filled out both pre and post surveys, which ultimately made it to the results, however there were also individuals who filled out one survey or did not fill out any surveys while still participating in the exercise intervention.

Given that this study was a pilot and the exercise science lab which was used had limited space, a small sample size was effective in allowing the management and implementation of the RT class. Future research should look into finding larger spaces which would allow for more participants. In addition, the program should try to advertise the classes better in order to diversify the population which is involved in the study. Tactics that can be used to increase diversity and participation include incentives, promotional videos on campus, availability of classes, and cross campus communication.

Future research should address these issues in order to maximize the effectiveness of the employee Introduction to RT Class. Increasing the number of participants and diversifying the population of the study would allow for generalizability within different populations. Increasing the length of the study would allow for a more in-depth view into the key psychological constructs which play a role in exercise adherence (outcome expectancy and self-efficacy). These factors should be considered when planning the employee Introduction to RT Class for upcoming terms.

CONCLUSION

The purpose of this study was to evaluate the effectiveness of the EIM-OC employee Introduction to RT class. The results demonstrate that the program was effective in increasing key psychological constructs which related to exercise adherence and participation. A four-week 2 session per week intervention of RT showed positive increases in self-efficacy and outcome expectancy. Further studies should be conducted in order to provide more evidence for the effectiveness of the EIM-OC employee RT class. This study adds to the growing body of knowledge that currently exists on EIM-OC and WHPPs. Through effort on part of the EIM-OC team at CSUMB the program was successful, although different results might be attained in a more diverse population.

ACKNOWLEDGEMENTS

The authors thank the Undergraduate Research Opportunity Center (UROC) and the McNair Scholars Program for helping fund this project. This project would not be feasible without the Kinesiology department and Associate Professors supporting the process of planning and implementation of the program, along with mentorship of student leaders.

REFERENCES

1. Danaei, G., Ding, E. L., Mozaffarian, D., Taylor, B., Rehm, J., Murray, C. J., & Ezzati, M. (2009) The preventable causes of death in the United States: Comparative risk assessment of dietary, lifestyle, and metabolic risk factors. *PLoS Medicine*, 6(4), 1-23. *doi:10.1371/journal.pmed.1000058*
2. Cunningham, C., Sullivan, R. O., Caserotti, P., & Tully, M. A. (2020) Consequences of physical inactivity in older adults: A systematic review of reviews and meta-analyses. *Scandinavian Journal of Medicine & Science in Sports*, 30(5), 1-12. *doi: 10.1111/sms.13616*
3. Siegel, R. L., Miller, K. D., & Jemal, A. (2020) Cancer statistics, 2020. CA: *A Cancer Journal for Clinicians*, 70(1), 7–30. *doi: 10.3322/caac.21590*
4. Cormie, P., Zopf, E. M., Zhang, X., & Schmitz, K. H. (2017) The impact of exercise on cancer mortality, recurrence, and treatment-related adverse effects. *Epidemiologic Reviews*, 39(1), 71–92. *doi: 10.1093/epirev/mxx007*
5. U.S. Department of Health and Human Services. Physical Activity Guidelines for Americans, 2nd edition, *https://health.gov/sites/default/files/2019-09/Physical_Activity_Guidelines_2nd_edition.pdf* (accessed June 2020)
6. Sol, B. G., Graaf, Y. V., Petersen, R. V., & Visseren, F. L. (2011) The effect of self-efficacy on cardiovascular lifestyle. *European Journal of Cardiovascular Nursing*, 10(3), 180-186. *doi:10.1016/j.ejcnurse.2010.06.005*
7. Bandura, A. (1998) Health promotion from the perspective of social cognitive theory. *Psychology & Health*, 13, 623-649. *doi:10.1080/08870449808407422*
8. Mcauley, E., & Jacobson, L. (1991) Self-efficacy and exercise participation in sedentary adult females. *American Journal of Health Promotion*, 5(3), 185-207. *doi:10.4278/0890-1171-5.3.185*
9. Hallam, J. S., & Petosa, R. (2004) The long-term impact of a four-session work-site intervention on selected social cognitive theory variables linked to adult exercise adherence. *Health Education & Behavior*, 31(1), 88-100. *doi:10.1177/1090198103259164*
10. Mache, S., Jensen, S., Jahn, R., Steudtner, M., Ochsmann, E., & Preuß, G. (2015) Worksite health program promoting changes in eating behavior and health attitudes. *Health Promotion Practice*, 16(6), 826–836. *doi:10.1177/1524839915596310*
11. Hill-Mey, P., Hyatt-Neville, B., Kumpfer, K., Merrill, R., Reel, J., & Richardson, G. (2015) Worksite health promotion programs in college settings. *Journal of Education and Health Promotion*, 4(1), 1-7. *doi:10.4103/2277-9531.154019*
12. Leininger, L. J., Dames, K. D., Adams, K. J., Climstein, M., & Beliso, M. D. (2019) Positive impacts of a university walking program: A case study. *Journal of Physical Activity Research*, 4(1), 57-61. *doi:10.12691/jpar-4-1-7*
13. Aldana, S. G. (2001) Financial impact of health promotion programs: A comprehensive review of the literature. *American Journal of Health Promotion*, 15(5), 296-320. *doi:10.4278/0890-1171-15.5.296*

14. Bopp, M., Bopp, C. M., Duffey, M. L., Ganim, R., & Proctor, D. N. (2015) Implementation and evaluation of an Exercise is Medicine™ on campus week. *Evaluation and Program Planning*, 52, 176–181. doi:10.1016/j.evalprogplan.2015.06.003
15. Melton, B., Williamson, J. A., Bland, H., & Zhang, J. (2016) Using the Exercise is Medicine® on Campus platform to assess college students' practice of physical activity in a rural setting. *Journal of the Georgia Public Health Association*, 5(4), 360-364. doi:10.21633/jgpha.5.402
16. Lynn, J, Urda, J, Winters, C (2015)Slippery Rock University A Case Study of Success in Exercise is Medicine® On Campus, *ACSM's Health & Fitness Journal*, 19(4), 34-36. doi: 10.1249/FIT.0000000000000130
17. Hadley, K., & Morrissey, J. (2019) Psychological constructs as predictors of strength gains in a strength training course. *American Journal of Undergraduate Research*, 16(1), 41–48. *doi: 10.33697/ajur.2019.015*
18. Rodgers, W. M., Markland, D., Selzler, A., Murray, T. C., & Wilson, P. M. (2014) Distinguishing perceived competence and self-efficacy: An example from exercise. *Research Quarterly for Exercise and Sport*, 85, 527-539. *doi:10.1080/02701367.2014.961050*
19. Bandura, A. (1977) Self-efficacy: Toward a unifying theory of behavioral change. *Psychological Review*, 84(2), 191-215. *doi:10.1037/0033-295x.84.2.191*
20. Williams, D. M., Anderson, E. S., & Winett, R. A. (2005) A review of the outcome expectancy construct in physical activity research. *Annals of Behavioral Medicine*, 29(1), 70-79. *doi:10.1207/s15324796abm2901_10*
21. Godin, G. (2011) The Godin-Shepard Leisure-Time Physical Activity Questionnaire. *Health and Fitness Journal of Canada*, 4 (1), 18-22.
22. Lubans, D. R., Aguiar, E. J., & Callister, R. (2010) The effects of free weights and elastic tubing resistance training on physical self-perception in adolescents. *Psychology of Sport and Exercise*, 11(6), 497-504.
23. McAuley, E. (1993) Self-efficacy and the maintenance of exercise participation in the older adults. *Journal of Behavioral Medicine*, 16, 103-113.
24. McAuley, E., Lox, C., Duncan, T. E. (1993) Long-term maintenance of exercise, self-efficacy and psychological change in older adults. *Journal of Gerontology: Psychological Sciences,* 48(4), 218-224.
25. Knight, J. A. (2012) Review of physical inactivity: Associated diseases and disorders. *Annals of Clinical & Laboratory Science*, 42(3), 320-337.
26. Liu-Ambrose, T., Davis, J. C., Nagamatsu, L. S., Hsu, C. L., Katarynych, L. A., & Khan, K. M. (2010) Changes in executive functions and self-efficacy are independently associated with improved usual gait speed in older women. *BMC Geriatrics*, 10(1) *doi:10.1186/1471-2318-10-25*

ABOUT STUDENT AUTHOR

Maximilian Gastelum-Morales will graduate from California State University, Monterey Bay in Fall 2020 with a Bachelor's degree in Kinesiology - Exercise Science. Maximilian is a McNair Scholar and an EIM-OC student leader. Max has had the opportunity to present research findings at the Hawaii International Conference on Education in January 2020, and the ACSM annual conference in May 2020. His future career goals include being a researcher professor within the field of Kinesiology. Areas of study that interest him include biomechanics, physiology, strength & conditioning, and sports medicine.

PRESS SUMMARY

Exercise is Medicine on Campus (EIM-OC) is a worldwide health initiative within higher education institutions. CSUMB's EIM-OC program included an Introduction to Resistance Training class which was offered to all employees. The research design was pre/post; Surveys were completed before the start of the first class and after the end of the last class. Results of this study indicate that employees who participated in EIM-OC improved upon Resistance Training Self-Efficacy and Outcome Expectancy, two variables which are related to exercise adherence. This study adds to the evidence that worksite exercise programs, including RT, can be effective at improving exercise adherence within female employees.

Axisymmetric Thermal Finite Element Analysis of Effects of Intraocular Projector in the Human Eye

John A. Stark[*a], Craig D. Foster[b], & Charles Yu[c]*

[a]*Department of Civil and Materials Engineering, University of Illinois at Chicago, IL*
[b]*Department of Civil and Materials Engineering, University of Illinois at Chicago, IL*
[c]*Department of Ophthalmology, Stanford University, CA*

https://doi.org/10.33697/ajur.2020.035

*Student: jstark24@uic.edu**
Mentor: fosterc@uic.edu

ABSTRACT
Millions of people worldwide live with corneal opacity, which continues to be one of the leading causes of blindness. Corneal opacity is treatable. However, the surgical methods for treating this condition, such as corneal transplantation and keratoprosthesis, have many complications. The use of an intraocular projector is a promising approach to treat corneal blindness. Like any device using electrical power, an intraocular projection device produces heat, which could potentially damage eye tissue. Australian and international standards state that there cannot be an increase of temperature of 2 °C caused by an implanted device. In order to determine if these standards are met, a 2D axisymmetric thermal analysis of the projector in the human eye is conducted in ANSYS Workbench. With the projector operating at its maximum wattage, our analysis shows that an air gap extension within the projector will help maintain the temperature increase below 2 °C.

KEYWORDS
Finite Element Analysis; Eye; Heat Dissipation; Axisymmetric; Thermal Conductivity; Internal Heat Generation; Corneal Blindness; ANSYS; Intraocular Projector

INTRODUCTION

Disease, infection, wounds, inflammation, scarring, or damage to the cornea of the human eye can cause corneal blindness. These causes can increase corneal opacity, resulting in an indistinct or no image on the retina.[1] Two well-known surgical procedures for treating corneal blindness are corneal transplantation, also known as keratoplasty, and keratoprosthesis. The process of corneal transplantation generally consists of replacing the damaged cornea with a donor cornea. This surgery has resulted in many complications including the loss of 30–40% of donor endothelial cells, transplant rejection, astigmatism, choroidal hemorrhage, and many more.[2] In addition to these complications, there is a shortage of donor corneas, with over 50% of the world population having no access to a donor cornea. This shortage results in about 13 million people on waitlists for this surgery.[3] The Boston Keratoprosthesis Type 1 is a common alternative to corneal transplantation considering this shortage of donor corneas. The process of this surgery consists of replacing the damaged cornea with an artificial nonbiologic cornea. However, this artificial cornea's design and material interact with the human eye, resulting in increased risk for infection.[4]

With all the complications, infections from these surgeries, and shortage of donated corneas, an intraocular projector, also known as a micro-camera, has been proposed, with prototypes developed.[4] The projector takes in video from an external camera, then sends it through a transmission coil, to be later sent to a receiver coil. The receiver transmits this video to a processor to be decoded and sent to a micro-display. The micro-display inside the internal camera projects the image onto the retina. The internal micro-camera consists of a plastic shell, reflector, glass lens, micro-display and LED.[4] As the camera operates, the LED and micro-display create heat. The micro-display stays at a constant power and the LED can be set at different wattages. The larger the wattage, the brighter the picture quality will be displayed on the retina. Generated heat coming from the LED and micro-display flows through the camera and out into the tissues of the human eye. The closest eye tissue to the camera is the iris. According to the AIMD safety standards (ISO 14708-1:2014 / EN 45502-1:1997), the camera cannot cause an increase in temperature of 2 °C on any eye tissue, therefore the heat generated by the LED and micro-display needs to be analyzed, especially at the iris.[5]

Thermal finite element analysis has already proven useful for a wide variety of applications in the eye. Scott performed one of the earliest thermal finite element analyses of the eye to examine heat flow.[6] She later used the model to examine the temperature rise due to infrared radiation.[7] Shabib used finite element analysis to evaluate potential thermal damage from an IR laser.[8] Jafarbadi *et al.* also examined the effects of laser radiation.[9] Opie *et al.* used a thermal finite element model of a cat eye to establish that a 5 × 5 mm suprachoroidal heating device cannot dissipate more than 135 mW through the retina in order to keep the temperature change within 2 °C.[10] Gosalia *et al.* utilized a 3D thermal finite element model of the human head and eye to discover the resulting temperature changes when implanted simulator chips of a retinal prosthesis are surgically placed in the eye.[11] Through this thermal modeling, Lazzi *et al.* determined that the smaller chip located in the center of the eye creates a higher temperature rise.[12] Wessapan and Rattanadecho evaluated potential thermal problems from sauna therapy.[13] Rafiq and Khanday incorporated blood perfusion and porosity into the thermal model.[14] Through such studies, the thermal properties of the various tissues in the eye have been well characterized.

The purpose of this study is to provide a preliminary analysis of the impact of the intraocular projector on the temperature inside the eye. A two-dimensional, axisymmetric model is an efficient way to conduct such analysis. The geometry creation, meshing, and analysis are all quicker in two dimensions than three. While the eye is relatively axisymmetric as described by Thompson *et al.*,[15] the projector is not. Hence, eventually a three-dimensional model will be developed. The 2D is useful, however, in examining how changes in the camera model affect the temperature in the iris, as well as verifying the 3D model.

METHODS AND PROCEDURES

Geometry of 2D Axisymmetric Human Eye Model with Intraocular Projector

Every part of the human eye and projector are modeled in Solidworks. Each part has its own sketch file which are transferred into an assembly file. There are three assembly files, one being without the camera, and two with the camera at different positions in the eye. The assembly files were then transferred into ANSYS Workbench Steady-State Thermal so that a thermal finite element analysis can be conducted in order to test the temperature change amongst the parts of the eye.

A 2D CAD model of the human eye was developed in Solidworks to be axisymmetric about the eye's central axis. The human eye consists of the following parts: cornea, iris, limbus, aqueous humor, ciliary body, cortex lens, nucleus lens, vitreous humor, retina, choroid, sclera, and optic nerve head. The dimensions for each part were based upon the dimensions from the U.S Army Research Laboratory[15] and an internal report.[16]

The cornea was modeled first, then the limbus, ciliary body, iris, retina, choroid, optic nerve head (ONH), and iris. For simplicity, the iris was modeled after the exact iris created by Pawar.[16] The aqueous humor and vitreous humor were then modeled; however, their shape is dependent on the parts surrounding it. The lens of the eye is split into two different regions called the cortex and nucleus lens. Equations from Thompson *et al.* were used to develop the cortex and nucleus lens.[15] A set of points and spline curve were then used to make the part of the zonule fibers that is flush with the vitreous humor. The other edges of the zonule fibers are made from the parts of the shells of the aqueous humor and ciliary body.[15, 16] Each part was given surface planes and then imported into a Solidworks Assembly file.

The model was then edited so that the zonule fibers, and lens were removed. These parts are physically removed during surgery to make space for the camera. The camera developed by the University of Illinois team was then modeled in Solidworks. The camera is not symmetric about a central axis, so dimensions were changed in order to conserve volume. The camera consists of a casing, reflector, micro-display, LED, and lens.[4] Each part was modeled in its own Solidworks file and was then imported into the assembly file without the zonule fibers and lens. The vitreous humor was remodeled in according to where the camera would be placed. The changed camera dimensions are displayed in **Figure 1**.

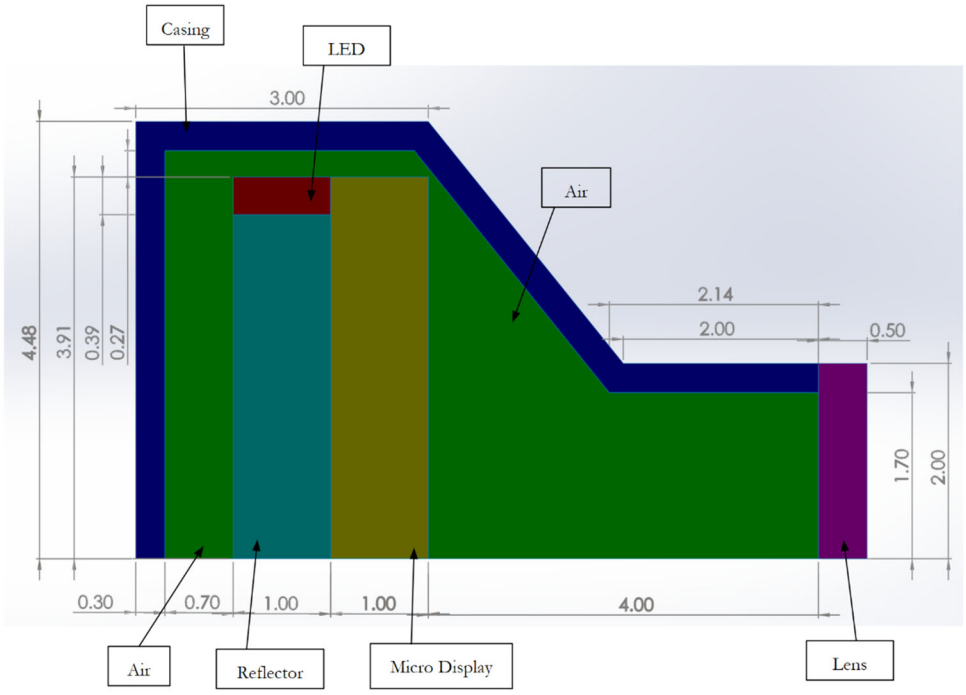

Figure 1. Intraocular Projector (Camera) with Part Descriptions and Dimensions (mm)

The original projector, at its highest power setting for the LED, caused a temperature increase greater than 2 °C in the iris at a temperature over 39 °C. Several solutions were attempted to improve the thermal dissipation, including changing materials, adding a thermal paste, and adding a conducting material that would dissipate more heat out of the front of the camera. The best solution was to extend the back of the camera 0.5 mm, adding an air gap that acts as an insulator. This insulation pushes more heat out the front and away from the closest living tissues. Only the results from this option and the original projector model are shown in this report. Models 1 and 2 are displayed below in **Figure 2** and **Figure 3** representing the eye model with the different cameras.

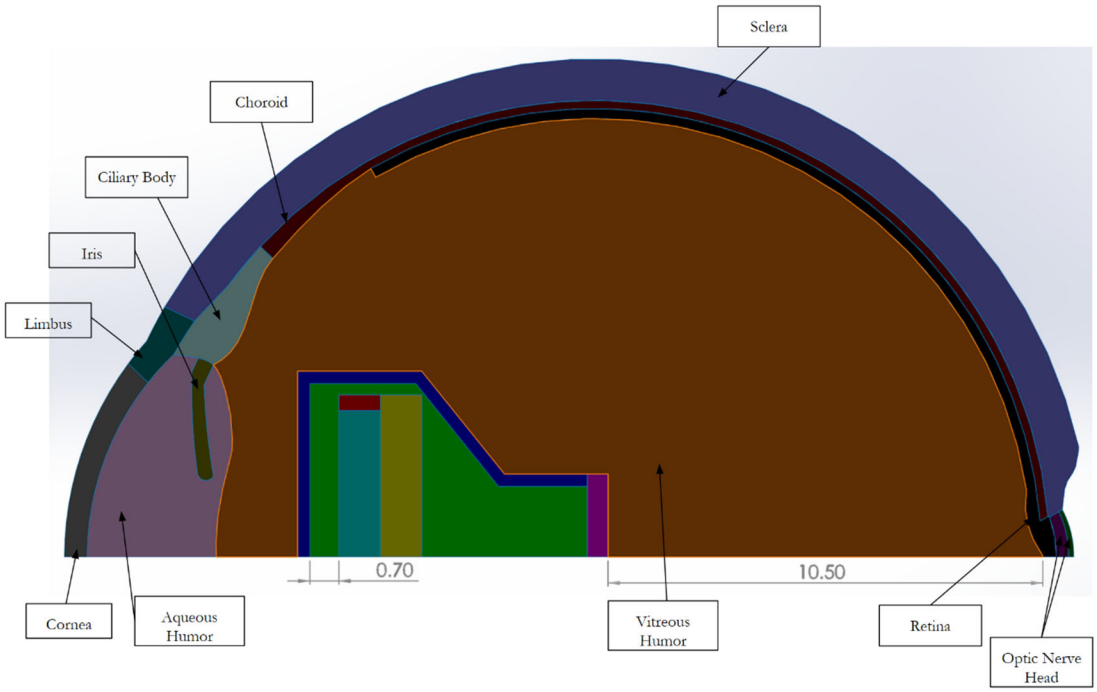

Figure 2. Model 1; Human Eye with Part Descriptions, Original Projector, and Dimensions (mm)

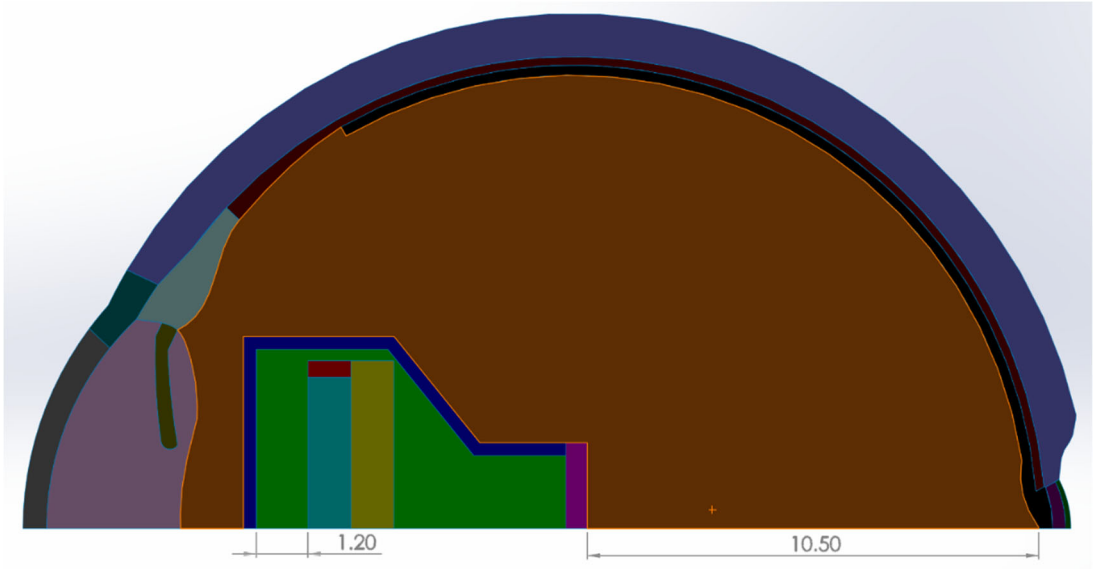

Figure 3. Model 2; Human Eye with Projector and 0.5 mm Air Gap Extension (mm)

Steady State Thermal Analysis

Models 1 and 2 were converted into IGS files which were then transferred into ANSYS Workbench. Steady-State Thermal Analyses were created for the assembly files. For the import geometry settings, the analysis was set to 2D with only surface bodies allowed to be imported. The 2D behavior for geometry was also set to axisymmetric.

Material Properties of Eye and Projector Parts

Each material in the eye and camera has a specific thermal conductivity value associated with it. Thermal conductivity values measure how easily heat is transferred through the eye. Therefore, they are important to accurately assess how quickly and in what directions heat will dissipate from the eye. The PMMA and ABS plastics can have somewhat different compositions and manufacturing conditions, and therefore have a range of thermal conductivity values. The values for air and glass were taken directly from ANSYS. The thermal conductivity values are displayed in **Table 1**.

Part	Thermal Conductivity (W/m °C)	Reference Number
Cornea	0.58	**10**
Sclera	0.58	**10**
Choroid	0.6	**10**
Iris	1.0042	**17**
Optic Nerve Head (ONH)	1.0042	**17**
Retina	0.565	**10**
Aqueous Humor	0.58	**17**
Ciliary Body	0.498	**17**
Limbus	0.58	**17**
Saline Solution	0.603	**18, 19**
Air	0.0242	
PMMA	0.1922 - 0.1986	**20**
ABS Plastic	0.14 - 0.21	**21**
Glass	0.8	

Table 1. Thermal Conductivity Values of Eye and Camera Parts

The eye parts were assigned their corresponding thermal conductivity values in ANSYS. During the procedure of inserting the camera into the eye, the vitreous humor will be replaced with saline solution, so that area was given the thermal conductivity value of saline solution. The LED and Reflector are made of ABS plastic. Considering this thermal conductivity value has a range, the decision was made to make the value 0.175 W/m °C which is the midpoint of this range of these values. Analysis was also

conducted at both extremes for the range of these values for ABS plastic, but there was no significant change in temperature of any part of the eye tissue. The micro-display and camera lens were given the material of glass. Lastly, the camera casing was given the material of PMMA. PMMA also has a range of thermal conductivity values, and these values are linearly related to temperature.[20] The value used in this study was 0.19289 W/m °C.

Meshing

The meshing for Models 1 and 2 were generated in ANSYS. To simplify the meshing process, Automatic Mesh Defeaturing was turned to Off. Model 1 consists of 5,270 nodes and 1,469 elements. Model 2 consists of 5,161 nodes and 1,430 elements. The mesh for both models were not further refined because the mesh was adequate for the analysis to be performed. The meshing for each model is shown in **Figure 4**.

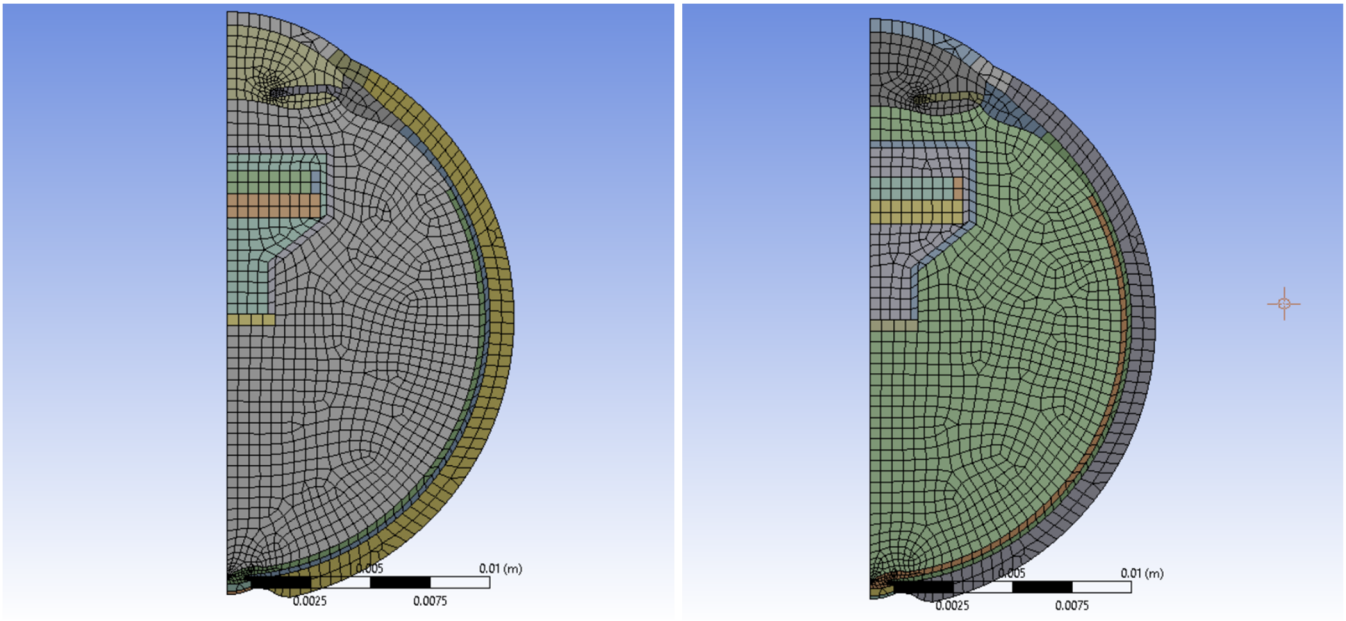

(a) (b)

Figure 4. (a) Meshing for Model 1; (b) Meshing for Model 2

Boundary Conditions

The thermal conditions at the boundary of the eye vary by location. A temperature of 37 °C is applied on the surface of the sclera because normal body temperature is 37 °C.[6] Convection of 37 °C with film coefficient 65 W/m^2 °C is applied on the surface of the sclera as well.[10] An external temperature of 40 °C is chosen for the cornea and limbus to represent an extreme outside temperature. A film coefficient 10 W/m^2 is also applied.[6] Outward heat flux of 40 W/m^2 and radiation with emissivity of 0.975 is applied on the surface of the cornea and limbus as well.[6] Internal heat generation is applied to the bodies of the micro-display and LED because these parts are a power source and are generating heat. The input for internal heat generation in ANSYS is in W/m^3. The micro-display will only be set at 25 mW for this analysis; however, the LED will be set at four different wattages of 25 mW, 50 mW, 75 mW, and 100 mW. Using these wattages and the geometry of the parts of the camera, the internal heat generation values were calculated and are shown in **Table 2**.

		Internal Heat Generation (W/m^3)			
Part	**Volume (m^3)**	25 mW	50 mW	75 mW	100 mW
LED	9.00×10^{-9}	2.78×10^{6}	5.56×10^{6}	8.33×10^{6}	1.11×10^{7}
Micro-Display	4.80×10^{-8}	5.21×10^{5}			

Table 2. Internal Heat Generation of Micro-Camera Parts at Different Wattages

The LED is set at these four wattages because as there is more power, there is more heat flowing through the eye and thereby causing a larger increase in temperature of an eye tissue. 25 mW is the minimum power that the LED will be set at in order for the camera to work properly. The maximum power at which the LED can be set is 100 mW. This setting provides the brightest picture to the retina. The goal is to pinpoint which wattage does not cause an increase of 2 °C to stay within AIMD standards.

RESULTS AND DISCUSSION

The analysis conducted in ANSYS was completed by solving for the final temperatures in Models 1 and 2. The final solutions for the analysis at 25 mW, 50 mW, and 75 mW did not display a temperature over 39 °C, which is 2 °C above the original temperature of the eye at 37 °C, at any eye tissue for these two models. At 100 mW the iris does exceed over 39 °C for Model 1 which does not abide by AIMD standards. The final solution for Model 1 is portrayed in **Figure 5**.

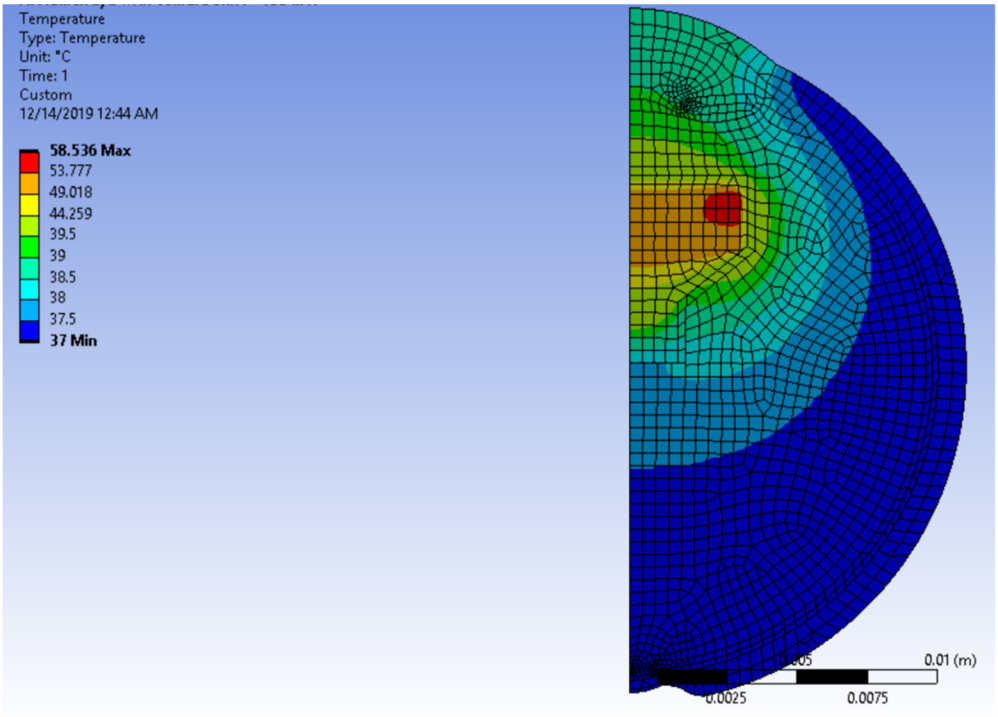

Figure 5. Model 1 Analysis Temperature Solution at 100 mW

The major heating issue is that too much heat escapes from the back of the camera and heats the iris, as shown in the heat flux plot in **Figure 6**.

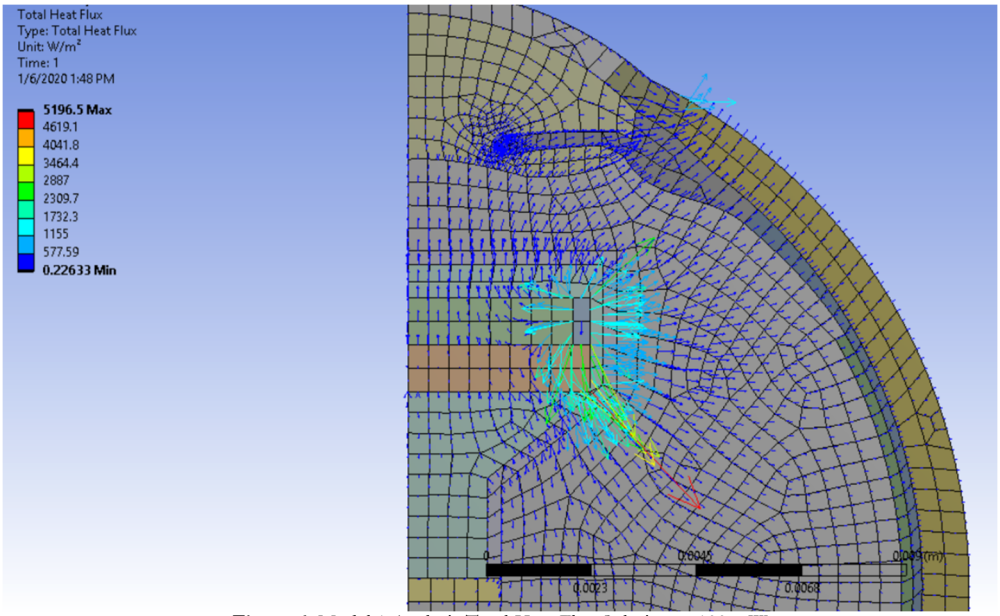

Figure 6. Model 1 Analysis Total Heat Flux Solution at 100 mW

Model 2 contains an extended air gap of 0.5 mm within the camera. Air is a great insulator if it can be contained and with this update in geometry compared to Model 1, iris temperatures were kept below 39 °C at all wattages. **Figure 7** displays the solution for Model 2 at 100 mW.

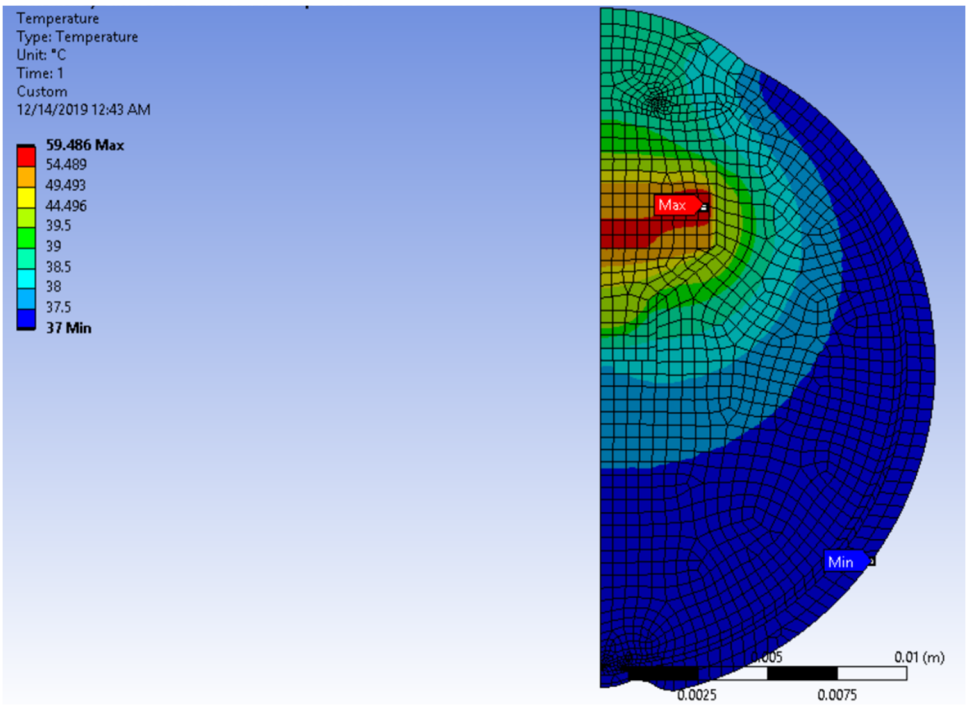

Figure 7. Model 2 Analysis Temperature Solution at 100 mW

The final maximum temperatures of the iris for both Models are below in **Table 3**. As seen in the table, the maximum iris temperature at 100mW for Model 1 exceeds 39 °C by 0.002 °C. For Model 2, the iris temperature achieved a maximum of 38.766 °C which is below 39 °C thereby not resulting in more than a 2 °C increase.

Power (mW)	Model 1 Max Iris Temperature (°C)	Model 2 Max Iris Temperature (°C)
25	38.006	37.928
50	38.337	38.207
75	38.67	38.486
100	39.002	38.766

Table 3. Maximum Iris Temperatures for Models 1 and 2 at 100 mW

There is roughly a linear relationship between the wattage of the LED and the maximum temperature of the iris. This relationship is portrayed in a graph in **Figure 8**.

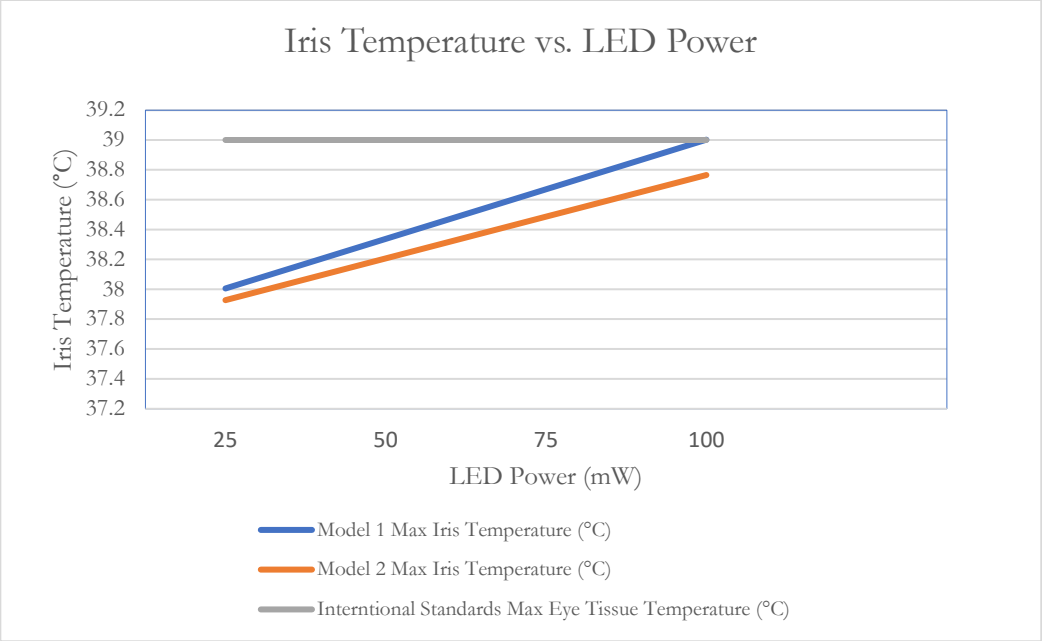

Figure 8. Graphical Representation of the Linear Relationship between Maximum Iris Temperature and LED Power

CONCLUSIONS

In this study, the temperature distribution across two 2D axisymmetric eye models were analyzed. AIMD standards have stated that a device, such as this intraocular projector, cannot cause more than a 2 °C increase in eye tissue temperature. Two Solidworks models were imported into ANSYS with specific boundary conditions to study if these standards were met. These two models consisted of one model with the original projector design, and another model including the second projector with an added 0.5 mm air gap. The two models were tested at 25 mW, 50 mW, 75 mW, and 100 mW of power produced in the LED. Model 1 showed an increase of at least 2 °C for 100 mW. Considering the camera works best at 100 mW, because it outputs the best image onto the retina, Model 2 had a 0.5 mm air gap extension to insulate heat better within the camera. This caused temperatures of the iris to stay within 39 °C. Based upon this eye model with the 0.5 mm air gap, the intraocular projector can safely be operated with 100 mW of power from the LED.

ACKNOWLEDGEMENTS

The first author gratefully acknowledges support of the University of Illinois at Chicago College of Engineering Guaranteed Paid Internship Program. The authors would like to thank Dipika Gongal, Siddhant Tahkur, Ashay Panse, Rahul Pawar and Torna Patil for their help with dimensions of the eye model and guidance in the finite element analysis. This research is partially funded by US Department of Defense grant *VR180058* and US NIH National Eye Institute grant *K08EY27469*, and that support is gratefully acknowledged.

REFERENCES

1. Whitcher, Srinivasan J. M., and Upadhyay, M. (2001) Corneal blindness: a global perspective, *Bull World Health Organ.*, 214-221.
2. Tan, D., Dart, J., Holland, E. and Kinoshita, S. (2012) Corneal transplantation, *The Lancet*, 379(9827), 1749-1761. *https://doi.org/10.1016/s0140-6736(12)60437-1*
3. Gain, P., *et al.*, (2016) Global Survey of Corneal Transplantation and Eye Banking, *JAMA Ophthalmology*, 134(2), 167. *https://doi.org/10.1001/jamaophthalmol.2015.4776*
4. Yu, C. *et al.*, (2019) Feasibility of Intraocular Projection for Treatment of Intractable Corneal Opacity, *Cornea*, 38(4), 523-527. *https://doi.org/10.1097/ico.0000000000001852*
5. ISO 14708-1:2014, ISO, 2019. Available: https://www.iso.org/standard/52804.html. (Accessed: 26- Nov- 2019).
6. Scott, J. (1988) A finite element model of heat transport in the human eye, *Physics in Medicine and Biology*, 33(2), 227-242. *https://doi.org/10.1088/0031-9155/33/2/003*
7. Scott, J. (1988) The computation of temperature rises in the human eye induced by infrared radiation, *Physics in Medicine and Biology*, 33(2), 243-257. *https://doi.org/10.1088/0031-9155/33/2/004*
8. Shibib, K. (2012) Finite element analysis of cornea thermal damage due to pulse incidental far IR laser, *Lasers in Medical Science*, 28(3), 871-877. *https://doi.org/10.1007/s10103-012-1168-2*

9. Mirnezami, S. Rajaei Jafarabadi, M. and Abrishami, M., (2013) Temperature Distribution Simulation of the Human Eye Exposed to Laser Radiation, *Journal of lasers in medical sciences*, 4, 176-182. *https://doi.org/10.22037/jlms.v4i4.3928*

10. Opie, N., Burkitt, A., Meffin, H., Grayden, D. (2012) Heating of the Eye by a Retinal Prosthesis: Modeling, Cadaver and In Vivo Study, *IEEE Transactions on Biomedical Engineering*, 59(2), 339-345. *https://doi.org/10.1109/tbme.2011.2171961*

11. Gosalia, K., Weiland, J., Humayun, M., and Lazzi, G. (2004) Thermal Elevation in the Human Eye and Head Due to the Operation of a Retinal Prosthesis, *IEEE Transactions on Biomedical Engineering*, 51(8), 1469-1477. *https://doi.org/10.1109/tbme.2004.827548*

12. Lazzi, G. (2005) Thermal effects of bioimplants, *IEEE Engineering in Medicine and Biology Magazine*, 24(5), 75-81. *https://doi.org/10.1109/memb.2005.1511503*

13. Wessapan, T., and Rattanadecho, P. (2015) Heat Transfer Analysis of the Human Eye During Exposure to Sauna Therapy, *Numerical Heat Transfer, Part A: Applications*, 68(5), 566-582. *https://doi.org/10.1080/10407782.2014.986393*

14. Rafiq, A., and Khanday, M. (2016) Thermal behavior of human eye in relation with change in blood perfusion, porosity, evaporation and ambient temperature, *Journal of Thermal Biology*, 62, 138-142. *https://doi.org/10.1016/j.jtherbio.2016.06.024*

15. Thompson, K., Bhardwaj, R., Nguyen, T. (2017) Development of an Anatomically Accurate Finite Element Human Ocular Globe Model for Blast-Related Fluid-Structure Interaction Studies. US Army Research Laboratory report ARL-TR-7945

16. Pawar, R. (2018) Design and Finite Element Analysis of effects of Therapeutic Hypothermia in Human Eye, University of Illinois at Chicago.

17. Wessapan, T., and Rattanadecho, P. (2015) Heat Transfer Analysis of the Human Eye During Exposure to Sauna Therapy, *Numerical Heat Transfer, Part A: Applications*, 68(5), 566-582. *https://doi.org/10.1080/10407782.2014.986393*

18. Nayar, K., Sharqawy, M., Banchik, L., and Lienhard, J. (2016) Thermophysical properties of seawater: A review and new correlations that include pressure dependence, *Desalination*, 390, 1-24. *https://doi.org/10.1016/j.desal.2016.02.024*

19. Sharqawy, M., Lienhard, J., and Zubair, S. (2010) Thermophysical properties of seawater: a review of existing correlations and data, *Desalination and Water Treatment*, 16(1-3), 354-380. *https://doi.org/10.5004/dwt.2010.1079*

20. Assael, M., Botsios, S., Gialou, K., and Metaxa, I. (2005) Thermal Conductivity of Polymethyl Methacrylate (PMMA) and Borosilicate Crown Glass BK7, *International Journal of Thermophysics*, 26(5), 1595-1605. *https://doi.org/10.1007/s10765-005-8106-5*

21. The Thermal Conductivity of Unfilled Plastics - C-Therm - Thermal Conductivity Instruments, https://ctherm.com/resources/blog/the_thermal_conductivity_of_unfilled_plastics/. (Accessed: 26- Nov- 2019).

ABOUT THE AUTHORS

John Stark is a Junior Civil Engineering Student at the University of Illinois at Chicago (UIC) and plans on graduating with a bachelor's degree in May 2022. John has been working on this project since the summer of 2019 through the Guaranteed Paid Internship Program at UIC. He plans to continue researching the method of finite element analysis and develop a focus in structural engineering within his major.

Craig Foster is a professor of Civil and Materials Engineering at University of Illinois at Chicago. His research focuses on numerical modeling, especially finite element analysis, of mechanical, thermal, and multiphysics problems.

Charles Yu is an ophthalmologist at the Byers Eye Institute at Stanford University. His research focuses on medical devices for vision restoration.

PRESS SUMMARY

Corneal blindness continues to be a problem for millions of people across the world. An intraocular projector, also known as a micro-camera, is a novel proposed solution to this problem and is surgically placed inside the eye. The projector creates heat, which must be dissipated without causing damage to eye tissue. Australian and international standards state that there cannot be an increase of temperature of more than 2 °C from an implanted device; therefore, a simulation needs to be conducted to test if these standards are met. The eye and projector were designed in the CAD software, Solidworks, as a 2D axisymmetric model. The model was then analyzed in ANSYS Workbench finite element software to study the temperature change in the eye tissue as the projector is operating.

Prime Factors and Divisibility of Sums of Powers of Fibonacci and Lucas Numbers

*Spirit Karcher, Mariah Michael**

Department of Mathematics, Christopher Newport University, Newport News, VA

https://doi.org/10.33697/ajur.2020.036

*Students: spirit.karcher.13@cnu.edu, mariah.michael.16@cnu.edu**
Mentor: jessica.kelly@cnu.edu

ABSTRACT
The Fibonacci sequence, whose first terms are $\{0, 1, 1, 2, 3, 5, \ldots\}$, is generated using the recursive formula $F_{n+2} = F_{n+1} + F_n$ with $F_0 = 0$ and $F_1 = 1$. This sequence is one of the most famous integer sequences because of its fascinating mathematical properties and connections with other fields such as biology, art, and music. Closely related to the Fibonacci sequence is the Lucas sequence. The Lucas sequence, whose first terms are $\{2, 1, 3, 4, 7, 11, \ldots\}$, is generated using the recursive formula $L_{n+2} = L_{n+1} + L_n$ with $L_0 = 2$ and $L_1 = 1$. In this paper, patterns in the prime factors of sums of powers of Fibonacci and Lucas numbers are examined. For example, $F_{3n+4}^2 + F_{3n+2}^2$ is even for all $n \in \mathbb{N}_0$. To prove these results, techniques from modular arithmetic and facts about the divisibility of Fibonacci and Lucas numbers are utilized.

KEYWORDS
Fibonacci Sequence; Lucas Sequence; Modular Arithmetic; Divisibility Sequence

INTRODUCTION

In the year 1202, Leonardo of Pisa, later known as Fibonacci, published a book entitled *Liber Abacci* or *Book of Calculation* which was one of the first European texts on algebra.[1, 2] Since Fibonacci was a merchant, the majority of his book focused on the Hindu-Arabic numerals and their practical applications in money conversions, profit margins, and other areas in commerce. However, at the end of *Liber Abbaci*, Fibonacci added a section of brain teasers and the solution to his most famous problem is still being studied today. The question posed was this:

If a pair of rabbits is placed in an enclosed area, how many pairs of rabbits will there be after a year if the following assumptions are made:

1. *Every month a pair of rabbits produces another pair*
2. *Rabbits begin to bear young two months after their birth and*
3. *None of the rabbits die*

To solve this problem, the pairs of rabbits at the end of each month are counted. Initially, one pair of rabbits is in the enclosed area ($F_0 = 1$). After the first month, there will still be one pair of rabbits as the first pair is still unable to bear young ($F_1 = 1$). After the second month, there will be two pairs of rabbits as the original pair will produce a pair of young ($F_2 = 2$). After third month, there will be three pairs of rabbits as only one pair (the original) will be able to reproduce ($F_3 = 3$). After the fourth month, there will be two pairs able to reproduce so there will be five total pairs ($F_4 = 5$). After the fifth month, there will be three pairs able to reproduce so there will be eight total pairs ($F_5 = 8$). Continuing in this manner, the pairs of rabbits may be counted for infinitely many months.

The sequence of numbers that results from this riddle is:

$$1,\ 1,\ 2,\ 3,\ 5,\ 8,\ 13,\ 21,\ 34,\ 55,\ 89,\ 144,\ \ldots \qquad \textbf{Equation } 1.$$

This sequence was named the Fibonacci sequence after its creator and its terms became known as Fibonacci numbers. This sequence has numerous special properties and a variety of applications in the field of mathematics. Although it has been studied for centuries, the Fibonacci sequence continues to be a topic of study by mathematicians today. In fact, *The Fibonacci Quarterly* is a journal entirely dedicated to advances in mathematics related to Fibonacci numbers.[3]

Related to the Fibonacci sequence is the Lucas sequence.[2] The Fibonacci and Lucas sequences share the same recursive formula but the initial conditions differ. These well-known sequences are two members of a larger family of recursive sequences.[4–6] The focus of this paper is exploring patterns in the prime factors of sums of powers of Fibonacci and Lucas numbers.

Background

The recursive relationship of the Fibonacci sequence is formally defined as

$$F_{n+2} = F_{n+1} + F_n, \text{ for } n \in \mathbb{N}_0 \text{ with } F_0 = 0 \text{ and } F_1 = 1. \qquad \textbf{Equation } 2.$$

Notice that the the sequence in **Equation** 1. relates to the sequence defined in **Equation** 2. by $F_m = F_{n+1}$ for $m \in \mathbb{N}_0$. The enumeration of the sequence defined in **Equation** 2. simplifies calculations and will be used for the remainder of the paper.

For the Lucas sequence, the recursive relationship is defined as

$$L_{n+2} = L_{n+1} + L_n, \text{ for } n \in \mathbb{N}_0 \text{ with } L_0 = 2 \text{ and } L_1 = 1. \qquad \textbf{Equation } 3.$$

The Fibonacci and Lucas number sequences are two members of a larger family of recursive sequences. This larger family contains sequences called the general Lucas sequences of the first and second kind.[4–6]

For integers P and Q, the nth term of general Lucas sequence of the first kind, $U_n(P,Q)$, is defined by

$$U_{n+2}(P,Q) = PU_{n+1}(P,Q) - QU_n(P,Q), \text{ for } n \in \mathbb{N}_0$$

$$\text{with } U_0(P,Q) = 0 \text{ and } U_1(P,Q) = 1\,,$$

while the nth term of a general Lucas sequence of the second kind, $V_n(P,Q)$, is defined by

$$V_{n+2}(P,Q) = PV_{n+1}(P,Q) - QV_n(P,Q), \text{ for } n \in \mathbb{N}_0$$

$$\text{with } V_0(P,Q) = 2 \text{ and } V_1(P,Q) = 1\,.^4$$

For $P = 1$ and $Q = -1$, the Lucas sequence of the first kind is the Fibonacci numbers, while the Lucas sequence of the second kind is the Lucas numbers.

Motivation

The motivation for working with sums of powers of Fibonacci and Lucas numbers came from the results of Arangala et al.[7] The authors explore finding closed form equations for sums of even powers of Fibonacci and Lucas numbers with indices that differ by two. For example,

$$F_n^2 + F_{n-2}^2 = 3F_{n-1}^2 + 2(-1)^{n-1}\,.$$

The proofs of Arangala et al. provide a foundation for useful techniques involving the identities and equations from above to manipulate sums of powers of Fibonacci numbers. The theorems were extended to Fibonacci numbers that had indices which differed by $k \equiv 0 \bmod 4$ rather than differing by 2. For example, when extended to have the indices differ by $k \equiv 0 \bmod 4$ the result above becomes:

$$F_n^2 + F_{n-k}^2 = L_k F_{n-\frac{k}{2}}^2 + 2F_{\frac{k}{2}}^2(-1)^{n-\frac{k}{2}} \text{ where } L_k \text{ is the } k^{th} \text{ Lucas number.}$$

Expanding on the ideas of Arangala et al., the results in this paper come from answering the following questions:

- Are there patterns in the prime factors of the sum $F_n^2 + F_{n-2}^2$ for all $n \geq 2$?
- If so, what are they? And can these patterns be written in a way that holds for all $n \in \mathbb{N}_0$?
- How can the result for Fibonacci numbers be extended to the Lucas numbers and more generally, Lucas sequences of the first and second kind?

Studying results related to powers and the divisibility of Fibonacci and Lucas numbers is of particular interest to numerous mathematicians.[5, 6, 8–16]

PRELIMINARIES

Recall that given an integer m and an integer n such that $0 \leq n \leq m$, there exists integers k and r with $0 \leq r < n$ such that $m = kn + r$. The integer, r, is called the remainder modulo n. Working with the remainder r as opposed to the number m itself is called modular arithmetic. Modular arithmetic is similar to standard arithmetic in many ways but it does have a few special properties. In modular arithmetic there is not strict equality. Rather there is congruence of numbers using their remainders.

Definition: Let n be a positive integer and let a and b be any integers. Then a is *congruent* to $b \bmod n$ written, $a \equiv b \bmod n$, if a and b have the same remainder when divided by n.

Modular arithmetic is useful when working with large integers because it simplifies problems by replacing an integer, m, with its remainder, r, when divided by a fixed positive integer, n.

Definition: An integer, a, is *divisible* by n, if $a \equiv 0 \bmod n$. Equivalently, if there exists an integer, k, such that $a = nk$.

For example, $7 \equiv 1 \bmod 2$ as $7 = 2(3) + 1$; that is the remainder of 7 when divided by 2 is 1. As well as, $10 \equiv 0 \bmod 2$ since $10 = 2(5) + 0$; the remainder is 0. In other words, 10 is divisible by 2.

Recall that all odd numbers can be written as $2k + 1$ where k is an integer and all even numbers can be written as $2k$ for some integer k. Then it follows that for any integer m:

$$m \equiv \begin{cases} 0 \bmod 2 & \text{if m is even} \\ 1 \bmod 2 & \text{if m is odd.} \end{cases}$$

Three propositions related to modular arithmetic are presented below. Proposition 1 utilizes the definition for even and odd integers. Additionally, Propositions 2 and 3 concern sums and products under modular arithmetic. For the interested reader, additional results related to modular arithmetic may be found in any introduction discrete mathematics or number theory book.[17–19]

Proposition 1.

i. The sum of two odd numbers is an even number.

ii. The sum of two even numbers is an even number.

iii. The sum of an even number and an odd number is an odd number.

iv. The product of two even numbers is an even number.

v. The product of two odd numbers is an odd number.

vi. The product of an even number and an odd number is an even number.

The proof for iii and vi are shown below and the proofs for the other results are left to the reader.

Proof. For iii:

Without loss of generality, let n and m be an even and odd number respectively. Then,

$$n = 2k \text{ and } m = 2l + 1$$

for integers k and l. Then,

$$n + m = 2k + (2l + 1) = (2k + 2l) + 1 = 2(k + l) + 1\,.$$

Since the integers are closed under addition, $k + l$ is an integer. Therefore $n + m$ is an odd number. □

Proof. For vi:

Without loss of generality, let n be an even number and m be an odd number. Then,

$$n \cdot m = 2k(2l + 1) = 4kl + 2k = 2(2kl + k)\,.$$

Since the integers are closed under addition, $2kl + k$ is an integer. Therefore, nm is an even number. □

Addition of numbers under modular arithmetic works as expected. Computations may be done with only the remainders.

Proposition 2.

$$(a \bmod n) + (b \bmod n) \equiv (a + b) \bmod n.$$

Proof. Suppose there exist two numbers, such that the first is congruent to a mod n and the second is congruent to b mod n; then the first is may be written as $nk + a$ and the second as $nl + b$ for integers k and l. Then the sum of these two numbers under mod n arithmetic is given by

$$(a \bmod n) + (b \bmod n) \equiv (nk + a) + (nl + b)\,.$$

The right hand side may be rewritten as

$$\begin{aligned}(nk + a) + (nl + b) &= (nk + nl) + (a + b)\\ &= n(k + l) + (a + b)\,.\end{aligned}$$

Therefore,

$$(nk + a) + (nl + b) \equiv (a + b) \bmod n\,,$$

and

$$(a \bmod n) + (b \bmod n) \equiv (a + b) \bmod n$$

from the definition of congruence mod n from above. □

Note that this property for addition under modular arithmetic provides an alternative proof for the properties (i)-(iii) of even and odd numbers in Proposition 1. For example, the proof of Proposition 1(iii) is simplified to: For an odd number, m, and even number, n, $m \equiv 1 \bmod 2$ and $n \equiv 0 \bmod 2$, and so $m + n \equiv (1 + 0) \bmod 2 \equiv 1 \bmod 2$.

Proposition 3.

$$(a \bmod n) \cdot (b \bmod n) \equiv (a \cdot b) \bmod n.$$

Note that this property for multiplication under modular arithmetic provides an alternative proof for the properties (iv)-(vi) of even and odd numbers in Proposition 1.

These propositions allow us to easily determine when a sum (or product) of Fibonacci and Lucas numbers is divisible by a given n. For example, using **Equation** 2., for any F_n if the sum of the previous two is equivalent to $0 \bmod n$ then the sum is divisible by n.

From the properties of modular arithmetic, it may be observed that the Fibonacci numbers follow an interesting pattern under mod 2 arithmetic. As $F_1 = F_2 = 1$, both are congruent to 1 mod 2. From Proposition 1(i), the sum of two odd numbers is even; so $F_1 + F_2 = 1 + 1 \equiv 0 \bmod 2$. However by **Equation** 2., $F_1 + F_2 = F_3$. From here, $F_2 + F_3$, is an odd number plus an even number so $F_4 \equiv 1 \bmod 2$. The pattern of the Fibonacci numbers under mod 2 arithmetic continues throughout the entire sequence as follows:

$$1,\ 1,\ 0,\ 1,\ 1,\ 0,\ 1,\ 1,\ 0,\ 1,\ 1,\ 0,\ \ldots$$

This observation that every third Fibonacci number is divisible by 2 demonstrates a much more powerful property of the Fibonacci numbers. It is a well known result that the Fibonacci numbers are an example of a divisibility sequence.[10, 11]

Definition: A *divisibility sequence* is an integer sequence, $\{a_n\}$, indexed by positive integers n, such that if m divides n then a_m divides a_n.

There are many well known properties that follow from the Fibonacci numbers forming a divisibility sequence. These will be used to prove conjectures about the prime factors in sums of squares and cubes of Fibonacci numbers later in the paper.

Proposition 4. *i. Two divides every third Fibonacci number.*

ii. Three divides every fourth Fibonacci number.

iii. Five divides every fifth Fibonacci number.

Proof. To show (i), recall that $F_3 = 2$. From the definition of a divisibility sequence, this means that F_3 divides F_{3k} for all $k \in \mathbb{N}_0$. Therefore, all Fibonacci numbers whose index is divisible by 3 are divisible by 2. To show (ii), recall that $F_4 = 3$. From the definition of a divisibility sequence, this means that F_4 divides F_{4k} for all $k \in \mathbb{N}_0$. Therefore, all Fibonacci numbers whose index is divisible by 4 are divisible by 3. Lastly, to show (iii), recall that $F_5 = 5$. From the definition of a divisibility sequence, this means that F_5 divides F_{5k} for all $k \in \mathbb{N}_0$. Therefore, all Fibonacci numbers whose index is divisible by 5 are divisible by 5. □

The reader may observe interesting patterns in Tables 1 and 2 when looking at the Fibonacci numbers under addition and multiplication using modular arithmetic. The properties of addition allow us to move horizontally across the row of $F_n \bmod n$ in Tables 1 and 2; the patterns will continue indefinitely by Proposition 2. The properties of multiplication under modular arithmetic give us the column entries. For example, $F_7 = 13 \equiv 1 \bmod 2$. In order to find $F_7^3 \bmod 2$, it is only necessary to look at $1^3 \bmod 2$ which is much simpler than calculating 13^3 and then reducing that value mod 2.

While the Fibonacci numbers form a divisibility sequence, it is straightforward to show that this property is not applicable to the Lucas numbers or more general Lucas sequences. For example, while 2 divides 4, $L_2 = 3$ does not divide $L_4 = 7$. Notice that $L_2 = 3$ does divide $L_6 = 18$ and $L_{10} = 123$. The Lucas sequence is, however, an odd divisibility sequence.

Definition: An *odd divisibility sequence* is an integer sequence, $\{a_n\}$, indexed by positive integers n, such that if n/m is an odd integer, then a_m divides a_n.

F_n	1	1	2	3	5	8	13	21	34	55	89	144	233	377	610	987
F_n mod 3	1	1	2	0	2	2	1	0	1	1	2	0	2	2	1	0
F_n^2 mod 3	1	1	1	0	1	1	1	0	1	1	1	0	1	1	1	0
F_n^3 mod 3	1	1	2	0	2	2	1	0	1	1	2	0	2	2	1	0

Table 1. Powers of F_n under mod 3, with $n \geq 1$

F_n	1	1	2	3	5	8	13	21	34	55	89	144	233	377	610	987
F_n mod 5	1	1	2	3	0	3	3	1	4	0	4	4	3	2	0	2
F_n^2 mod 5	1	1	4	4	0	4	4	1	1	0	1	1	4	4	0	4
F_n^3 mod 5	1	1	3	2	0	2	2	1	4	0	4	4	2	3	0	3

Table 2. Powers of F_n under mod 5, with $n \geq 1$

Being an odd divisibility sequence is a much weaker property than being a divisibility sequence. As such, many of the results applicable to the Fibonacci numbers are not relevant to the Lucas numbers. For example, our results for Fibonacci numbers cannot be directly extended to the Lucas numbers.

Bala presents several new sequences based upon Lucas sequences of the first and second kind that do form divisibility sequences.[4] As an example, for a Lucas sequence of the second kind with $n \in \mathbb{N}_0$ and $r \in \mathbb{Z}$, the sequences:

$$\begin{aligned} Z^1_{rn} &= V_{rn} - V_{3rn} \\ Z^2_{rn} &= V_{rn} - 3V_{3rn} + 3V_{5rn} - V_{7rn} \\ Z^3_{rn} &= V_{rn} - 5V_{3rn} + 10V_{5rn} - 10V_{7rn} + 5V_{9rn} - V_{11rn} \\ &\vdots \end{aligned}$$

each form a divisibility sequence.[4] These "sequences of sequences" will be the focus of results for Lucas numbers.

RESULTS

Fibonacci Numbers

The main results in this section come from examining patterns in the prime factors of the sum $F^2_{kn} + F^2_{kn-2}$. This quantity, a sum of squared Fibonacci numbers, is of interest similar quantities were studied elsewhere, such as in Arangala et. al.[7], where a related sum $F^2_{kn+l} + F^2_{mn+r}$ is studied. This sum has specific indices which will allow the sum to be divisible by certain primes for all $n \geq 0$. The patterns are observed in Tables 1 and 2. Additionally, the sum $F^3_n + F^3_{n-2}$ is examined for specific primes that are not contained in the factors of the sum $F^2_n + F^2_{n-2}$.

Observing the prime factors for $F^2_n + F^2_{n-2}$ for n from 2 to 50, the first pattern was found for sums containing 2 as a prime factor.

Lemma 1. *For all $n \geq 0$,*

$$F^2_{3n+4} + F^2_{3n+2} \text{ is divisible by 2.}$$

Proof. Begin by using the recursive definition in **Equation** 2. for the Fibonacci numbers to rewrite F_{3n+4} in terms of F_{3n+3} and F_{3n+2}:

$$F^2_{3n+4} + F^2_{3n+2} = (F_{3n+3} + F_{3n+2})^2 + F^2_{3n+2}$$

then expanding and combining like terms,

$$= F^2_{3n+3} + 2F_{3n+3}F_{3n+2} + 2F^2_{3n+2}.$$

It is clear that $2F_{3n+3}F_{3n+2}$ and $2F^2_{3n+2}$ are divisible by 2 and thus even numbers. In order for the entire sum to be even, F^2_{3n+3} must also be even.

From Proposition 4(i) on the divisibility of Fibonacci numbers, F_n is even when n is divisible by 3. Clearly, F_{3n+3}

is even for all $n \geq 0$ since $3n+3$ is divisible by 3 for all $n \geq 0$. Lastly, if F_{3n+3} is even then so too is F_{3n+3}^2 by Proposition 1(iv) on even and odd numbers.

Therefore, $F_{3n+4}^2 + F_{3n+2}^2$ is the sum of even terms and is itself even for all $n \geq 0$. □

The second prime which appears in regular intervals as a factor of $F_n^2 + F_{n-2}^2$ is 5. Unlike the factor of 2, not only does the factor of 5 show up in a consistent pattern but it always shows up in the factorization of two consecutive n values.

Lemma 2. *For all $n \geq 0$,*

a. $F_{5n+3}^2 + F_{5n+1}^2$ *is divisible by 5.*

b. $F_{5n+4}^2 + F_{5n+2}^2$ *is divisible by 5.*

Proof. To prove the first statement, first recall from Table 2 that F_n will be divisible by 5 if and only if $n \equiv 0 \bmod 5$, or equivalently there is a F_{5n} term in the sum. So, begin by using the recursive definition of the Fibonacci numbers to rewrite F_{5n+3}

$$F_{5n+3}^2 + F_{5n+1}^2 = (F_{5n+2} + F_{5n+1})^2 + F_{5n+1}^2$$

By expanding and combining like terms, the righthand side becomes

$$= F_{5n+2}^2 + 2F_{5n+2}F_{5n+1} + 2F_{5n+1}^2$$

Using **Equation** 2. again, rewrite F_{5n+2}^2 as follows:

$$= (F_{5n+1} + F_{5n})^2 + 2F_{5n+2}F_{5n+1} + 2F_{5n+1}^2$$

then again, expand and combine like terms:

$$= 3F_{5n+1}^2 + F_{5n}^2 + 2F_{5n+1}F_{5n} + 2F_{5n+2}F_{5n+1}$$

Lastly, rewrite the F_{5n+2} in the last term using **Equation** 2.. The goal of this process is to have either a coefficient of 5 or F_{5n} in each term. So, expanding and combining like terms:

$$= 5F_{5n+1}^2 + F_{5n}^2 + 4F_{5n+1}F_{5n}\,.$$

The first term is clearly a multiple of 5. Since the second and third terms both have an F_{5n} this implies that they are divisible by 5 by Proposition 4(iii). Therefore, $5F_{5n+1}^2 + F_{5n}^2 + 4F_{5n+1}F_{5n} \equiv 0 \bmod 5$ as all three terms are divisible by 5. The second result follows similarly. □

Unlike the factor of 2, 5 appears in "pairs" for consecutive n. Using a numerical experiment, it is observed that 5 was a factor of the sum $F_n^2 + F_{n-2}^2$ for $n = 3,\ 4,\ 8,\ 9,\ 13,\ 15, \ldots$ where the n values coincide with the indices in Lemma 2. At first this pattern is seemingly random, however Table 2 can provide insight as to why this occurs. The pattern in the F_n^2 for $n \geq 1$ under mod 5 is as follows:

$$1,\ 1,\ 4,\ 4,\ 0,\ 4,\ 4,\ 1,\ 1,\ 0,\ 1,\ 1,\ 4,\ 4,\ 0,\ 4,\ 4,\ 1,\ 1,\ 0, \ldots$$

So F_n^2 will be either $0, 1,$ or 4 mod 5 for all $n \geq 1$, which means in order to have the sum be equivalent to 0 mod 5 it will either have to occur when both terms are equivalent to 0 mod 5 or when one term is equivalent to 1 mod 5 and the other is equivalent to 4 mod 5. Since the indices of the sum $F_n^2 + F_{n-2}^2$ are two units apart, there will never have the case where both terms are equivalent to 0 mod 5. However, based on the pattern above, it becomes clear that the terms which are equivalent to 1 mod 5 and 4 mod 5 are two units apart and appear in pairs resulting in pairs of sums which are divisible by 5 appearing at equal intervals. For example, when $n = 3$ the sum is $F_3^2 + F_1^2 \equiv 1 \bmod 5 + 4 \bmod 5$ which from Proposition 2 is equivalent to $(1 + 4) \bmod 5 \equiv 0 \bmod 5$.

So far a pattern in this sum with a prime factor of 2 as well as a very interesting "pairing" pattern for a prime factor of 5, has been observed. Curiously, based on initial observations 3 is not a factor of $F_n^2 + F_{n-2}^2$ for $2 \leq n \leq 100$. Now it will be shown that 3 is not be a divisor of $F_n^2 + F_{n-2}^2$ for all $n \in \mathbb{N}_0$.

Lemma 3. *For all $n \geq 2$,*

$$F_n^2 + F_{n-2}^2 \text{ will never be divisible by 3.}$$

Proof. This result will be proved by contradiction. Assume that $F_n^2 + F_{n-2}^2$ has a factor of 3, or equivalently, $F_n^2 + F_{n-2}^2 \equiv 0 \bmod 3$. From the properties of addition under modular arithmetic this will happen when either:

a. F_n^2 and F_{n-2}^2 both have a factor of 3; that is, they are both congruent to 0 mod 3, or

b. F_n^2 is congruent to 1 mod 3 and F_{n-2}^2 is congruent to 2 mod 3 or vice versa.

In case a: using Proposition 4(ii) and properties of modular arithmetic, F_n will have a factor of 3 if and only if $n \equiv 0 \bmod 4$. Then, it follows that F_n^2 will also have a factor of 3 when $n \equiv 0 \bmod 4$. The same will hold for F_{n-2}^2. Without loss of generality, assume that $n - 2 \equiv 0 \bmod 4$. Proposition 2 implies that $n \equiv 2 \bmod 4$. Therefore only one of n or $n - 2$ can be equivalent to 0 mod 4. Thus, the assumption that $F_n^2 + F_{n-2}^2$ has a factor of 3 leads to a contradiction, so $F_n^2 + F_{n-2}^2$ does not have a factor of 3.

So consider case b: assume that $F_n^2 \equiv 1 \bmod 3$ and $F_{n-2}^2 \equiv 2 \bmod 3$. Using Table 1, observe that $F_n^2 \not\equiv 2 \bmod 3$ for any n. This can be proved rigorously using Proposition 2. Thus, the assumption that $F_n^2 \equiv 1 \bmod 3$ and $F_{n-2}^2 \equiv 2 \bmod 3$ (or vice versa) leads to a contradiction.

Therefore, the original assumption is false. Hence, $F_n^2 + F_{n-2}^2$ will never have a factor of 3 for any integer $n \geq 2$. □

Lemma 3 shows there will never be a factor of three in a sum of squares. However, it is conjectured that a factor of three may show up in a sum of cubes. Recall from Table 1, that F_n^3 can be equivalent to 0, 1, or, 2 mod 3 so although, F_n and F_{n-2} cannot both be equivalent to 0 mod 3, when considering a sum of cubes, there is now the possibility of having F_n^3 mod 1 mod 3 and F_{n-2}^3 mod 2 mod 3 or vice versa.

Lemma 4. *For all $n \geq 0$,*

$$F_{4n+3}^3 + F_{4n+1}^3 \text{ is divisible by 3.}$$

Proof. In order for $F_{4n+3}^3 + F_{4n+1}^3$ to be divisible by 3, it is necessary to show that it can be written as a sum of terms which are all divisible by 3. Begin by using **Equation** 2. to rewrite the first term.

$$F_{4n+3}^3 + F_{4n+1}^3 = (F_{4n+2} + F_{4n+1})^3 + F_{4n+1}^3$$

Expanding $(F_{4n+2} + F_{4n+1})^3$ and then combining terms

$$= F_{4n+2}^3 + 3F_{4n+2}^2 F_{4n+1} + 3F_{4n+2}F_{4n+1}^2 + 2F_{4n+1}^3$$

Again, using **Equation** 2. to rewrite F_{4n+2}^3

$$= (F_{4n+1} + F_{4n})^3 + 3F_{4n+2}^2 F_{4n+1} + 3F_{4n+2}F_{4n+1}^2 + 2F_{4n+1}^3$$

Expanding $(F_{4n+1} + F_{4n})^3$ and combining terms

$$= 3F_{4n+1}^3 + 3F_{4n+1}^2 F_{4n} + 3F_{4n+1}F_{4n}^2 + 3F_{4n+2}^2 F_{4n+1} + 3F_{4n+2}F_{4n+1}^2 + F_{4n}^3$$

It is clear that every term whose coefficient is 3 is divisible by 3. Now check that F_{4n}^3 is divisible by 3 for all n. Recall from Table 1 and divisibility that F_m is divisible by 3 when m is a multiple of 4. Therefore, F_{4n} is divisi-

ble by 3 for all n and thus, so is F_{4n}^3. Since $F_{4n+3}^3 + F_{4n+1}^3$ is the sum of terms, each divisible by 3, it too will be divisible by 3. □

Lucas Numbers

Extending the results of the last section to the Lucas numbers is not possible using the same techniques as the Lucas numbers do not form a divisibility sequence. The arguments of the work with Fibonacci numbers heavily rely on the fact that the Fibonacci numbers form a divisibility sequence.

To move around this difficulty, the results of Bala[4] are utilized. Recall that the Lucas numbers are a Lucas sequence of the second kind with $P = 1$ and $Q = -1$. This is denoted by $\{L_n\}_{n\in\mathbb{N}_0} = \{V_n(1,-1)\}_{n\in\mathbb{N}_0}$. In each of the theorems below, a divisibility sequence $\{Z_{rn}\}$ is created from terms of Lucas numbers. Then the focus is on the sequences, $\{W_{rn}\}$, made of sums of terms from $\{Z_{rn}\}$. In particular, the objective is to see when the terms will be divisible by two.

Theorem 1. *Let $\{L_n\}$ be the Lucas sequence, and define $Z_{rn} = L_{rn} - L_{3rn}$ and $W_{rn} = Z_{rn}^2 + Z_{r(n-1)}^2$ for all $n \in \mathbb{N}_0$.*

For all $n \geq 0$ and $r \equiv 0 \mod 3$, W_{rn} is divisible by 2.

Proof. The aim is to show for all $n \in \mathbb{N}$, W_{rn} will be even when $r = 3k$. In other words, $W_{rn} \equiv 0 \mod 2$ if and only if $r \equiv 0 \mod 3$. There are three cases to study: $r \equiv 0, 1$ or $2 \mod 3$.

Case 1 ($r \equiv 0 \mod 3$): When $r \equiv 0 \mod 3$, $rn \equiv 0 \mod 3$ and $r(n-1) \equiv 0 \mod 3$. Therefore L_{rn}, L_{3rn}, $L_{r(n-1)}$, and $L_{3r(n-1)}$ will all be even for any $n \in \mathbb{N}_0$. Therefore, Z_{rn} and $Z_{r(n-1)}$ will be even and W_{rn} will also be even.

Case 2 ($r \equiv 1 \mod 3$): When $r \equiv 1 \mod 3$, $rn \equiv 0 \mod 3$ only when $n \equiv 0 \mod 3$. Similarly, $r(n-1) \equiv 0 \mod 3$ only when $n - 1 \equiv 0 \mod 3$. It is impossible to choose $n \in \mathbb{N}_0$ such that $n \equiv 0 \mod 3$ and $n - 1 \equiv 0 \mod 3$. Therefore either L_{rn} or $L_{r(n-1)}$ is odd. Hence either Z_{rn} or $Z_{r(n-1)}$ is odd and consequently W_{rn} is odd.

Case 3 ($r \equiv 2 \mod 3$): When $r \equiv 2 \mod 3$, $rn \equiv 0 \mod 3$ only when $n \equiv 0 \mod 3$. Similarly, $r(n-1) \equiv 0 \mod 3$ only when $n - 1 \equiv 0 \mod 3$. As in Case 2, it is impossible to choose $n \in \mathbb{N}_0$ such that $n \equiv 0 \mod 3$ and $n - 1 \equiv 0 \mod 3$. Therefore either L_{rn} or $L_{r(n-1)}$ is odd. Hence either Z_{rn} or $Z_{r(n-1)}$ is odd and consequently W_{rn} is odd. □

DISCUSSION AND CONCLUSIONS

The Fibonacci numbers have other well-known properties about divisibility that were not discussed in this paper. For example, 29 divides every 14^{th} Fibonacci number. This follows since $F_{14} = 29$ and the Fibonacci sequence is a divisibility sequence. Using numerical results, it has been observed that $F_n^2 + F_{n-2}^2$ when $n = 5, 11, 19, 25, \ldots$ so the authors conjecture that

$$F_{14n+5}^2 + F_{14n+3}^2 \text{ is divisible by } 29$$

and

$$F_{14n+11}^2 + F_{14n+9}^2 \text{ is also divisible by } 29.$$

Similar to the "pairing" nature of sums with a factor of 5, the values of n for which $F_n^2 + F_{n-2}^2$ has a factor of 29 are spaced out at repeating intervals of 6 then 8 which results in the two separate conjectures. It is also interesting to note that each pair of these intervals adds up to a difference in n of 14 and this coincides with the divisibility property that states 29 will divide every 14^{th} Fibonacci number.

The results of this paper pertaining to the Lucas sequence could be further expanded by looking at other Lucas sequence-based divisibility sequences such as those found in the work of Bala[4] or Somer.[5, 6] For example generalizing the results for all integers P and Q and using the Lucas sequence of the second kind. Additionally, based on preliminary numerical experiments the following conjectures based are proposed:

For all $n \geq 0$,

$$L_{3n+5}^2 + L_{3n+3}^2 \text{ is divisible by 2.}$$

and

$$L_{n+3}^3 + L_{n+1}^3 \text{ is divisible by 5.}$$

ACKNOWLEDGMENTS
The authors are grateful to the anonymous reviewers for their suggestions on improving the presentation and content of this paper.

REFERENCES

1. Katz, V. (1998) *A history of mathematics: an introduction* 2nd ed., Addison-Wesley.
2. Tannenbaum, P. (2014) *Excursions in modern mathematics* 8th ed., Pearson.
3. *Fibonacci Quarterly*, *https://www.fq.math.ca/index.html*, (accessed Dec 2020)
4. Bala, P. Lucas sequences and divisibility sequences, *https://oeis.org/A273622/a273622.pdf*, (accessed Feb 2016)
5. Somer, L. (1992) Divisibility of terms in Lucas sequences by their subscripts, in *Applications of Fibonacci numbers* (Bergum, G., Philippou, A., and Horadam A., Eds.) 515–525, Springer, Dordrecht. *https://doi.org/10.1007/978-94-011-2058-6_ 52*
6. Somer, L. (1996) Divisibility of terms in Lucas sequences of the second kind by their subscripts, in *Applications of Fibonacci numbers* (Bergum, G., Philippou, A., and Horadam A., Eds.) 473–486, Springer, Dordrecht. *https://doi.org/10.1007/978-94-009-0223-7_ 39*
7. Arangala, C., Hrovat, B., and Kelner, J. (2016) Sums of powers of Fibonacci and Lucas numbers. *Minnesota J. of Undergrad. Math.* 2 (1), 1–12.
8. Brillhart, J., Montgomery, P., and Silverman, R. (1988) Tables of Fibonacci and Lucas factorizations, *Math. Comput.*, 50 (181), 251-260. *https://doi.org/10.1090/S0025-5718-1988-0917832-6*
9. Clary, S., and Hemenway, P. (1993) On sums of cubes of Fibonacci numbers, in *Applications of Fibonacci numbers* (Bergum, G., Philippou, A., and Horadam A., Eds.) 123-136, Springer, Dordrecht. *https://doi.org/10.1007/978-94-011-2058-6_ 12*
10. Gandhi, K. (2011) Divisibility properties of Fibonacci numbers. *South Asian J. Math.*, 1 (3), 140–144.
11. Hoggatt, V., and Long, C. (1974) Divisibility properties of generalized Fibonacci polynomials. *Fibonacci Quart.* 12, 11-3-120.
12. Jaidee, M., and Pongsriiam, P. (2019) Arithmetic Functions of Fibonacci and Lucas Numbers. *Fibonacci Quart.*, 57 (3), 246-254.
13. Melham, R. (2000) Alternating sums of fourth powers of Fibonacci and Lucas numbers. *Fibonacci Quart.* 38 (3), 254–259.
14. Melham, R. (2008/2009) Some conjectures concerning sums of odd powers of Fibonacci and Lucas numbers. *Fibonacci Quart.* 46/47 (4), 312-315.
15. Pongsriiam, P. (2014) Exact divisibility by powers of the Fibonacci and Lucas numbers, *J. of Integer Seq.* 17, 1-12. *https://doi.org/10.3934/math.2020433*
16. Thongmoon, M. (2009) New identities for the even and odd Fibonacci and Lucas numbers. *Int. J. Contemp. Math. Sci.* 4 (14), 671-676.
17. Jones, G., and Jones, J. (1998) *Elementary number theory*, Springer, London. *https://doi.org/10.1007/978-1-4471-0613-5*
18. Richmond, B. and Richmond, T. (2004) *A discrete transition to advanced mathematics*, Amer. Math. Soc., Rhode Island.
19. Sundstrom. T. (2013) *Mathematical reasoning: writing and proof*, *https://scholarworks.gvsu.edu/books/24/*, (accessed Dec 2020)

ABOUT STUDENT AUTHORS

Spirit Karcher graduated from Christopher Newport University in 2018. She is a member of the Pi Mu Epsilon, a national mathematics honor society; Alpha Delta Pi; and Order of Omega, a leadership honor society. Currently, Spirit is studying to earn her Ph.D. in mathematics education at Florida State University.

Mariah Michael graduated from Christopher Newport University in 2020 with a B.S. in mathematics. She is a member of the Pi Mu Epsilon and Sigma Alpha Omega. She is currently studying to earn her M.S. in mathematics at George Mason University.

PRESS SUMMARY

This paper focuses on two specific types of recursive sequences; the Fibonacci sequence and Lucas sequence. The paper defines and examines the properties of divisibility and the sums of power of these two sequences. The work focuses on the patterns that result from manipulating the sequences. The work done in this paper can be expanded upon further by looking at higher sums of power in recursive sequences.

A Survey of Inhibitors for the Main Protease of Coronaviruses with the Potential for Development of Broad-Spectrum Therapeutics

Alyssa Sanders[*a], *Samuel Ricci*[b], *Sarah Uribe*[a], *Bridget Boyle*[a], *Brian Nepper*[b], *& Nathaniel Nucci*[a,b]

[a]*Department of Molecular & Cellular Biosciences, Rowan University, Glassboro, NJ*
[b]*Department of Physics & Astronomy, Rowan University, Glassboro, NJ*

https://doi.org/10.33697/ajur.2020.037

Students: sandersa8@students.rowan.edu, *riccis1@students.rowan.edu, uribes2@students.rowan.edu, bridget.boyle@jefferson.edu, nepperb@gmail.com*
Mentor: nucci@rowan.edu

ABSTRACT
The coronaviruses plaguing humanity in the 21st century share much in common: a spontaneous route of origin from wild animals, a propensity to take human life, and, importantly, a highly conserved set of biological machinery necessary for viral replication. Most recently, the SARS-CoV-2 is decimating economies around the world and has claimed over two million human lives, reminding the world of a need for an effective drug against present and future coronaviruses. To date, attempts to repurpose clinically approved antiviral medications show minimal promise, highlighting the need for development of new antiviral drugs. Nucleotide analog inhibitors are a promising therapeutic candidate, but early data from clinical studies suggests these compounds have limited efficacy. However, novel compounds targeting the main protease responsible for critical steps in viral assembly are gaining considerable interest because they offer the potential for broad-spectrum coronavirus therapy. Here, we review the literature regarding potential inhibitors for the main protease of coronaviruses, especially SARS-CoV-2, analyze receptor-drug interactions, and draw conclusions about candidate inhibitors for future outbreaks. Promising candidates for development of a broad-spectrum coronavirus protease inhibitor include the neuraminidase inhibitor 3K, the peptidomimetic inhibitor 11a and 11b, the α-ketoamide inhibitor 13b, the aldehyde prodrug, and the phosphate prodrug developed by Pfizer. *In silico* and *in vitro* analyses have shown that these inhibitors strongly interact with the active site of the main protease, and to varying degrees, prevent viral replication via interactions with the largely conserved active site pockets.

KEYWORDS
Severe Acute Respiratory Syndrome Coronavirus; Middle East Respiratory Syndrome Coronavirus; Severe Acute Respiratory Syndrome Coronavirus 2; Replicase Polypeptide; Protease; Neuraminidase Inhibitor; Peptidomimetic Inhibitor; α-Ketoamide Inhibitor; Molecular Docking

INTRODUCTION

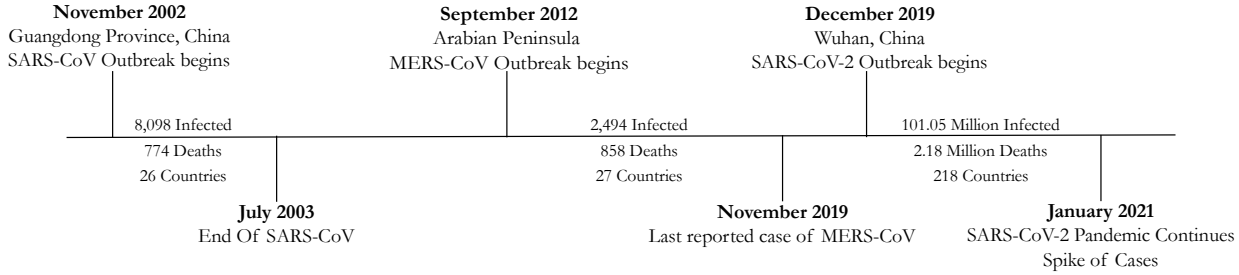

Figure 1. A timeline of the recent coronavirus outbreaks, with the case total and death total from the World Health Organization.[1–3] Reported data are from January 29, 2021.

Severe acute respiratory syndrome coronavirus (SARS-CoV), Middle East respiratory syndrome coronavirus (MERS-CoV), and severe acute respiratory syndrome coronavirus 2 (SARS-CoV-2) are three highly pathogenic coronaviruses that have emerged in the 21st century. Each of these have zoonotic origins, and are genetically similar to coronaviruses in bats around the world.[4, 5] As seen in **Figure 1**, SARS-CoV was the first outbreak and originated in Guangdong Province, China, in November 2002. The SARS-CoV outbreak officially ended in July 2003.[6] Nine years later, MERS-CoV emerged in the Arabian Peninsula and continues to infect people today.[7] Both SARS-CoV and MERS-CoV spread to over two dozen countries, infected thousands of people, and have estimated death rates of 10 and 40%, respectively.[5, 6] The most recent outbreak, SARS-CoV-2, has spread globally to nearly

every nation and territory with confirmed cases in the tens of millions and more than two million deaths as of January, 2021. The estimated fatality rate for SARS-CoV-2 is 3.3% globally.[10] Prior to SARS-CoV, known coronavirus infections in humans presented mild symptoms and were isolated to specific regions of the world.[11] SARS-CoV-2, however, shows the potential for coronavirus outbreaks to reach pandemic proportions. Taken together, the evidence of zoonotic origins and capability of global infection support the possibility of another pandemic-level coronavirus emerging. A robust understanding of the coronavirus biology is therefore vital to the safety and wellbeing of the human population.

Despite the different time periods and severity of the outbreaks mentioned, the coronaviruses display a strong degree of genetic and structural conservation.[12] SARS-CoV, MERS-CoV, and SARS-CoV-2, are positive-sense, single-stranded RNA viruses with genomes of ~30,000 nucleotides.[13–15] Approximately two-thirds of this genome encodes the replicase machinery for the coronavirus.[16] The replicase gene consists of two open reading frames (ORF), ORF1a and ORF1b. ORF1a is found upstream and encodes for polyprotein (pp) 1a. When transcribed together, ORF1a and ORF1b encode a larger polyprotein, pp1ab.[16] The polyproteins contain the chymotrypsin-like (M^{Pro} or CL^{Pro}) and papain-like (PL^{Pro}) proteases which cleave the polyprotein into 16 non-structural proteins (Nsp).[17] The PL^{Pro} cleaves at five sites, working in the N-terminal direction, Nsp1-4, and the M^{Pro}, which is Nsp5, cleaves the polyprotein at eleven sites working in the C-terminal direction. M^{Pro} auto cleaves itself from the polyprotein and subsequently cleaves Nsp6-16 (**Figure 2**).[18] These non-structural proteins form two major complexes: the cytoplasmic enzyme complex and the replicase complex.[14, 16] PL^{Pro} cleaves Nsp1 which is responsible for suppressing the host gene expression by degrading the host cell's RNA, improving viral gene expression efficiency.[20] This occurs by Nsp1 binding to the 40S ribosomal subunit in the host cell and inactivating it. This suppresses the cap-dependent and internal ribosome entry site (IRES)-mediated translation, protecting the RNA of the coronavirus.[20] PL^{Pro} also cleaves Nsp2 which has an unclear function.[18] In previous studies, the deletion of Nsp2 resulted in decrease viral RNA synthesis and growth, inferring that Nsp2 plays a crucial role in viral RNA synthesis, although the specific mechanism of action requires further research. Nsps3-6 work together to form double membrane vesicles involved in RNA synthesis. Nsp7 and 8 form a large super complex that supports viral replication.[18, 19] Nsp9 plays a role in the binding of ssRNA and dsDNA and affects viral growth.[20, 21] Nsp10 and 11 also play a role in viral RNA synthesis, and Nsp10 forms a part of the viral mRNA cap methylation complex.[15, 22] Nsp12 is responsible for priming the dependent RNA polymerase.[15, 23] Nsp13, a helicase with RNA and DNA unwinding capabilities, possesses dNTPase activity, helping form the 5' cap of viral mRNA.[24, 25] Nsp14 removes one nucleotide at a time from viral ssRNA and dsDNA.[29] The function of Nsp15 is unknown, however the role of Nsp16 is to add Nsp10 and Nsp14 to form the mRNA cap methylation complex.[18] PL^{Pro} cleaves Nsps1-4, which are proteins necessary for colonizing, and the M^{Pro} cleaves the Nsps needed to support the replication machinery.

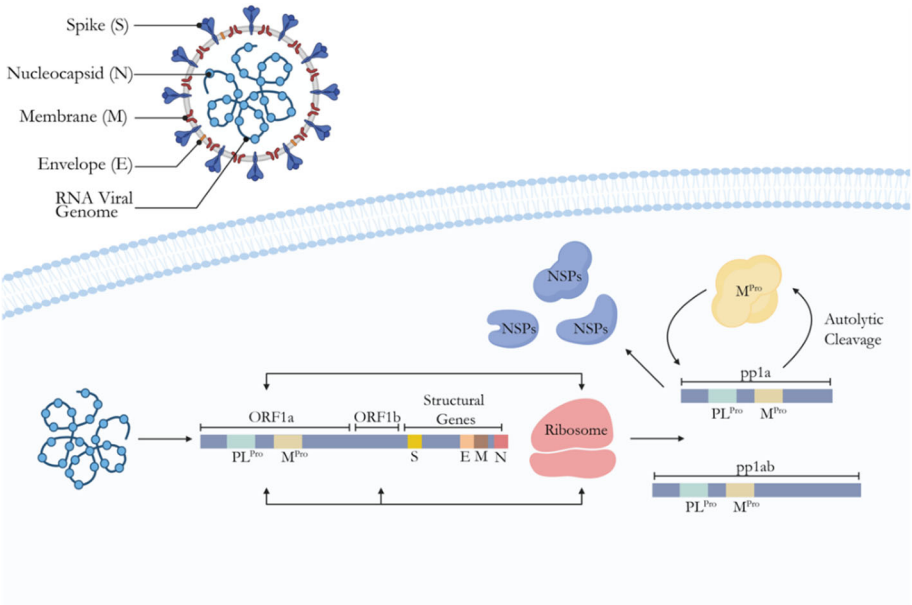

Figure 2. Coronavirus replication pathway. After inserting the viral RNA, ORF1a or ORF1a and ORF1b are translated into the polyproteins pp1a or pp1ab, respectively. The main protease, M^{Pro}, automatically cleaves itself from the translated polyprotein and begins to cleave nonstructural proteins from the remainder of the protein. The nonstructural proteins then combine to form the necessary replication machinery. This image was created with BioRender.com.

Although the M^{Pro} and PL^{Pro} both cleave Nsps, inhibiting the M^{Pro} has some advantages over PL^{Pro} inhibition: the M^{Pro} has a larger role in viral replication, it displays high genetic and structural conservation, and there are no human analogues,[30, 31] thus an inhibitor would be less likely to target human proteins and lead to unwanted side effects. Additionally, the spike protein – the protein necessary for the coronavirus to attach to human epithelial cells – is a popular target for drug design, but the efficacy of this target is limited because flexible glycans shield the protein from molecular detection.[32]

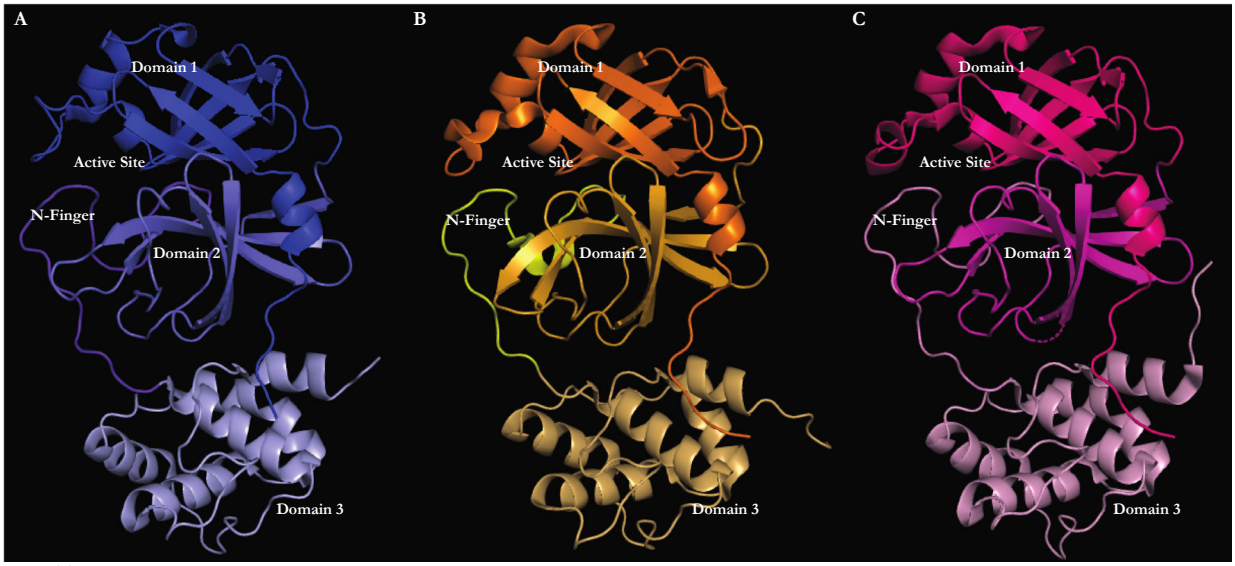

Figure 3. The monomer structures of the M^{Pro} from the three coronaviruses responsible for major outbreaks of human infection are shown with color code to distinguish their structural domains. A. SARS-CoV M^{Pro} (PDB: 1UK3)[33]: Domain I (residues 1-97), Domain II (98-175), Domain III (200-306), N-finger (176-199). B. MERS-CoV M^{Pro} (PDB: 4WME)[34]: Domain I (1-97), Domain II (98-178), Domain III (201-306), N-finger (179-200). C. SARS-CoV-2 M^{Pro} (PDB: 6YB7)[35]: Domain I (1-97), Domain II (98-175), Domain III (200-306), N-Finger (176-199). This figure was made through the use of PyMOL.[36]

The M^{Pro} is catalytically active as a homodimer, and each monomer has three domains, **Figure 3**. Domains I and II include antiparallel β-sheets and form the active site of the protease. Domain III includes five α-helices in a globular cluster and mediates dimerization. Interactions between the helices of monomers are the primary driver of dimerization. The C-terminal domain III is linked to the N-terminal domains I and II via a long loop referred to as the N-finger.

As shown in **Figure 3**, the structures of the SARS-CoV, MERS-CoV, and SARS-CoV-2 M^{Pro} are highly similar. SARS-CoV and SARS-CoV-2 are genetically nearly identical, sharing 96% of their nucleotide sequence.[37] MERS-CoV shares 87% genetic similarity with SARS-CoV-2.[38] There are 108 non-conservative and 45 conservative amino acid mutations between the main proteases of SARS-CoV and MERS-CoV, **Figure 4**. A considerable portion, 43%, of non-conservative mutations are found in domain III, showing active site conservation. This observation is further corroborated by a lower root mean square deviation in atomic position of overlays of domains I and II compared to domain III, 0.311, 0.455, and 1.062 Å respectively.[39] Despite the comparatively larger variance of the MERS-CoV M^{Pro}, only one significant structural change is evident. The N-finger of MERS-CoV M^{Pro} is distinct from the other two, demonstrated by the addition of an α-helix (**Figure 5**, shown in yellow). There are only five non-conservative mutations and four conservative amino acid mutations between SARS-CoV and SARS-CoV-2. The only evident structural difference is caused by a non-conservative mutation of Ala46 in SARS-CoV M^{Pro} to Ser in MERS-CoV and SARS-CoV-2 M^{Pro} in the first domain. This replacement of a hydrophobic side chain with a hydrophilic one induces the change of a small α-helical turn to an apparently more flexible loop (**Figure 5**, at the active site on the outside of domain I). The N-finger is crucial for catalytic activity, but not for dimerization.[38] Mutated proteases lacking the N-finger show C-terminal mediated dimerization but cannot cleave the substrate.[38] Given the strongly conserved nature of the flexible N-finger, the extension may regulate the active site's exposure to ligands. Although this is not fully understood, the specific mechanism warrants further study.[40] All three coronaviruses have minor genetic and amino acid differences, MERS-CoV to a greater extent than SARS-CoV to SARS-CoV-2, but there is an important structural and functional conservation shared in the makeup of the enzymes' active sites.[40]

Structural features found to contribute to the catalytic mechanism of M^{Pro} are highly conserved across coronavirus lines. A Cys145-His41 catalytic dyad is the central functional unit of the protease. Mutation of either the Cys or His to Ala leaves the enzyme nonfunctional.[41] Catalysis begins with the binding of the polypeptide substrate to the enzyme, forming a Michaelis complex. Cleavage of the substrate at the conserved Glu-Ala (or Ser) bond triggers the release of the N-terminal half of the peptide. The C-terminal end of the peptide substrate acylates the active site, and the His41 residue acts as a base in the deacylation step, releasing the C-terminal end.[42] A GSCGS motif, **Figure 4** and **Figure 5,** is essential to catalytic activity; mutations in this motif towards smaller, hydrophobic amino acid residues result in a sharp reduction in catalytic efficiency.[39] The motif starts the catalytic process by forming hydrogen bonds with pp1a. In tandem with the GSCGS motif, all three M^{Pro} sequences contain a partial negative charge cluster composed of amino acid residues Arg40, Tyr54, and Asp190.[39] Mutations of Asp190 to nonpolar and polar-uncharged amino acids fail to cleave the peptide substrate, demonstrating the importance of the negative charged group. Arg40 interacts with, and potentially balances, the negative charge associated with Asp190. Mutations of Arg40 to aliphatic residues inhibit the enzyme's ability to successfully cleave the peptide. Tyr54 directly interacts with Arg30 via π-cation interactions, limiting the negative charge, so the resultant charge of these interactions is partially negative.[39] Thermodynamic simulations support the need for a conserved water molecule to link the GSCGS motif and partial negative charge cluster.[39] Although these analyses were performed on SARS-CoV and MERS-CoV only, these findings provide meaningful insight to the catalytic mechanism of the coronavirus's main protease, and both the motif and partial negative charge cluster, are present in the SARS-CoV-2 M^{Pro}.

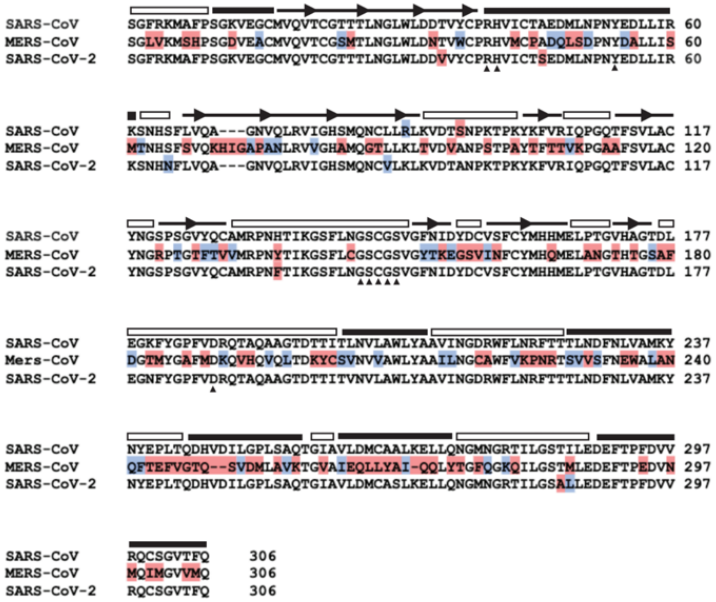

Figure 4. Amino acid sequence alignment of the M^{Pro} from SARS-CoV, MERS-CoV, and SARS-CoV-2. Black amino acids represent complete conservation, blue amino acids represent a conservative mutation, and red amino acids represent non-conservative mutations. The black triangles under the amino acid sequence show conserved amino acid residues within the active site pocket.

The active site, formed between domains I and II and the N-finger, is vital for the proteases' function and has become an increasing target for inhibitor design.[43] Targeting the active site would prevent cleavage of non-structural proteins from pp1a and pp1ab.[30, 42] As shown in **Figure 5**, there are four unique subsites, S_1, S_1', S_2, and S_4, which independently interact with the polypeptide, increasing the overall binding affinity. The S_1 subsite spans parts of domains I and II of the M^{Pro}, whereas the S_1' subsite is strictly in domain I. The S_2 subsite is located between domain I and the N-finger and is comprised of those resulting amino acids. The S_4 subsite is located between the N-finger and domain II. The location of these subsites is conserved across strains, indicating the importance of the overall active site structure. In the S_1 subsite, the polypeptide backbone displays multiple hydrogen bonding donors and acceptors available for bonding with a potential inhibitor.[30, 42] Another key characteristic of the S_1 subsite is the oxyanion hole, which is made up of amino acid residues 138 through 145 for SARS-CoV and SARS-CoV-2, and residues 141 through 148 for MERS-CoV. The hole, also referred to as the oxyanion loop, donates two hydrogen atoms during dimerization, further stabilizing the transition state of the catalysis reaction.[45] Subsite S_1' has three crucial, exposed amino acid residues, His41, Cys145, and Gly143.[45] Subsite S_1' has three crucial, exposed amino acid residues, His41, Cys145, and Gly143. Inhibitor interaction with these pocket residues gives rise to potent antiviral activity. The S_2 and S_4 pockets are typically large and are lined by hydrophobic side chains. Previous studies show that drug compounds with bulky, hydrophobic structures interact

with these pockets to further increase binding affinity. The S_2 and S_4 pockets have hydrogen bonding at the carboxyl oxygen of His164, providing an anchor point for these inhibitors.

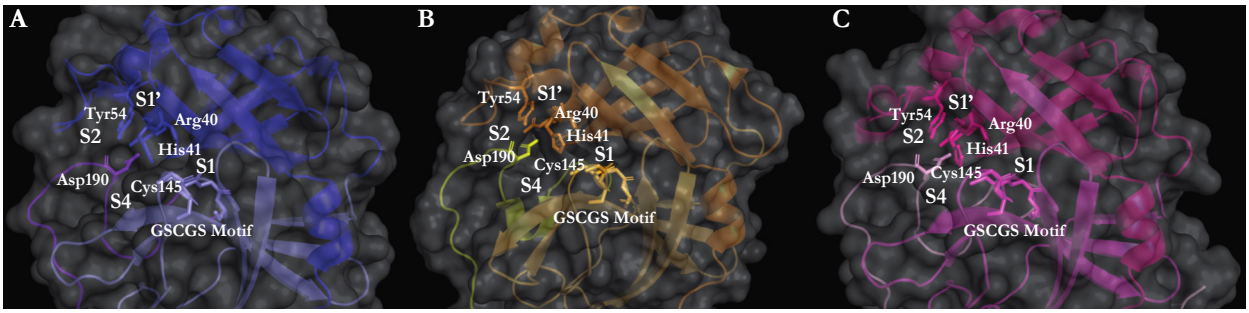

Figure 5. Conserved structures within the active sites of A. SARS-CoV (PDB: 1UK3)[33], B. MERS-CoV (PDB: 4WME)[34], and C. SARS-CoV-2 (PDB: 6YB7)[35] main proteases. Shown are the cysteine-histidine dyad, the GSCGS motif, and the partial negative charge cluster. The subsites of the active site pocket are also shown. This figure was with PyMOL.[36]

POTENTIAL INHIBITORS

Efforts to identify inhibitors against SARS-CoV-2 have involved both repurposing previously discovered antiviral drugs and development of novel inhibitors. Repurposed inhibitors, used for treatment of diseases such as HIV, hepatitis, influenza or asthma, include Atazanavir [46], Darunavir [47], Ebselen [48, 49], Lopinavir in combination with Ritonavir [50–52], Boceprevir [53], Oseltamivir [54], calpain inhibitors II and XII [53], and Montelukast [55], **Table 1.**

	Inhibitor	Classification	Viral Line	Method	IC_{50}	Reference
Repurposed	Atazanavir	HIV Inhibitor	SARS-CoV-2	*In vitro*	NR	46
	Darunavir	HIV Inhibitor	SARS-COV-2	Clinical Trial	NA	47
	Ebselen	Bi-Polar Disorder	SARS-CoV-2	*In vitro*	.67μM	48,49
	Lopinavir/ Ritonavir	HIV Antiviral	SARS-CoV MERS-CoV SARS-CoV-2	Clinical Trial	NR	50–52
	Boceprevir	Hepatitis Inhibitor	SARS-CoV-2	*In vitro*	4.13 μM	53
	Oseltamivir	Influenza Inhibitor	SARS-CoV-2	*In vitro* Clinical Trial	>100 μM	54
	Calpain Inhibitor II	Calpain Inhibitor	SARS-CoV-2	*In vitro*	2.07 μM	53
	Calpain Inhibitor XII	Calpain Inhibitor	SARS-CoV-2	*In vitro*	0.49 μM	53
	Montelukast	Anti-asthma	SARS-CoV-2	Computational	NR	55
Novel	Compound 6d	Peptidomimetic inhibitor	SARS-CoV MERS-CoV	*In vitro*	1.7 μM 4.7 μM	57
	3K	Neuraminidase (NA) Inhibitor	SARS-CoV MERS-CoV	*In vitro*	SARS 6.4 MERS 5.8	44
	11a	Peptidomimetic Inhibitors	SARS-CoV-2	*In vitro*	0.053 μM	61
	11b	Peptidomimetic Inhibitors	SARS-CoV-2	*In vitro*	.040 μM	61
	13a	Alpha-Ketoamides Inhibitor	SARS-CoV-2	*In vitro*	2.39 μM	43,65
	13b	Alpha-Ketoamides Inhibitor	SARS-CoV-2	*In vitro*	0.67 μM	43,65
	GC-376	Aldehyde Prodrug	SARS-CoV-2	*In vitro*	0.03 μM	63
	PF-07304814	Phosphate Prodrug	SARS-CoV SARS-CoV-2	*In vitro* Clinical Trial	NR	62

Table 1. A selection of the inhibitors that have been tested on M^{Pro}.

The repurposed inhibitors that have been tested in clinical trials show little efficiency for inhibiting the coronavirus M^{Pro}. The HIV inhibitor, Darunavir did not have an anti-viral effect on SARS-CoV-2 and is a poor therapeutic option for the M^{Pro} of coronaviruses.[47] In the clinical trial using Lopinavir in combination with ritonavir, hospitalization times and symptoms were

comparable to the control.[51] On day 28 of this combination therapy, patients' SARS-CoV-2 RNA levels plateaued at 40% of the viral load documented at the start of the trial. This led to the belief that the combination of Lopinavir and ritonavir does not inhibit the viral M^{Pro}. The patients treated with Lopinavir and Ritonavir suffered adverse side effects and the trial was halted.[51] Though some docking experiments suggest these repurposed inhibitors should work, they have consistently shown insignificant improvements in clinical outcomes, at best. The evidence now strongly indicates that repurposed drugs show marginal promise and present no guarantee of working on future coronaviruses. Therefore, designing and testing novel compounds and inhibitors is crucial in the fight against coronavirus related illnesses. Some novel inhibitors that show promise include neuraminidase (NA) inhibitors (3K) [44], multiple peptidomimetic inhibitors like compound 6d, 11a, and 11b [56–61], phosphate prodrug PF-07304814 [62], an aldehyde prodrug GC-376 [63], and lastly alpha-ketoamides inhibitors 13a and 13b [64], **Table 1.** The novel inhibitors that seem to have the most promise based on our analysis of the reported IC_{50} values are the 3K inhibitor, 11a, 11b, 13a, GC-376, and PF-07304814.

Inhibitor	Covalent Bonds	Hydrogen Bonds	Hydrophobic Interactions	Reference
3K - SARS	None	*Leu141* (S_1), Ser144 (S_1'), His163 (S_1), *Glu166* (S_1)	His41 (S_1'), Leu49 (S_2), Gln192 (S_4), Leu170 (S_4), Gln195 (S_4), Val193 (S_4)	44
3K - MERS	None	Ser147 (S_1'), His166 (S_1), *Glu169* (S_1)	His41 (S_1'), Leu 49 (S_2), Gln192 (S_4), Leu 170 (S_4), Gln195 (S_4), Val193 (S_4)	44
11a	Cys145 (S_1')	*Cys145* (S_1'), *Gly143* (S_1'), His163 (S_1), *Glu166* (S_1), *Phe140* (S_1)	Met49 (S_2), Try54 (S_2), Met165 (S_2), Asp187 (S_2), Pro168 (S_4), Gln189 (S_4)	61
11b	Cys145 (S_1')	Gln189 (S_4), *Gly143* (S_1'), *Cys145* (S_1'), His163 (S_1), *His164* (S_1), *Ph140* (S_1), *Glu166* (S_1)	His41 (S_1'), Met49 (S_2), Met165 (S_4), Val186 (S_2), Tyr54 (S_2), Asp187 (S_2)	61
13b	Cys145 (S_1')	His41 (S_1'), *Gly143* (S_1'), *Ser144* (S_1'), *Glu166* (S_1), *Phe140* (S_1), *Gly143* (S_1'), *Cys145* (S_1'), His164 (S_2), *Thr26* (S_1'), His172 (S_4)	Met165 (S_4), Gln189 (S_4), His41 (S_1'), Met49 (S_2), Asp187 (S_2), Asn142 (S_4), Pro168 (S_4)	43, 65
GC-376	Cys145 (S_1')	*Gly143 (S_1'), Ser144 (S_1'),* His163 (S_1), *Cys145 (S_1'), Glu166 (S_1),* Glu166 (S_1), *Phe140 (S_1),* Gln 189 (S_4), His41 (S_1')	His41 (S1'), Met49 (S_2), Met169 (S_2)	63
PF-07304814	Cys145 (S_1')	*Met165 (S_4),* Cys145 (S_1'), *His164 (S_2), Phe140 (S_1),* His163 (S_1), *Glu165 (S_1),* Glu166 (S_1)	His41 (S_1'), Met49 (S_2), Tyr54 (S_2), Pro168 (S_4), Asp187 (S_2)	62

Table 2. Potential novel inhibitors for the M^{Pro} of coronaviruses and the interactions that they have with the amino acids (sub pockets) of the active site as reported by the cited references. Hydrogen bond lists indicate protein-inhibitor H-bonds formed with side chains only (plain text), with backbone only (italicized), or with both backbone and side chains (italicized and underlined).These interaction were determined or confirmed by our analysis of the M^{Pro}-drug structures using PyMOL.[36]

A Neuraminidase (NA) Inhibitor (3k)

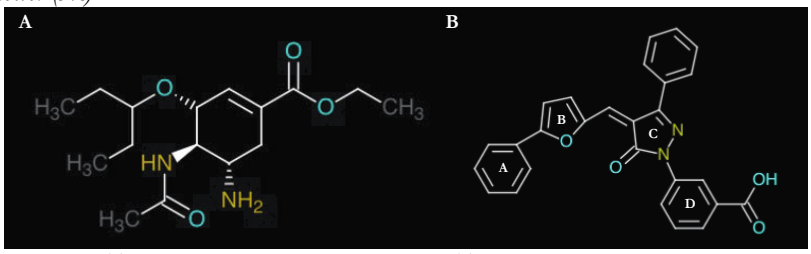

Figure 6. A. The chemical structure of Oseltamivir. **B.** The chemical structure of the 3K inhibitor.

Neuraminidase (NA) inhibitors are antiviral agents that work against both influenza A and influenza B. These types of inhibitors work by blocking the neuraminidase enzyme – which functions to free viruses from infected cells contributing to further spread – to prevent further infection.[66] Two NA inhibitors used to inhibit the M^{Pro} of coronaviruses are Oseltamivir and 3K (**Figure 6**).[44, 54] The most significant structural change between Oseltamivir and the 3K inhibitor is the expanded aromatic functionalization in 3K. The increased size and hydrophobicity of the 3K inhibitor predicts the increased performance of 3K over Oseltamivir is a result of the bulky, hydrophobic subgroups. Both Oseltamivir and the 3K inhibitor are capable of forming six hydrogen bonds with the active site.

Tan, *et al.,* performed molecular docking and *in vitro* studies of Oseltamivir (**Figure 6A**), a competitive neuraminidase inhibitor widely used in the clinic to treat influenza A and B, on several structures found within the SARS-CoV-2.[54] *In silico* analysis predicted a potential binding energy of -7.5 kcal/mol for Oseltamivir carboxylic acid and the active site of the SARS-CoV-2 M^{Pro}.[54] Successful binding *in silico* for this repurposed inhibitor did not, however, translate to antiviral activity with *in vitro* analysis providing an IC_{50} greater than 100 μM.[54] The high IC_{50} value indicated an ineffective inhibition of Oseltamivir to the M^{Pro}. However, a previous study by Kumar, *et al.*, experimentally examined 19 different NA inhibitors in complex with SARS-CoV and

MERS-CoV,[44] and determined the IC_{50} values for the inhibitors via a fluorometric assay. A fluorogenic peptide is placed in solution with the M^{Pro} and cleavage of the peptide increases the fluorescence intensity, allowing for a quantitative measure of enzyme efficacy. The most promising compound was 3K, shown in **Figure 6B**. The 3K inhibitor in complex with SARS-CoV M^{Pro} shows an IC_{50} of 6.4 ± 1.2 μM, and an IC_{50} of 5.8 ± 1.6 μM with MERS-CoV M^{Pro}. Modeling of 3K binding showed that the inhibitor does not occupy the S_1' subsite.[44] Instead, the phenyl group shows a preference for the hydrophobic pocket at S_4. However, the phenyl group had a tighter fit in the S_4 pocket of the MERS-CoV M^{Pro} due to the smaller pocket size in this variant. The hydrophobicity of ring A creates a strong binding interaction with the S_2 subsite, **Table 2**. In the S_1 pocket of SARS-CoV, the 3K inhibitor forms hydrogen bonds with Ser144 and Leu141. In MERS-CoV, the 3K inhibitor forms hydrogen bonds in the S_1 pocket with Ser147 and Glu169. The promise of 3K shown in this study requires confirmation using cell-based assays to further verify the predicted effects. Given the strong similarities between the M^{Pro} active sites, NA inhibitors based on the 3K structure may be strong candidates for the development of broad-spectrum inhibitors of coronavirus replication. With the 3K inhibitor showing efficacy to the M^{Pro} of SARS-CoV and MERS-CoV, there is a hope that it may have a similar efficacy towards SARS-CoV-2. This study demonstrates that neuraminidase inhibitors are capable of interacting with the active site of the SARS-CoV-2 M^{Pro}, but further studies are necessary to discover an inhibitor capable of stopping viral replication *in vitro.*

Peptidomimetic Inhibitors (11a and 11b)

Peptidomimetics are a class of inhibitors designed to mimic the structure of peptides. Interest for these molecules is growing because they demonstrate high potency, strong target selectivity, and a prolonged duration of activity when compared to natural peptides.[59] Peptidomimetic inhibitor studies in SARS-CoV and SARS-CoV-2 show efficacy in targeting and inhibiting the viral M^{Pro}, thus making them a promising strategy of inhibition.[56, 61] Wong, *et al.,* examined the effects of 5 different inhibitors on SARS-CoV M^{Pro} with IC_{50} values between 5 and 52 μM. The most promising formed a covalent bond with Cys145, completely preventing enzymatic proteolysis.[56] In a more recent study by Chuck, *et al.,* peptidomimetic inhibitors showed the ability to inhibit the M^{Pro} of SARS-CoV.[67] Four inhibitors were tested and demonstrated IC_{50} values ranging from 4.6 to 49 μM.[67] The significant range in IC_{50} is a result of minor alterations of functional groups on each moiety.

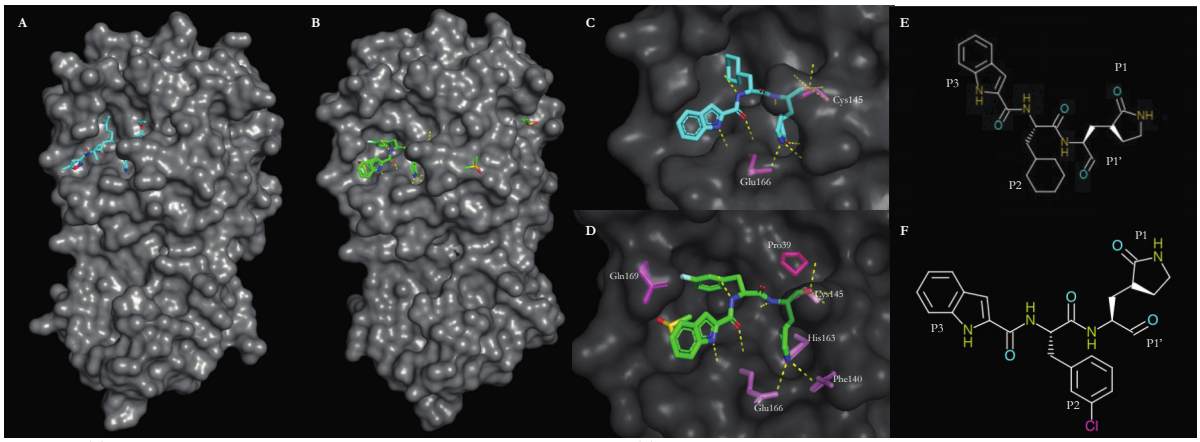

Figure 7. A. The M^{Pro} of SARS-CoV-2 with compound 11a (PDB: 6LZE).[68] B. The M^{Pro} of SARS-CoV-2 with compound 11b interacting with the active site (PDB: 6M0K).[68] C, D. Polar interactions between the protease and inhibitor 11a or 11b, respectively, are shown by dashed yellow lines. E. The chemical structure of compound 11a. F. The chemical structure of compound 11b. This figure was prepared with PyMOL.[36]

Dai, *et al.*, investigated the efficacy of peptidomimetic aldehyde-based inhibitors, shown in **Figure 7**, against the SARS-CoV-2 M^{Pro}.[61] An antiviral activity assay was performed in Vero E6 cells that had been infected with SARS-CoV-2. Synthesized compounds 11a and 11b showed robust SARS-CoV-2 inhibitory activity. Compound 11a differs from 11b in the P_2 site; 11a contains a cyclohexyl group whereas 11b has an aryl group. Compounds 11a and 11b potently inhibit SARS-CoV-2 M^{Pro} with IC_{50} values of 0.053 ± 0.005 μM and 0.040 ± 0.002 μM respectively, **Table 1**. The low IC_{50} values are a result of strong interactions that occur between the inhibitors and the M^{Pro}. Compound 11a and 11b predominantly interact with amino acids in the S_1 and S_1' subsites. Interactions in the S_1' subsite include a covalent bond formed between the aldehyde at the P_1' site of 11a and Cys145 as well as hydrogen bond formed with the backbone of Cys145 and Gly143. In the S_1 pocket of the M^{Pro} the (S)-y-Lactam ring at the P_1 site of 11a forms hydrogen bonds with the side chains His163 and Glu166, and the main chain of Phe140. The P_2 site of 11a forms hydrophobic interactions with the side chains of Met49, Tyr54, Met165 and Asp187 in the S_2 pocket of the M^{Pro}. The S_4 subsite interacts with the P_3 of 11a by hydrophobic interactions between Pro168 and Gln189. Together, the interactions between 11a and the M^{Pro} form a stable interaction which inhibits viral activity. Similarly, 11b exhibits the same interactions in the S_1, S_1', and S_4 subsites of the M^{Pro}, but the aryl group at the P_2 site of 11b results in different interactions with the S_2 subsite. Specifically, 11b forms hydrophobic interactions in the S_2 subsite with His41, Met49, Met165, and Val186. Additionally, a hydrogen bond

forms between the side chain of Gln189 and 11b to stabilize the inhibitor in the active site.[61] Both of these compounds form a covalent bond with Cys145, which is essential for antiviral activity. However, neither of these inhibitors form a hydrogen bond with His41, a mechanism commonly found in several other successful inhibitors. Strong interactions between compounds 11a and 11b with the active site pocket of M^{Pro} suggest these compounds are promising candidates in preventing viral replication, warranting further research.

Alpha-Ketoamide Inhibitor (13b)

Another class of inhibitors, α-ketoamide inhibitors, show great potential in targeting the M^{Pro} of coronaviruses. Zhang, *et al.,* reported the design of various modified α-ketoamide inhibitors of the M^{Pro} of beta coronaviruses, alpha coronavirus, and 3C proteases of enteroviruses.[65] Previously, the group had developed an α-ketoamide inhibitor, 11r, with a low EC_{50} against the SARS-CoV M^{Pro} and an EC_{50} value of 400 pM against MERS-CoV.[64] With the goal of preventing SARS-CoV-2 M^{Pro} from cleaving Nsps, the group modified the α-ketoamide inhibitor and studied its efficacy *in silico* and *in vitro*. The designed α-ketoamide inhibitor (13b) includes a pyridine ring (**Figure 8**) that sterically clashes with Gln189.[64] However, previous computational studies indicate Gln189 is flexible, and may allow for proper binding *in vitro*. Computational docking studies provide a suggested mechanism of interaction between 13b and the M^{Pro} of SARS-CoV-2. A nucleophilic attack of the catalytic Cys145 onto the α-ketoamide 13b inhibitor initiates binding, forming a thiohemiacetal in a reversible reaction. The α-ketoamide inhibitor 13b structure then interacts with the catalytic dyad of the cysteine protease, which behaves as an "oxyanion hole" during catalysis, via hydrogen bonds.[65] This interaction prevents catalysis. Zhang, L., *et al.,* identified some of the necessary interactions that 13b has with the M^{Pro} of SARS-CoV-2 to prevent viral replication. A subsequent study by Gimeno, *et al.*, completed the understanding of these interactions between 13b and the M^{Pro}.

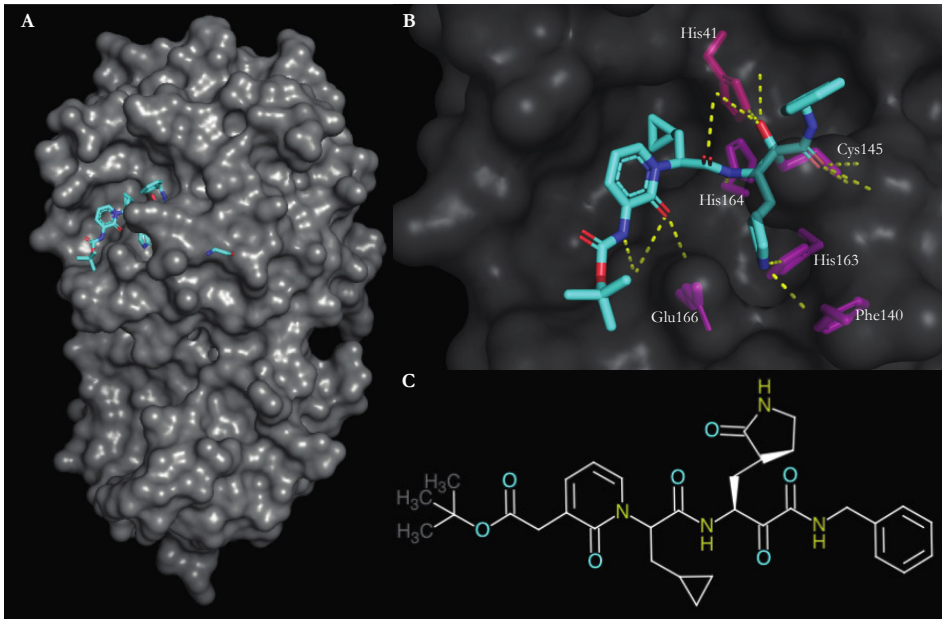

Figure 8. A. Compound 13b bound to the M^{Pro} of SARS-CoV-2 (PDB: 6Y2G).[65] B. The active site of the M^{Pro} and the polar interactions it has with compound 13b, as shown by dashed yellow lines. C. The chemical structure of inhibitor 13b. This figure was made through the use of PyMOL.[36]

Gimeno, *et al.*, found 13b forms hydrogen bonds and has hydrophobic interactions with other amino acids in the active site, as seen in **Table 2**. Some of the most important observed interactions include a hydrogen bond with the carbonyl oxygen of His164 that acts as an anchoring point as shown in **Figure 8b**. The hydrophobic interactions that occur in the S_4 and S_2 subsites act as a "hydrophobic grip" on the inhibitor and increase binding affinity. In the S_1 subsite, 13b hydrogen bonds with Glu166, the backbone of Phe140 and the side chain of His163.[43] Given that 13b forms a covalent bond with Cys145 and has other strong interactions with the M^{Pro}, it is a strong candidate for a broad-spectrum inhibitor of coronaviruses.[43] Though this promise has been revealed by computational analysis, cellular assays are necessary to provide further insight regarding the efficacy of 13b as a coronavirus inhibitor.

Aldehyde Prodrug (GC-376)

GC-376 is an aldehyde prodrug and demonstrates strong affinity for the M^{Pro} of SARS-CoV-2.[63] This is accomplished by GC-376 structurally mimicking the Nsps that the M^{Pro} cleaves. X-ray crystallography has revealed the binding interactions between GC-376 and the M^{Pro} of SARS-CoV-2 (**Figure 9**).[63] This inhibitor is unique due to its two different conformations in the active site where the oxyanion hole is located. In the S conformation the oxyanion hole is occupied by the thioacetal hydroxide. However, in the R conformation the thioacetal hydroxide sticks out and forms a hydrogen bond with His41. Like the α-ketoamide inhibitors, a covalent bond forms between GC-376 and Cys145, locking the inhibitor into the active site. GC-376 also forms a number of hydrogen bonds and has hydrophobic interactions with the S_2 and S_4 subsites of the active site. The γ-lactam ring occupies the S_1 subsite and forms hydrogen bonds with the side chains of His163 and Glu166 as well as the main chain of Phe140. In the S_1' subsite, GC-376 forms a hydrogen bond with His41 or has a hydrophobic interaction with this amino acid, due to the two different conformations mentioned above. The S_2 subsite of the M^{Pro} is occupied by an isobutyl group that forms hydrophobic interactions with Met49 and Met146. Other hydrophobic interactions occur in the S_4 subsite which is occupied by the phenyl-methyl ester of GC-376. In addition to structural analysis of binding, the GC-376 inhibitor has also been studied in cell cultures to determine the efficiency of antiviral activity, demonstrating an IC_{50} value of 0.03 μM.[63]

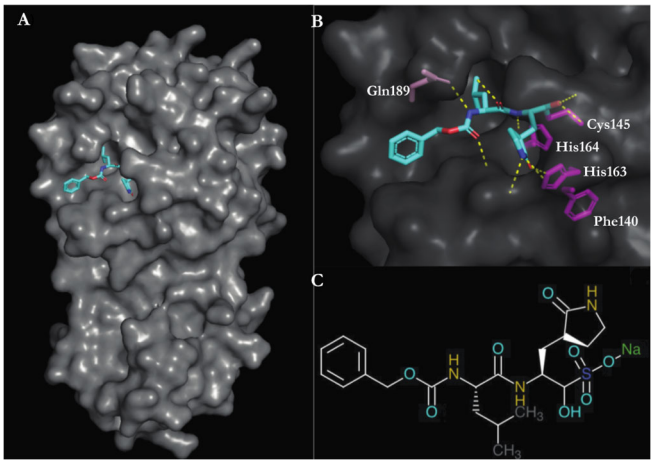

Figure 9. A. The SARS-CoV-2 M^{Pro} in complex with the inhibitor GC-376 (PDB: 6WTT).[63] B. The active site of the M^{Pro} with GC-376 and polar interactions between them, as shown by dashed yellow lines. C. The chemical structure of GC-376. This image was made with the use of PyMOL.[36]

Phosphate Prodrug PF-07304814

PF-07304814 (**Figure 10**) is a highly soluble, phosphate prodrug capable of inhibiting 12 different coronavirus strains across the α, β, and γ coronavirus families.[62] Alkaline phosphatase enzymes rapidly cleave the phosphate molecule, metabolizing it into the active moiety, PF-00835231.[62] Analysis by Boras, B., *et al,*. shows PF-07304814 strongly inhibits the M^{Pro} of SARS-CoV. The inhibitor forms an irreversible covalent bond with Cys145 at the active site of the M^{Pro}. Binding of this drug induces a melting temperature shift of 14.6 °C, indicating tight binding of the molecule and protein. PF-0083521 demonstrates a low affinity for human proteases and, therefore, shows strong selectivity towards coronavirus M^{Pro}s. Nonhuman-primate studies demonstrate that PF-07304814 has strong preclinical safety features and robust antiviral activity. A limitation of this drug is the requirement for intravenous delivery, which complicates delivery of the drug beyond the clinic. The cellular assays alone provide robust support for the potential of a novel M^{Pro} inhibitor capable of broad-spectrum coronavirus activity.[62] Structural analysis of inhibitor interactions with the binding site provides further insight.

A structural inventory of protein-drug interactions confirms that PF-00835231 forms a covalent bond with Cys145 (**Figure 10B**). It also forms hydrogen bonds with the side chains of Phe140, His163, and Glu166. Additional hydrogen bonds, indicated by yellow dashes, in **Figure 10B** are formed with the backbone moieties of Met165, Cys145, and His164. From our analysis, we were able to determine polar interactions and hypothesize the hydrophobic interactions. A comparison of hydrophobic interactions of other inhibitors determined how the M^{Pro} may interact with the hydrophobic areas of the prodrug. We identified hydrophobic contacts with the side chains of His41, Met49, Tyr54, and Pro168, as well as with the aliphatic portion of the Asp187 side chain. These hydrophobic interactions increase the attraction between the inhibitor and the active site of the M^{Pro}. It is important to note that an inventory based on structure will need to be confirmed by other, more rigorous, analysis like *in silico* docking.

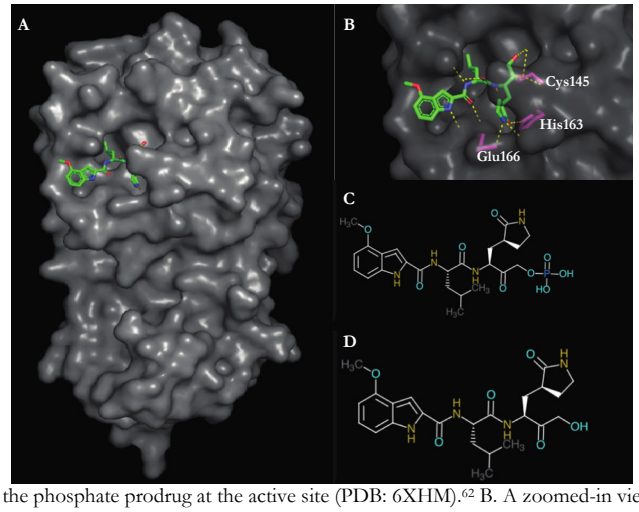

Figure 10. A. SARS-CoV-2 M^{Pro} with the phosphate prodrug at the active site (PDB: 6XHM).[62] B. A zoomed-in view of the active site with the phosphate prodrug and the polar interactions between them, showed by the dashed yellow lines. **C.** Chemical structure of PF-07304814, the prodrug. D. Chemical structure of PF-00835231, the active form. This figure was made through the use of PyMOL.[36]

CONCLUSION

The highly pathogenic coronavirus outbreaks of the past two decades show similarity in structure and function of the M^{Pro}. SARS-CoV and SARS-CoV-2 share the most similarities, and MERS-CoV is less similar. However, the active site of the main proteases demonstrates a high degree of structural conservation across all coronavirus lines, specifically the Cys145-His41 catalytic dyad and GSCGS recognition site. Spanning domains I and II as well as the N-finger, the active site holds relevance as a center point for therapeutic targeting and rational drug design across the three viruses. This review catalogs four groups of novel inhibitors that target the main protease of coronaviruses. The 3k inhibitor, a neuraminidase inhibitor, shows efficacy in inhibiting the M^{Pro}s of SARS-CoV and MERS-CoV.[44] 3k interacts with the active site via a combination of hydrogen bonds and hydrophobic interactions, but this compound does not form a covalent bond with the Cys145, a property of other compounds known to improve inhibition.[44] However, *in silico* models of this drug in the active site provides evidence that the S_4 pocket of the M^{Pro} in MERS-CoV is smaller than the S_4 pocket of the M^{Pro} in the SARS-CoV.[44] This understanding allows for a simple modification in the inhibitor to better fit into the smaller hydrophobic pocket. Another class of inhibitors, peptidomimetic inhibitors, readily allow for chemical modifications to better fit the protease's binding pocket.[56, 61] The two most promising candidates in this class of inhibitors are 11a and 11b, which covalently bind to the M^{Pro} of SARS-CoV-2. These inhibitors also form hydrogen bonds and have hydrophobic interactions with the M^{Pro}. Their low IC_{50} values show that they are promising inhibitors for further study. Compound 13b is a modified α-ketoamide inhibitor capable of covalently binding Cys145 and has a low IC_{50} value.[64] All four inhibitors show high efficacy either *in silico* or *in vitro*, yet all four lack animal studies to validate their efficacy *in vivo.* An aldehyde prodrug, GC376, is another promising novel coronavirus inhibitor because it has a very low IC50 value (0.03 uM) and forms a covalent bond with Cys145, blocking viral replication.[63] The phosphate prodrug PF-07304814 is a novel compound shown to inhibit the main protease of coronaviruses and decrease viral load in nonhuman primates.[62] Importantly, *in vitro* assays show the prodrug's ability to inhibit the main protease of a dozen different coronaviruses, showing the potential for broad spectrum therapy against coronaviruses. Taken together, the information reviewed in this article suggests inhibitors designed for one coronavirus protease are likely to be effective against M^{Pro} of other coronaviruses. Ideally, modification of these inhibitors will produce drugs with great efficacy. Regardless of the challenges, the potential for broad-spectrum, coronavirus therapeutic design appears possible and within reach. The implications of universal inhibitor design offer hope for clinicians during both today's coronavirus pandemic, and any future outbreaks.

REFERENCES

1. WHO | Cumulative Number of Reported Probable Cases of SARS. (2015). WHO.
2. WHO *Coronavirus Disease (COVID-19) Dashboard | WHO Coronavirus Disease (COVID-19) Dashboard.* (n.d.). Retrieved January 29, 2021, from *https://covid19.who.int/*
3. WHO *EMRO | MERS outbreaks | MERS-CoV | Health topics.* (n.d.). Retrieved January 29, 2021, from *http://www.emro.who.int/health-topics/mers-cov/mers-outbreaks.html*
4. Ye, Z.-W., Yuan, S., Yuen, K.-S., Fung, S.-Y., Chan, C.-P., & Jin, D.-Y. (2020). Zoonotic origins of human coronaviruses. *International Journal of Biological Sciences*, *16*(10), 1686–1697. *https://doi.org/10.7150/ijbs.45472*
5. Drexler, J. F., Corman, V. M., & Drosten, C. (2014). Ecology, evolution and classification of bat coronaviruses in the aftermath of SARS. In *Antiviral Research* (Vol. 101, Issue 1, pp. 45–56). *https://doi.org/10.1016/j.antiviral.2013.10.013*
6. LeDuc, J. W., & Barry, M. A. (2004). SARS, the First Pandemic of the 21st Century. In *Emerging Infectious Diseases* (Vol. 10,

Issue 11, p. e26). *https://doi.org/10.3201/eid1011.040797_02*
7. Al-Osail, A. M., & Al-Wazzah, M. J. (2017). The history and epidemiology of Middle East respiratory syndrome corona virus. In *Multidisciplinary Respiratory Medicine* (Vol. 12, Issue 1). BioMed Central Ltd. *https://doi.org/10.1186/s40248-017-0101-8*
8. WHO | Update 49 - SARS case fatality ratio, incubation period. (2015). *WHO*.
9. Donnelly, C. A., Malik, M. R., Elkholy, A., Cauchemez, S., & Van Kerkhove, M. D. (2019). Worldwide Reduction in MERS Cases and Deaths since 2016. In *Emerging infectious diseases* (Vol. 25, Issue 9, pp. 1758–1760). *https://doi.org/10.3201/eid2509.190143*
10. Dong, E., Du, H., & Gardner, L. (2020). An interactive web-based dashboard to track COVID-19 in real time. In *The Lancet Infectious Diseases* (Vol. 20, Issue 5, pp. 533–534). Lancet Publishing Group. *https://doi.org/10.1016/S1473-3099(20)30120-1*
11. Jaiswal, N. K., & Saxena, S. K. (2020). Classical Coronaviruses. In *Coronavirus Disease 2019 (COVID-19): Epidemiology, Pathogenesis, Diagnosis, and Therapeutics* (pp. 141–150). *https://doi.org/10.1007/978-981-15-4814-7_12*
12. Tang, X. C., Zhang, J. X., Zhang, S. Y., Wang, P., Fan, X. H., Li, L. F., Li, G., Dong, B. Q., Liu, W., Cheung, C. L., Xu, K. M., Song, W. J., Vijaykrishna, D., Poon, L. L. M., Peiris, J. S. M., Smith, G. J. D., Chen, H., & Guan, Y. (2006). Prevalence and Genetic Diversity of Coronaviruses in Bats from China. *Journal of Virology*, *80*(15), 7481–7490. *https://doi.org/10.1128/jvi.00697-06*
13. Kim, Y., Cho, Y., Kim, D., Yang, J., Kim, H., Park, S., Han, Y. W., Yun, M., Lee, H. S., Kim, A., Heo, D. R., Kim, J. A., Kim, S. J., Jung, H., Kim, N., Yoon, S., Nam, J., Kang, H. J., Cheong, H., … Kim, S. S. (2015). *Complete Genome Sequence of Middle East Respiratory Syndrome*. *3*(4), 3–4. *https://doi.org/10.1128/genomeA.00787-15.Copyright*
14. Marco, A., Steven, J. M., Caroline, R., & Robert, A. (2003). *The Genome sequence of the SARS-associated coronavirus* .
15. Khailany, R. A., Safdar, M., & Ozaslan, M. (2020). Genomic characterization of a novel SARS-CoV-2. *Gene Reports*, *19*. *https://doi.org/10.1016/j.genrep.2020.100682*
16. *THE CORONAVIRUS REPLICASE: INSIGHTS INTO A SOPHISTICATED ENZYME MACHINERY*. (n.d.).
17. Woo, P. C. Y., Huang, Y., Lau, S. K. P., & Yuen, K. Y. (2010). Coronavirus genomics and bioinformatics analysis. In *Viruses* (Vol. 2, Issue 8, pp. 1805–1820). MDPI AG. *https://doi.org/10.3390/v2081803*
18. Neuman, B. W., Chamberlain, P., Bowden, F., & Joseph, J. (2014). Atlas of coronavirus replicase structure. *Virus Research*, *194*, 49–66. *https://doi.org/10.1016/j.virusres.2013.12.004*
19. Báez-Santos, Y. M., St. John, S. E., & Mesecar, A. D. (2015). The SARS-coronavirus papain-like protease: Structure, function and inhibition by designed antiviral compounds. In *Antiviral Research* (Vol. 115, pp. 21–38). Elsevier B.V. *https://doi.org/10.1016/j.antiviral.2014.12.015*
20. Kamitani, W., Huang, C., Narayanan, K., Lokugamage, K. G., & Makino, S. (2009). A two-pronged strategy to suppress host protein synthesis by SARS coronavirus Nsp1 protein. *Nature Structural and Molecular Biology*, *16*(11), 1134–1140. *https://doi.org/10.1038/nsmb.1680*
21. Zhai, Y., Sun, F., Li, X., Pang, H., Xu, X., Bartlam, M., & Rao, Z. (2005). Insights into SARS-CoV transcription and replication from the structure of the nsp7-nsp8 hexadecamer. *Nature Structural and Molecular Biology*, *12*(11), 980–986. *https://doi.org/10.1038/nsmb999*
22. Bartlam, M., Yang, H., & Rao, Z. (2005). Structural insights into SARS coronavirus proteins. In *Current Opinion in Structural Biology* (Vol. 15, Issue 6, pp. 664–672). *https://doi.org/10.1016/j.sbi.2005.10.004*
23. Sutton, G., Fry, E., Carter, L., Sainsbury, S., Walter, T., Nettleship, J., Berrow, N., Owens, R., Gilbert, R., Davidson, A., Siddell, S., Poon, L. L. M., Diprose, J., Alderton, D., Walsh, M., Grimes, J. M., & Stuart, D. I. (2004). The nsp9 Replicase Protein of SARS-Coronavirus, Structure and Functional Insights. *Structure*, *12*(2), 341–353. *https://doi.org/10.1016/j.str.2004.01.016*
24. Egloff, M.-P., Ferron, F., Rie Campanacci, V., Longhi, S., Rancurel, C., Lè Ne Dutartre, H., Snijder, E. J., Gorbalenya, A. E., Cambillau, C., & Canard, B. (2004). *The severe acute respiratory syndrome-coronavirus replicative protein nsp9 is a single-stranded RNA-binding subunit unique in the RNA virus world. www.pnas.orgcgidoi10.1073pnas.0307877101*
25. Bouvet, M., Debarnot, C., Imbert, I., Selisko, B., Snijder, E. J., Canard, B., & Decroly, E. (2010). In vitro reconstitution of sars-coronavirus mRNA cap methylation. *PLoS Pathogens*, *6*(4), 1–13. *https://doi.org/10.1371/journal.ppat.1000863*
26. van Dinten, L. C., van Tol, H., Gorbalenya, A. E., & Snijder, E. J. (2000). The Predicted Metal-Binding Region of the Arterivirus Helicase Protein Is Involved in Subgenomic mRNA Synthesis, Genome Replication, and Virion Biogenesis. *Journal of Virology*, *74*(11), 5213–5223. *https://doi.org/10.1128/jvi.74.11.5213-5223.2000*
27. Tanner, J. A., Watt, R. M., Chai, Y. B., Lu, L. Y., Lin, M. C., Peiris, J. S. M., Poon, L. L. M., Kung, H. F., & Huang, J. D. (2003). The severe acute respiratory syndrome (SARS) coronavirus NTPasefhelicase belongs to a distinct class of 5' to 3' viral helicases. *Journal of Biological Chemistry*, *278*(41), 39578–39582. *https://doi.org/10.1074/jbc.C300328200*
28. Ivanov, K. A., Thiel, V., Dobbe, J. C., van der Meer, Y., Snijder, E. J., & Ziebuhr, J. (2004). Multiple Enzymatic Activities Associated with Severe Acute Respiratory Syndrome Coronavirus Helicase. *Journal of Virology*, *78*(11), 5619–5632. *https://doi.org/10.1128/jvi.78.11.5619-5632.2004*
29. Minskaia, E., Hertzig, T., Gorbalenya, A. E., Campanacci, V., Cambillau, C., Canard, B., & Ziebuhr, J. (2006). Discovery of an RNA virus 3'→5' exoribonuclease that is critically involved in coronavirus RNA synthesis. *Proceedings of the National Academy of*

Sciences of the United States of America, *103*(13), 5108–5113. *https://doi.org/10.1073/pnas.0508200103*

30. Rathnayake, A. D., Zheng, J., Kim, Y., Perera, K. D., Mackin, S., Meyerholz, D. K., Kashipathy, M. M., Battaile, K. P., Lovell, S., Perlman, S., Groutas, W. C., & Chang, K.-O. (2020). 3C-like protease inhibitors block coronavirus replication in vitro and improve survival in MERS-CoV-infected mice. *Science Translational Medicine*, *5332*(August), eabc5332. *https://doi.org/10.1126/scitranslmed.abc5332*

31. Jin, Z., Zhao, Y., Sun, Y., Zhang, B., Wang, H., Wu, Y., Zhu, Y., Zhu, C., Hu, T., Du, X., Duan, Y., Yu, J., Yang, X., Yang, X., Yang, K., Liu, X., Guddat, L. W., Xiao, G., Zhang, L., … Rao, Z. (2020). Structural basis for the inhibition of SARS-CoV-2 main protease by antineoplastic drug carmofur. *Nature Structural and Molecular Biology*, *27*(6), 529–532. *https://doi.org/10.1038/s41594-020-0440-6*

32. Casalino, L., Gaieb, Z., Goldsmith, J. A., Hjorth, C. K., Dommer, A. C., Harbison, A. M., Fogarty, C. A., Barros, E. P., Taylor, B. C., McLellan, J. S., Fadda, E., & Amaro, R. E. (2020). Beyond Shielding: The Roles of Glycans in the SARS-CoV-2 Spike Protein. *ACS Central Science. https://doi.org/10.1021/acscentsci.0c01056*

33. Yang, H., Yang, M., Ding, Y., Liu, Y., Lou, Z., Zhou, Z., Sun, L., Mo, L., Ye, S., Pang, H., Gao, G. F., Anand, K., Bartlam, M., Hilgenfeld, R., & Rao, Z. (2003). The crystal structures of severe acute respiratory syndrome virus main protease and its complex with an inhibitor. *Proceedings of the National Academy of Sciences of the United States of America*, *100*(23), 13190–13195. *https://doi.org/10.1073/pnas.1835675100*

34. Needle, D., Lountos, G. T., & Waugh, D. S. (2015). Structures of the Middle East respiratory syndrome coronavirus 3C-like protease reveal insights into substrate specificity. *Acta Crystallographica Section D: Biological Crystallography*, *71*, 1102–1111. *https://doi.org/10.1107/S1399004715003521*

35. *RCSB PDB - 6YB7: SARS-CoV-2 main protease with unliganded active site (2019-nCoV, coronavirus disease 2019, COVID-19).* (n.d.).

36. Schrodinger LLC. (2015). *The PyMOL Molecular Graphics System, Version 1.8*.

37. Kaur, N., Singh, R., Dar, Z., Bijarnia, R. K., Dhingra, N., & Kaur, T. (2020). Genetic comparison among various coronavirus strains for the identification of potential vaccine targets of SARS-CoV2. *Infection, Genetics and Evolution*, 104490. *https://doi.org/10.1016/j.meegid.2020.104490*

38. Tahir ul Qamar, M., Alqahtani, S. M., Alamri, M. A., & Chen, L. L. (2020). Structural basis of SARS-CoV-2 3CLpro and anti-COVID-19 drug discovery from medicinal plants. *Journal of Pharmaceutical Analysis*, *10*(4), 313–319. *https://doi.org/10.1016/j.jpha.2020.03.009*

39. Wang, H., He, S., Deng, W., Zhang, Y., Li, G., Sun, J., Zhao, W., Guo, Y., Yin, Z., Li, D., & Shang, L. (2020). Comprehensive Insights into the Catalytic Mechanism of Middle East Respiratory Syndrome 3C-Like Protease and Severe Acute Respiratory Syndrome 3C-Like Protease. *ACS Catalysis*, *10*(10), 5871–5890. *https://doi.org/10.1021/acscatal.0c00110*

40. Zhong, N., Zhang, S., Zou, P., Chen, J., Kang, X., Li, Z., Liang, C., Jin, C., & Xia, B. (2008). Without Its N-Finger, the Main Protease of Severe Acute Respiratory Syndrome Coronavirus Can Form a Novel Dimer through Its C-Terminal Domain. *Journal of Virology*, *82*(9), 4227 LP – 4234. *https://doi.org/10.1128/JVI.02612-07*

41. Huang, C., Wei, P., Fan, K., Liu, Y., & Lai, L. (2004). 3C-like Proteinase from SARS Coronavirus Catalyzes Substrate Hydrolysis by a General Base Mechanism. *Biochemistry*, *43*(15), 4568–4574. *https://doi.org/10.1021/bi036022q*

42. Chang, G.-G. (2009). Quaternary Structure of the SARS Coronavirus Main Protease. *Molecular Biology of the SARS-Coronavirus*, 115–128. *https://doi.org/10.1007/978-3-642-03683-5_8*

43. Gimeno, A., Mestres-Truyol, J., Ojeda-Montes, M. J., Macip, G., Saldivar-Espinoza, B., Cereto-Massagué, A., Pujadas, G., & Garcia-Vallvé, S. (2020). Prediction of novel inhibitors of the main protease (M-pro) of SARS-CoV-2 through consensus docking and drug reposition. *International Journal of Molecular Sciences*, *21*(11). *https://doi.org/10.3390/ijms21113793*

44. Kumar, V., Tan, K. P., Wang, Y. M., Lin, S. W., & Liang, P. H. (2016). Identification, synthesis and evaluation of SARS-CoV and MERS-CoV 3C-like protease inhibitors. *Bioorganic and Medicinal Chemistry*, *24*(13), 3035–3042. *https://doi.org/10.1016/j.bmc.2016.05.013*

45. Verschueren, K. H. G., Pumpor, K., Anemüller, S., Chen, S., Mesters, J. R., & Hilgenfeld, R. (2008). A structural view of the inactivation of the SARS coronavirus main proteinase by benzotriazole esters. *Chemistry & Biology*, *15*(6), 597–606. *https://doi.org/10.1016/j.chembiol.2008.04.011*

46. Fintelman-Rodrigues, N., Sacramento, C., Lima, C. R., da Silva, F. S., Ferreira, A., Mattos, M., de Freitas, C., Soares, V. C., Gomes Dias, S. da S., Temerozo, J., Miranda, M., Matos, A., Bozza, F., Carels, N., Alves, C. R., Siqueira, M., Bozza, P., & Souza, T. M. (2020). *Atazanavir inhibits SARS-CoV-2 replication and pro-inflammatory cytokine production. https://doi.org/10.1101/2020.04.04.020925*

47. De Meyer, S., Bojkova, D., Cinatl, J., Van Damme, E., Buyck, C., Van Loock, M., Woodfall, B., & Ciesek, S. (2020). Lack of antiviral activity of darunavir against SARS-CoV-2. *International Journal of Infectious Diseases*, *97*, 7–10. *https://doi.org/10.1016/j.ijid.2020.05.085*

48. Jin, Z., Du, X., Xu, Y., Deng, Y., Liu, M., Zhao, Y., Zhang, B., Li, X., Zhang, L., Peng, C., Duan, Y., Yu, J., Wang, L., Yang, K., Liu, F., Jiang, R., Yang, X., You, T., Liu, X., … Yang, H. (2020). Structure of Mpro from SARS-CoV-2 and discovery of its inhibitors. *Nature*, *582*(7811), 289–293. h*ttps://doi.org/10.1038/s41586-020-2223-y*

49. Sies, H., & Parnham, M. J. (2020). Potential therapeutic use of ebselen for COVID-19 and other respiratory viral infections.

Free Radical Biology and Medicine, *156*(June), 107–112. *https://doi.org/10.1016/j.freeradbiomed.2020.06.032*

50. Sisay, M. (2020). 3CLpro inhibitors as a potential therapeutic option for COVID-19: Available evidence and ongoing clinical trials. *Pharmacological Research*, *156*, 104779. *https://doi.org/10.1016/j.phrs.2020.104779*

51. Cao, B., Wang, Y., Wen, D., Liu, W., Wang, J., Fan, G., Ruan, L., Song, B., Cai, Y., Wei, M., Li, X., Xia, J., Chen, N., Xiang, J., Yu, T., Bai, T., Xie, X., Zhang, L., Li, C., … Wang, C. (2020). A trial of lopinavir-ritonavir in adults hospitalized with severe covid-19. *New England Journal of Medicine*, *382*(19), 1787–1799. *https://doi.org/10.1056/NEJMoa2001282*

52. Yao, T. T., Qian, J. D., Zhu, W. Y., Wang, Y., & Wang, G. Q. (2020). A systematic review of lopinavir therapy for SARS coronavirus and MERS coronavirus—A possible reference for coronavirus disease-19 treatment option. *Journal of Medical Virology*, *92*(6), 556–563. *https://doi.org/10.1002/jmv.25729*

53. Ma, C., Sacco, M. D., Hurst, B., Townsend, J. A., Hu, Y., Szeto, T., Zhang, X., Tarbet, B., Marty, M. T., Chen, Y., & Wang, J. (2020). Boceprevir, GC-376, and calpain inhibitors II, XII inhibit SARS-CoV-2 viral replication by targeting the viral main protease. *Cell Research*, *30*(8), 678–692. *https://doi.org/10.1038/s41422-020-0356-z*

54. Tan, Q., Duan, L., Ma, Y., Wu, F., Huang, Q., Mao, K., Xiao, W., Xia, H., Zhang, S., Zhou, E., Ma, P., Song, S., Li, Y., Zhao, Z., Sun, Y., Li, Z., Geng, W., Yin, Z., & Jin, Y. (2020). Is oseltamivir suitable for fighting against COVID-19: In silico assessment, in vitro and retrospective study. *Bioorganic Chemistry*, *104*, 104257. *https://doi.org/10.1016/j.bioorg.2020.104257*

55. Wu, C., Liu, Y., Yang, Y., Zhang, P., Zhong, W., Wang, Y., Wang, Q., Xu, Y., Li, M., Li, X., Zheng, M., Chen, L., & Li, H. (2020). Analysis of therapeutic targets for SARS-CoV-2 and discovery of potential drugs by computational methods. *Acta Pharmaceutica Sinica B*, *10*(5), 766–788. *https://doi.org/10.1016/j.apsb.2020.02.008*

56. Wong, K. B., Wan, D. C. C., & Chow, H. F. (2014). Substrate specificity and rational design of peptidomimetic inhibitors for SARS coronavirus main protease. *Hong Kong Medical Journal*, *20*(4), 18–21.

57. Kumar, V., Shin, J. S., Shie, J. J., Ku, K. B., Kim, C., Go, Y. Y., Huang, K. F., Kim, M., & Liang, P. H. (2017). Identification and evaluation of potent Middle East respiratory syndrome coronavirus (MERS-CoV) 3CLPro inhibitors. *Antiviral Research*, *141*, 101–106. *https://doi.org/10.1016/j.antiviral.2017.02.007*

58. Tomar, S., Johnston, M. L., John, S. E. S., Osswald, H. L., Nyalapatla, P. R., Paul, L. N., Ghosh, A. K., Denison, M. R., & Mesecar, A. D. (2015). Ligand-induced dimerization of Middle East Respiratory Syndrome (MERS) Coronavirus nsp5 protease (3CLpro): Implications for nsp5 regulation and the development of antivirals. *Journal of Biological Chemistry*, *290*(32), 19403–19422. *https://doi.org/10.1074/jbc.M115.651463*

59. Vagner, J., Qu, H., & Hruby, V. J. (2008). Peptidomimetics, a synthetic tool of drug discovery. *Current Opinion in Chemical Biology*, *12*(3), 292–296. *https://doi.org/10.1016/j.cbpa.2008.03.009*

60. Ghosh, A. K., Xi, K., Ratia, K., Santarsiero, B. D., Fu, W., Harcourt, B. H., Rota, P. A., Baker, S. C., Johnson, M. E., & Mesecar, A. D. (2005). Design and Synthesis of Peptidomimetic Severe Acute Respiratory Syndrome Chymotrypsin-like Protease Inhibitors. *Journal of Medicinal Chemistry*, *48*(22), 6767–6771.

61. Dai, W., Zhang, B., Jiang, X.-M., Su, H., Li, J., Zhao, Y., Xie, X., Jin, Z., Peng, J., Liu, F., Li, C., Li, Y., Bai, F., Wang, H., Chen, X., Cen, X., Hu, S., Yang, X., Wang, J., … Liu, H. (2020). *Structure-Based Design, Synthesis and Biological Evaluation of Peptidomimetic Aldehydes as a Novel Series of Antiviral Drug Candidates Targeting the SARS-CoV-2 Main Protease. https://doi.org/10.1101/2020.03.25.996348*

62. Boras, B., Jones, R. M., Anson, B. J., Arenson, D., Aschenbrenner, L., Bakowski, M. A., Beutler, N., Binder, J., Chen, E., Eng, H., Hammond, J., Hoffman, R., Kadar, E. P., Kania, R., Kimoto, E., Kirkpatrick, M. G., Lanyon, L., Lendy, E. K., Lillis, J. R., … Allerton, C. (2020). Discovery of a Novel Inhibitor of Coronavirus 3CL Protease as a Clinical Candidate for the Potential Treatment of COVID-19. *BioRxiv*, 2020.09.12.293498. *https://doi.org/10.1101/2020.09.12.293498*

63. Ma, C., Sacco, M. D., Hurst, B., Townsend, J. A., Hu, Y., Szeto, T., Zhang, X., Tarbet, B., Marty, M. T., Chen, Y., & Wang, J. (2020). Boceprevir, GC-376, and calpain inhibitors II, XII inhibit SARS-CoV-2 viral replication by targeting the viral main protease. *Cell Research*, *30*(8), 678–692. *https://doi.org/10.1038/s41422-020-0356-z*

64. Zhang, L., Lin, D., Kusov, Y., Nian, Y., Ma, Q., Wang, J., Von Brunn, A., Leyssen, P., Lanko, K., Neyts, J., De Wilde, A., Snijder, E. J., Liu, H., & Hilgenfeld, R. (2020). α-Ketoamides as Broad-Spectrum Inhibitors of Coronavirus and Enterovirus Replication: Structure-Based Design, Synthesis, and Activity Assessment. *Journal of Medicinal Chemistry*, *63*(9), 4562–4578. *https://doi.org/10.1021/acs.jmedchem.9b01828*

65. Zhang, L., Lin, D., Sun, X., Curth, U., Drosten, C., Sauerhering, L., Becker, S., Rox, K., & Hilgenfeld, R. (2020). Crystal structure of SARS-CoV-2 main protease provides a basis for design of improved a-ketoamide inhibitors. *Science*, *368*(6489), 409–412. *https://doi.org/10.1126/science.abb3405*

66. McAuley, J. L., Gilbertson, B. P., Trifkovic, S., Brown, L. E., & McKimm-Breschkin, J. L. (2019). Influenza virus neuraminidase structure and functions. *Frontiers in Microbiology*, *10*(JAN). *https://doi.org/10.3389/fmicb.2019.00039*

67. *Since January 2020 Elsevier has created a COVID-19 resource centre with free information in English and Mandarin on the novel coronavirus COVID- 19 . The COVID-19 resource centre is hosted on Elsevier Connect , the company ' s public news and information* . (2020). *January*.

68. Dai, W., Zhang, B., Jiang, X. M., Su, H., Li, J., Zhao, Y., Xie, X., Jin, Z., Peng, J., Liu, F., Li, C., Li, Y., Bai, F., Wang, H., Cheng, X., Cen, X., Hu, S., Yang, X., Wang, J., … Liu, H. (2020). Structure-based design of antiviral drug candidates targeting the SARS-CoV-2 main protease. *Science*, *368*(6497), 1331–1335. *https://doi.org/10.1126/science.abb4489*

ABOUT STUDENT AUTHORS

Alyssa Sanders is a senior at Rowan University, graduating with a B.S. in Translational Biomedical Science. She intends to pursue a Ph.D. degree following her graduation.

Samuel Ricci is a graduate of Rowan University with a B.S. in Biophysics. He is currently advancing his training as an NIH Intramural Research Training Award recipient in the laboratory of Dr. Christine Alewine at the National Cancer Institute.

Sarah Uribe graduated from Rowan University in May of 2020 with a B.S. in Translational Biomedical Science. She is pursuing her M.S. in Pharmaceutical Science at Rowan University.

Bridget Boyle graduated from Rowan University in May of 2020 with a B.S. in Translational Biomedical Science. Bridget is currently pursuing a Ph.D. degree at Thomas Jefferson University with a focus on neuroscience.

Brian Nepper graduated from Rowan University in May of 2020 with a B.S. in Physics. He is currently perusing a M.S. in Mechanical Engineering at Rowan University with a focus on nanotechnology.

PRESS SUMMARY

The coronaviruses plaguing humanity in the 21st century share much in common: a spontaneous route of origin from wild animals, a propensity to take human life, and, importantly, a highly conserved set of biological machinery necessary for viral replication. Most recently, the SARS-CoV-2 is decimating economies around the world and has claimed over two million human lives, reminding the world of a need for an effective drug against present and future coronaviruses. To date, attempts to repurpose clinically approved antiviral medications show minimal promise, highlighting the need for development of new antiviral drugs. While vaccines attempt to help the body form antibodies against the viral spike protein, vaccines will be unlikely to protect against future emerging strains. The main protease of the coronavirus is an attractive alternative target for developing broad-spectrum inhibitors that may help protect against future outbreaks. This protease is responsible for cleaving proteins needed to replicate the virus. Here, we review the literature regarding potential inhibitors for the main protease of coronaviruses-with a specific focus on SARS-CoV-2. We analyze receptor-drug interactions and draw conclusions about candidate inhibitors for future outbreaks. Promising candidates for development of a broad-spectrum coronavirus protease inhibitor include the neuraminidase inhibitor 3k, the peptidomimetic inhibitor 11b, the α-ketoamide inhibitor 13b, the aldehyde prodrug, and the phosphate prodrug developed by Pfizer. *In silico* and *in vitro* analysis show that these inhibitors strongly interact with the active site of the main protease, and to varying degrees, prevent viral replication via interactions with the largely conserved active site pockets.

Print Edition ISSN 1536-4585
Online Edition ISSN 2375-8732